UNIVERSITY OF CRETE

DEPARTMENT OF MATERIALS SCIENCE AND TECHNOLOGY

Rheological signatures and origin of dynamic arrest in macromolecular systems of complex architecture

Master's Thesis

Nikolaos Kalafatakis

Heraklion, February 2021

Acknowledgements

First of all, I would like to thank from the deepest of my heart my supervisor Professor Dimitris Vlassopoulos. His is one of the most inspiring and motivating persons in my life. During my undergraduate years in the Materials Science and Technology Department he taught me Thermodynamics but more importantly he introduced me to the fascinating world of Polymer Physics when I attend his advanced course. His contribution to my progress is not limited to this. He trusted me and he gave me the opportunity to work with him, something that I do really appreciate and is an honor for me. He taught me also to be careful with my experiments and that good data may need months to be collected. He gave me fascinating samples to work with and he had no doubt about my results. But most importantly I think that he taught me ethos and behavior, something really important for me. On top of that he also gave me the life's opportunity to do my Ph.D. under his supervision something that I believe to be a privilege. I will be always grateful for his unconditioned support and patience when a health issue remembered me what is most important in life…

I am also grateful to Dr. Benoit Loppinet. He has unquestionably helped me to think out of the box, which I personally believe to be the most scientific way. He is one of the persons that gave me useful advice and he was always forward to discuss with me my questions regarding his expertise, scattering experiments. Not only that but he always tried to make me think about the big picture and see the real stuff.

I would also like to thank Prof. George Petekidis for introducing me to the world of colloids during my undergraduate and for the challenging discussions that we had during these two and a half years.

Moving to my lab mates I have to start with the senior members, Antje and Antonis. I am really grateful to them for all the knowledge they have shared with me these two and a half years. They were always willing to help me with the most important things. Antje has helped me a lot and introduced me to light scattering. Antonis was always available to give me the most valuable advices when I needed them. My experiments would be more difficult without his help, ranging from physics to mechanics.

To my fellow lab mates, I do have to start with my best friend Manos with whom I have shared among others some of the most beautiful moments in the lab and during our undergraduate years. He is more than a friend for me. He introduced me to the lab and the fascinating world of rheometry and he was always there to help me with the most simple or complicated things. I could keep on writing about Manos but I think that I will need another Chapter.

I also thank Katerina R. for the initial training she provided me and her patience. I know that I was not the best student but she helped me a lot.

Dimitra was always there to remember me that I can't reach her level of anxiety and have a joke when the stress was rising. I do believe that she is one of the best students I have ever seen and I hope that she will continue academically at some point.

Nikos B. is the guy with whom I only share the same name, but I really enjoyed his company and hopefully I will continue to do.

Andreas was a nice lab mate willing to help in any way and we had nice time together in the lab.

Katerina P. was always silent but really skillful experimentally. She always discussed with me things that she was more involved and was always willing to share with me data.

Consiglia C. (CoCa) was always helpful to me with rheometry especially non-linear measurements.

Christina P. helped me a lot with rheometry and she was always there when I had a question.

Thanasis the Captain is one of the persons that I enjoy his company the most. He has made the life in lab more interesting with his stories and always shares knowledge with us.

Mohandas the Brad was also very helpful with rheometry and he helped me understand the AntonPaar Rheocompass software which I would need another master to go through. I also like the way he vortexes his samples…

I also thank former Ph.D. students of the lab Dr. Panagiota B. who helped me a lot with microgel suspensions and Dr. Thanasis B. for the interesting discussions. Also, thanks go to Dr. Leo G. for his useful advices and the discussions we had that made me better experimentally.

Moving to the current post-docs special thanks go to the dielectrics specialist Dr. Stylianos Alexandris. We had a lot of funny moments in the lab and out of it. He helped me a lot to understand the aspects of my star polymers and he also inspired experiments to reveal their special segmental dynamics.

Dr. Esmaeel M. has taught me a lot especially with my soft deformable microgels and the rheology of colloids. He was also always making fun of me in a good way…

Dr. Daniele Parisi what can I say? I will just thank you for all the information you have provided me and all the concentrated experience of rheometry you have shared with me. You are really a good teacher and you will turn to a great supervisor; I do believe it. I feel you a real friend.

This work would be purer without the catalytic help of Dr. Emmanouil Glynos. He gave me access to the DSC instrument and we also collaborated in the friendliest way in the polystyrene stars project. I do believe he is a friend of mine.

I want also to thank Dimitris Ch. And Georgia N. for their help with the DSC measurements.

I want also to thank Professor Dimitris Bikiaris from the Aristotle University of Thessaloniki for financial support.

Great thanks go to Professor George Floudas and his talented student Panagiotis Kardasis from the Physics Department of the University of Ioannina for the collaboration in the ultra-high functionality stars project.

I want to thank all my friends with whom I had the funniest moments and we grew up together. I thank them for their understanding when I had to be in FORTH forever…

Last but not least, I want to thank my parents Manolis and Rena who taught me the most important things. First to be responsible and also hard working because that is the only way to succeed. They did everything humanly possible to provide me all the goods and now I can see that they did it. I hope to be blessed enough to have children in the future that I will grow them with the same principles and love. I also thank my siblings for their support all these years. My mind now recalls my grandmother's Marika advising words "τα μάθια φοβούνται τη δουλειά αλλά τα χέρια όχι", also my grandfather Nikos who was a real man and probably I will not reach his ideals.

“Have fun on sea and land
Unhappy it is to become famous
Riches, honors, false glitters of this world
All is but soap bubbles”

From the Nobel Lecture of Pierre-Gilles de Gennes, 9/12/1991

Table of Contents

Abstract

This work examines some salient features of star polymers in the melt state, which make them unique hybrid materials interpolating between polymers and colloids. It is already known that their rich viscoelastic response depends on the two fundamental parameters, functionality (number of arms) and arm length. Stars with low functionality and entangled arms relax stress via arm retraction. As the functionality increases, a second slower relaxation process emerges and is assigned to colloidal hopping dynamics. Here, we focus on the behavior of stars with extreme functionalities and low molar mass (mainly unentangled) arms. In such situations, the slow process is characterized by an extended low-frequency plateau modulus which reflects the caged dynamics of jammed soft solid-like self-suspended nanoparticles. Additionally, the compact structure of such highly branched macromolecular objects displays layers of distinct segmental mobilities. By employing linear rheometry, calorimetric techniques and broadband dielectric spectroscopy (in collaboration) we unravel the above intriguing properties of these materials and therefore offer new design guidelines for core-shell nanoparticles and soft composites.

Περίληψη

Αυτή η εργασία εξετάζει μερικά σημαντικά χαρακτηριστικά των αστεροειδών πολυμερών (πολυμερή τα οποία ενώνονται στην μία άκρη τους σε ένα κοινό πυρήνα με την χαρακτηριστική μορφή αστεριού) στην μορφή τήγματος, τα οποία τα καθιστούν μοναδικά υβριδικά υλικά ανάμεσα σε πολυμερή και κολλοειδή. Είναι ήδη γνωστό ότι η πλούσια ιξωδοελαστική απόκριση τους εξαρτάται από τις θεμελιώδεις παραμέτρους, δηλαδή τον αριθμό των πλοκαμιών (πολυμερικών αλυσίδων που ενώνονται στον κοινό πυρήνα) και το μήκος τους. Αστέρια με μικρό αριθμό πλοκαμιών που παρουσιάζουν εμπλοκές χαλαρώνουν τις μηχανικές τάσεις μέσω ενός μηχανισμού χαλάρωσης γνωστό ως ανάκληση πλοκαμιού στον πυρήνα. Καθώς ο αριθμός των πλοκαμιών αυξάνεται, ένας δεύτερος μηχανισμός χαλάρωσης αναδύεται και οφείλεται σε κολλοειδή δυναμική. Εδώ, επικεντρωνόμαστε στην συμπεριφορά των αστεροειδών πολυμερών με τεράστιο αριθμό πλοκαμιών και μικρά μοριακά βάρη (κυρίως χωρίς εμπλοκές). Σε αυτή την περίπτωση, ο δεύτερος αργός μηχανισμός χαλάρωσης, χαρακτηρίζεται από ένα εκτεταμένο σε χαμηλές συχνότητές πλατό το οποίο αντικατοπτρίζει την παγιδευμένη δυναμική των περιορισμένων χαλαρών με συμπεριφορά στερεού αυτοδιεσπαρμένων νανοσωματιδίων. Επιπλέον, η συμπαγής μορφή τόσο διακλαδωμένων μακρομοριακών αντικειμένων καταδεικνύει στρώματα διαχωρισμένης τμηματικής δυναμικής. Επιστρατεύοντας ρεομετρία στην γραμμική περιοχή, θερμιδομετρικές τεχνικές και διηλεκτρική φασματοσκοπία σε συνεργασία αποσυνθέτουμε την περίπλοκη συμπεριφορά και κατανοούμε τις ενδιαφέρουσες ιδιότητες αυτών των υλικών και επιπλέον προσφέρουμε νέες κατευθυντήριες γραμμές για τον σχεδιασμό νανοσωματιδίων με μορφή πυρήνα-κορώνας και χαλαρών συνθετικών υλικών.

Chapter 1

Introduction

Soft matter is among the most interesting fields of materials science, due to its properties, applications and physics. The plethora of soft materials includes liquids, colloids, gels, rubbers, foams, liquid crystals, granular materials etc. Their applications are uncountable ranging from single use products, construction materials, cosmetics, personal care products like shampoos, viscosity modifiers, filters, safety products up to highly desired and technologically advanced products such as drug delivery agents, biomaterials, microelectronics etc.

Since the appearance of humans on Earth the history is strongly influenced by the availability and the ability of manipulating materials. The importance of materials is so high that eras of this history has been named after primary materials like stone (Stone Age), bronze (Bronze Age) or iron (Iron Age). Polymers were not known to people at that time but actually we are made out of them!! The biopolymers, namely macromolecules made in the living bodies are here from the very first day of human appearance.

People dealt with macromolecules like caoutchouc or natural rubber long time back, but chemists managed to synthesize polymers only during the middle of 19^{th} century. Even then they did not understand that they were synthesizing large molecules. The idea of polymers was introduced by Staudinger in 1920 with the macromolecular hypothesis: polymers are molecules made of covalently bonded elementary units, the monomers. Later on, in the next decades polymer science was established and synthetic methods were improved. Also, most of the foundations of the Polymer Physics known today were introduced during that time.

Understanding the properties of the abovementioned materials requires studying the fundamental aspects of their chemistry, viscoelastic properties, processing etc. All these materials share a common feature, i.e., the fact that their properties are associated with energetic changes of the order of a few kT.

The pioneering works of Kuhn on macromolecular sizes, the work of Flory on swelling of a single chain in good solvent, the work of Huggings and Flory on Thermodynamics were among the first studies dealing with polymers. The single-molecule models of polymer dynamics of Rouse and Zimm were built also at that time. In the sixties to eighties the main principles of modern polymer physics were born with Edwards' model and the very important confining tube, the view of semi-dilute solutions by des Cloizeaux and de Gennes and of course the reptation theory of polymeric chain developed by de Gennes and led to the Doi-Edwards theory for the flow properties of the polymer melts.

Polymer science is nowadays well-established and developed but there are still aspects of them that are far from understood. Polymers with associating groups bonded to their

chains, crystallization, liquid crystalline polymers and charged polymers are examples of areas of active research.

The outbreak of the coronavirus pandemic made the RNA vaccines known to everybody. This is another example of polymer science. The ability of this biopolymer to remain stable at temperatures convenient for vaccination, the production at very large scales or the mechanism of delivery in the human body would not be possible without the scientific research of doctors, chemists, biologists, material scientists, engineers etc.

In this work we deal with a specific type of polymer melts, namely star polymers. This type of polymers is important since this is the simplest case of branched polymers. In a star molecule, a number of *f* chains are covalently bonded onto a common core. This number of *f* arms can significantly vary from 2 (linear polymers thought as a two-arms star) up to order of 1000 arms. Here we study the case of low, intermediate and ultra-high functionalities to understand the effect of functionality in the terminal relaxation mechanisms of star polymers in the melt. We attempt a qualitative approach of the possible effect of monomer chemistry to the dynamics, more specifically the importance of stiffness and bulkiness of the monomer. In parallel the rich dynamics of these stars are studied to some extend with the case of ultra-high functionality stars to be of particular interest and discussed separately due to their complexity in the last chapter of this work.

In the following the main ideas and foundations of polymer dynamics are presented in brief. In chapter 2 the materials used in this study as well as the techniques utilized are presented. In chapter 3 we present and discuss the main findings of the large-scale dynamics for all the stars studied here. We also present preliminary data obtained by rheology, temperature-modulated differential scanning calorimetry and broad-band dielectric spectroscopy (in collaboration) on local scale dynamics. Finally, in Chapter 4 we present the data obtained on the local scale dynamics of the ultra-high functionality stars and the peculiarities found rheologically, as well as the data obtained on segmental dynamics using broad band dielectric spectroscopy that shed light in these observations.

1.1 Dynamics of unentangled polymers

Unentangled polymers are the simplest molecules to be studied. A polymer molecule has many internal degrees of freedom, for instance the rotational freedom about each C-C bond in the polyethylene molecule, and so it can take many different configurations. Because of this ideal flexibility we can assume a polymer molecule as a chain or a long piece of string, as depicted in the following cartoon. This chain can be modeled as following a regular lattice. The piece of chain lying within the lattice points are called “segments” and the rods connecting these points are “bonds”. Let now *b* be the length of each bond and *z* the coordination number of the lattice. If we assume that there is no correlation between the directions that different bonds take and that all the directions have the same probability, the configuration of the polymer is the same as a random walk on the lattice. This is the random walk model for polymers.

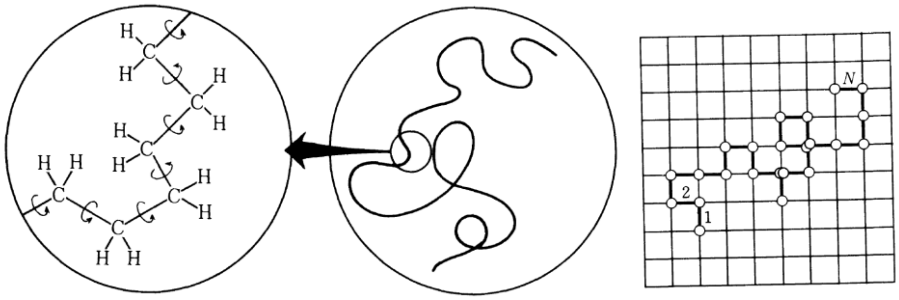

Figure 1. (from the left to the right subfigures). The atomic structure of polyethylene molecule, b. An overall view of the molecule, c. The random walk model of the polymer. White circles are the segments and the thick black lines correspond to the bonds. Cartoons reproduced from Reference[1]

For such a molecule the "end-to-end vector" *R* is given by $\langle R^2 \rangle = \sum_1^N \langle r_n^2 \rangle = Nb^2$, with *b* the length of a segment, so that the size of polymer is proportional to $N^{1/2}$. One can see that the probability distribution of the end-to-end vector for a random walk is:

$$P(R,N) = \left(\frac{3}{2\pi N b^2}\right)^{3/2} exp\left(-\frac{3R^2}{2Nb^2}\right).$$

This infinite flexibility of polymer segments means that the orientation of each bond is completely random and independent of the orientation of the previous bond. This means that the polymer segments can fold back on itself, something that is physically impossible. If we take this into consideration, we can calculate again the end-to-end vector which is again proportional to $N^{1/2}$ for large *N*.

Let now the bond vector *r*, then for a chain obeying Gaussian distribution the distribution of bond vector is given by:

$$p(r) = \left(\frac{3}{2\pi b^2}\right)^{3/2} exp\left(-\frac{3r^2}{2b^2}\right).$$

We can now assume the bond being equivalent to springs connecting the segments consisting of harmonic springs with *k* being the spring constant. This is the so-called bead spring model.

The Rouse model is the simplest version of the bead-spring model. It models a polymer chain as a string of beads each a distance *b* apart, where each bead is a chain segment, as described earlier. The beads move according to random walk statistics and chain dynamics can be incorporated by giving each bead a local friction coefficient and a corresponding thermal energy. The total friction coefficient of the whole Rouse chain is the sum of the contributions of each one of the *N* beads, so that the Rouse friction coefficient is $\zeta_{Rouse} = N\zeta$. The diffusion coefficient of the Rouse chain is obtained from the Einstein relation by:

$$D_{R(ouse)} = \frac{kT}{\zeta_R} = \frac{kT}{N\zeta}.$$

The polymer diffusion for a distance of the order of magnitude of its own size is given by a characteristic time, the so-called *Rouse time*, τ_R.

$$\tau_R \approx \frac{R^2}{D_R} \approx \frac{R^2}{\frac{\kappa T}{N\zeta}} = \frac{\zeta}{kT} N R^2.$$

This characteristic time has the significance that for time scales shorter than Rouse time, the chain exhibits viscoelastic modes, but for time scales larger than the Rouse time the motion of the chain is simply diffusive.

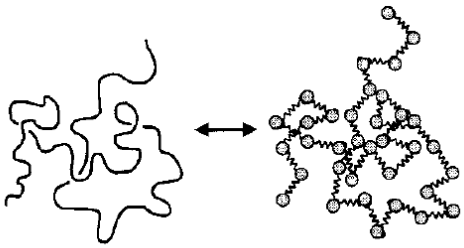

Figure 2. In the Rouse model a chain of N monomers is mapped onto a bead-spring chain of n beads connected by springs. Cartoon taken from Ref[2]

Rouse model successfully describes the polymer dynamics in the melt state, where hydrodynamic interactions are missing. But the fact that it only assumes interactions of the beads through the springs connecting them, yields to failure of the model in a dilute solution. This is not the case in this work, but we think that it is important to discuss the *Zimm model* for completeness, since it is referred in the following chapters. Zimm model include the hydrodynamic interactions of solvent molecules with the monomers of the chain, as well as hydrodynamic interactions between the monomers of a chain. In this case the model assumes that the chain drags with the solvent in its pervaded volume. The chain moves a solid object of size $R \approx bN^{\nu}$. The friction coefficient of the chain of size R being pulled through a solvent of viscosity η_s is given by Stokes law $\eta_{Z(imm)} = \eta_s R$. There is a coefficient 6π in Stokes law for a spherical object $\zeta = 6\pi\eta_s R$ but chains are 1-D objects so we drop all numerical coefficients.

In this case the chain moves a distance of order of its own size during the Zimm time τ_Z:

$$\tau_Z \approx \frac{R^2}{D_Z} \approx \frac{\eta_s}{kT} R^3 \approx \frac{\eta_s b^3}{kT} N^{3\nu} \approx \tau_0 N^{3\nu}.$$

τ_0 is the monomer relaxation time.

Polymers are self-similar objects exhibiting dynamic self-similarity, meaning that smaller sections of a chain with *n* monomers relax just like a whole chain that has *n* monomers. We can thus describe the relaxation of an unentagled chain using *N* different relaxation modes. The *p*th mode consists of *N/p* monomers and involves relaxation on the scale of chain sections with *N/p* monomers, the relaxation time of the p*th* mode has a similar form to the longest mode:

$$\tau_p \approx \tau_0 \left(\frac{N}{p}\right)^2 \text{ for } p=1, 2, \ldots, \text{N}.$$

The mode with index *p* breaks the chain into *p* sections of *N/p* monomers, and each of these relax as independent chains of *N/p* monomers on the time scale τ_p. At time τ_p segments with index higher than *p* have mostly relaxed, but modes with index lower than *p* have not relaxed yet.

Each unrelaxed mode contributes energy of order of *kT* to the stress relaxation modulus. The stress relaxation modulus after a strep deformation at time $t = \tau_p$ is proportional to the thermal energy *kT* and the number density of sections with *N/p* monomers, $\varphi/(b^3 N/p)$:

$$G(\tau_p) \approx \frac{kT}{b^3}\frac{\varphi}{N}p.$$

Also, the time dependence of the mode index *p* for the mode that relaxes at time $t = \tau_p$ is:

$$p \approx \left(\frac{\tau_p}{\tau_0}\right)^{-1/2} N$$

The relaxation modulus for Rouse modes can be given by:

$$G(t) \approx \frac{kT}{b^3}\varphi\left(\frac{t}{\tau_0}\right)^{-1/2} \quad for\ \tau_0 < t < \tau_P$$

$$and,\ G(t) \approx \frac{kT}{b^3}\varphi\left(\frac{t}{\tau_0}\right)^{-1/2} \exp\left(-\frac{t}{\tau_R}\right)\ for\ t > \tau_0.$$

Calculations for oscillatory shear leads to the storage and loss moduli that scale as:

$$G'(\omega) \cong G''(\omega) \sim \omega^{1/2} \text{ for } 1/\tau_R \ll \omega \ll 1/\tau_0.$$

For high frequencies $\omega > 1/\tau_0$ there are no relaxation modes in the Rouse model. The storage modulus becomes independent of ω, and equal to the short time stress relaxation modulus, which is *kT* per monomer. At low frequencies $\omega < 1/\tau_R$ (large time), the storage modulus is proportional to the square of ω and the loss modulus is proportional to the ω, as is the case for the terminal response of any viscoelastic liquid.

1.2 Dynamics of entangled polymers

The dynamical behavior of unentangled polymers was successfully described by the Rouse model in the melt state and Zimm model for dilute solutions. When the molecular weight and thus the size of a chain increases beyond a critical threshold the chain cannot any more diffuse a length of order of its own size due to constraints imposed by its surrounding neighbors. This is the entanglement state.

The dynamical behavior of entangled polymer melts was long the subject of various qualitatively unsuccessful theories until Edwards[3] introduced the idea that each chain is effectively confined to a tube around its coarse-grained or "primitive path",

subsequently developed into a systematic theory of linear polymer rheology by Doi and Edwards. A crucial dynamical feature of the tube is that in the absence of permanent cross-links, the chain is free to move along it: this mechanism was termed reptation by de Gennes in applying the idea to chains diffusing through networks[4]. The original Doi-Edwards model[5] assumed that the confined chain had, in effect, all the dynamical attributes of a Rouse chain in one dimension.

The tube mode represents these entanglements as an effective tube, where the chain is confined. The confinement length, i.e., the so-called tube diameter a, is a parameter of the model and represents the end-to-end distance of a chain of molecular weight identical to the entanglement mass M_e. The tube theory by pass the finer details of the structure of the confined chain at length scales smaller than a, and replaces the chain by a random walk, called the primitive path, of step length a. The primitive path is interpreted as the shortest path between the chain ends that is compatible with the topological constraints. According to the original tube model, the only available relaxation mechanism for the primitive path is diffusion back and forth along the tube axis. This mechanism is the above mentioned reptation. To resolve important discrepancies between the original model and experiments, refined tube models for linear chains[6–9] incorporate additional relaxation mechanisms of the primitive path, such as contour length fluctuations (CLF) and constraint release (CR).

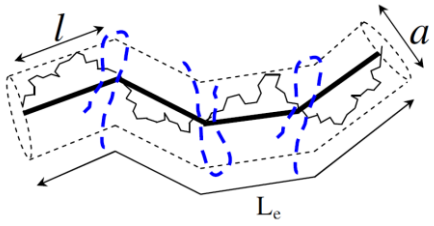

Figure 3. Cartoon of a chain in the tube. Thin line represents the real chain, thick line is the primitive path and dotted line are the entanglements that constrain the diffusion of the chain. Cartoon taken from Ref[10]

Because the experimental dependence observed for zero shear viscosity of entangled polymer melts follows a $M^{3.4}$ scaling[11] rather the anticipated M^3dependence predicted by pure reptation, it is clear that additional relaxation mechanisms besides curvilinear diffusion of the center of mass are required to correctly describe the relaxation of linear chains. Contour length fluctuations (CLF) are the second key ingredient of quantitative tube models. This process is a Rouse relaxation of the chain ends, which does not require the motion of the center of mass, already described by reptation. When the chain contracts within the tube and then stretches out again, the orientation of the ends of the initial tube is forgotten, and the stress associated with those portions is relaxed.

Doi and Edwards assumed that the tube constraining the motion of the test chain is fixed and immobile. The tube itself is able to move according to the motion of the surrounding chains. Tube motions chiefly affect the test chain in two different but related ways. First, “slow” tube motions allow large-scale lateral motions of internal segments, i.e., they induce a constraint release mechanism. Second, when motions of surrounding chains become fast at the observed time scale, the effect is equivalent to an increase of the “effective” tube diameter, which leads to an acceleration of the other relaxation processes (reptation, CLF). This mechanism is called “Dynamic Tube

Dilation" (DTD)[12]. This approach has first been proposed by Marrucci[13]. It is based on the concept that the "effective" tube of constraints around a chain widens as the relaxation proceeds. Indeed, the tube diameter is directly linked to the average distance that a chain can laterally cover without hitting topological constraints by the surroundings molecules. Where these obstacles fixed (i.e., a permanent network), the tube diameter would be a well-defined, time-independent quantity. However, because of the mobility of the surrounding chains, obstacles continuously disappear and reform, some of them more rapidly (near the chain end), others more slowly (far from the chain ends).

Therefore, the test chain will be able to move laterally and explore the surroundings more and more with time. In other words, the tube diameter must be taken as an increasing function of time during relaxation. This increase is calculated by assuming that the relaxed part of the polymer behaves like solvent. Therefore, the effective tube diameter depends on the unrelaxed fraction of the polymer, $\Phi(t)$ as:

$$G(t) = \frac{\rho RT}{M_e(t)^2}\Phi(t) = G_n^0\Phi(t)^{1+a}$$

The exponent *a* is the *dilution exponent* and takes values between 1 and 4/3[14].

1.3 Dynamics of entangled star polymers

All the discussion above was limited to linear chains. The molecular architecture of polymers, in our case star vs linear significantly alters the polymer dynamics. The reptation model described earlier and the modifications mentioned cannot be used in the case of star-shaped polymers. For a star with *f* arms, each arm should drag *f-1* arms along the tube of a single arm, significantly reducing the entropy of the star polymer. Therefore, the branch point of a star (core) is located in one cell of an entanglement net.

Stars relax stress and diffuse by arm retraction, which is large and thus entropically unfavorable fluctuations of the tube lengths of their arms. The easiest way for a star to relax its arms without crossing the arms from other stars is by retraction. Arm retraction reduces the length of the primitive path, by creating loops. The conformations with primitive path reduced by more than root-mean-square fluctuation *R* from its equilibrium length are exponentially unfavorable.

We can analyze the arm retraction as a thermally activated process with a potential $U(s) = F(L_a)$. Here L_a is the arm length and the distance of retraction is $s = \langle L_a\rangle - L_a$. Such a potential can be described as a parabola:

$$U(s) \approx \frac{\gamma kT}{2}\frac{(L_a - \langle L_a\rangle)^2}{N_a b^2} \approx \frac{\gamma kT}{2}\frac{s^2}{N_a b^2}.$$

The number of Kuhn monomers in each arm of the star is N_a and the effective spring constant of this harmonic potential is γ. The most probable length of the arm L_a is close to its equilibrium value $\langle L_a\rangle$ with small fluctuations from it corresponding to a potential change of order of the thermal energy kT. From time to time, there are large atypical fluctuations of the tube length that are exponentially unfavorable, since the number of conformations that allow this state is restricted.

The probability that the tube length will be reduced by *s* can be estimated by:

$$p(s) \sim exp\left(-\frac{U(s)}{kT}\right) \sim exp\left(-\frac{\gamma}{2}\frac{s^2}{N_a b^2}\right).$$

Then the average time between these large fluctuations *τ(s)* is inversely proportional to their probability *p(s)*.

The relaxation time of a star in an ocean of topological constrains is equal to the time it takes to completely retract its arms, which depends on the number of entanglements per arm:

$$\tau_{arm} = \tau(\langle L \rangle) \sim \left(\frac{N_a}{N_e}\right)^{5/2} exp\left(\frac{\gamma'}{2}\frac{\langle L \rangle^2}{N_a b^2}\right) \sim \left(\frac{N_a}{N_e}\right)^{5/2} exp\left(\frac{\gamma'}{2}\frac{N_a}{N_e}\right).$$

It is important here to make clear that the relaxation time of a star grows exponentially with the number of entanglements N_a/N_e per arm but it is independent of the number of arms *f* in the star. The coefficient in the exponential is weakly dependent on the relative amount of arm retraction $s/\langle L \rangle$, changing from γ at small retractions to γ' at full retraction, because the harmonic potential is only an approximation of the real potential.

The stress relaxation modulus is proportional to the average fraction of entanglements per arm that have not relaxed by having the free end of the arm visiting that tube section. If *s* is the length of the tube that has been retracted and relaxed during time $t=\tau(s)$ then the stress relaxation modulus at time *t* is:

$$G(t) \approx G_e \frac{\langle L_a \rangle - s}{L_a} \text{ for } \tau_e < t < \tau_{arm},$$

where G_e is the plateau modulus. The stress relaxation modulus of a star polymer has a time dependence similar to that of a linear polymer with molar mass $2\,M_a$ (the span molar mass of the star polymer) for times shorter than the Rouse time of the span. At the terminal time τ_{arm} there is of order one unrelaxed entanglement left per arm and the stress relaxation modulus is lower than the plateau modulus by the number of entanglements per arm:

$$G(\tau_{arm}) \approx \frac{N_e}{N_a} G_e.$$

The viscosity of entangled stars can be estimated as the product of the relaxation time and the terminal modulus:

$$\eta \approx G(\tau_{arm})\tau_{arm} \sim \left(\frac{N_a}{N_e}\right)^{3/2} exp\left(\frac{\gamma'}{2}\frac{N_a}{N_e}\right).$$

The main feature is the exponential growth of the viscosity with the number of entanglements per arm N_a/N_e. Another interesting feature of the viscosity of entangled stars is that it is independent of the number of arms *f*.

Finally, the diffusion coefficient $D \approx R^2/\tau$ of a linear polymer is the movement of the chain by a distance of order of its own size during their relaxation time. However, the diffusion of entangled stars is different because at the time scale of successful arm retraction, the branch point can only randomly hop between neighboring entanglement

cells by a distance of order one tube diameter a. For this, diffusion of an entangled star is much slower than the diffusion of a linear polymer with the same member of monomers:

$$D \approx \frac{a^2}{\tau_{arm}} \sim \left(\frac{N_a}{N_e}\right)^{-5/2} exp\left(-\frac{\gamma'}{2}\frac{N_a}{N_e}\right).$$

The main feature of the diffusion coefficient of stars is its exponential dependence on the number of entanglements per arm N_a/N_e related to the arm retraction time τ_{arm}.

1.4 Star polymers as soft colloids. Bringing the gap between polymers and colloids

Colloids are small particles suspended in a solvent. They can be dispersions of one substance in another such as smoke in air, emulsions, paints etc. The particles are of size of 10 nanometers up to few microns. Colloids can also be thought as single materials, such as rubbers reinforced with nanoparticles suspended in a polymeric matrix.

The motion of colloids was first observed by Robert Brown who discovered that small particles suspended in a liquid are in continual random motion. This phenomenon was named after him as Brownian motion and results from the fact that particles small enough gain thermal energy of the order of *kT* from the "bombardment" of the molecules consisting the suspending medium. Their ability to be affected by molecular forces such as Van der Waals interactions, electrostatic interaction and thermal energy gives them extremely interesting properties in terms of organization (liquid crystals, gels) and responsiveness (temperature, pH etc.). Their dynamics are governed by their attempt to find the minimum energy state, by trying to explore all the available conformations. This is not unlike atoms and molecules, except that their bigger size shifts the associated timescales to experimentally accessible values.

Colloids have been thought as representatives of atoms and molecules, due to their bigger size making them good candidates for research. Their size makes them experimentally observable using techniques such as rheology and confocal microscopy. The formation of a wide range of structures such as crystals and glasses bring colloids in the center of thermodynamics. Entropy governs their dynamics leading to phenomena such as depletion, osmotic pressure, free volume interactions and crystallization.

Several experimental techniques have been utilized to study the microstructure and directly relate the molecular characteristics to the material properties. Light-scattering, X-rays scattering, neutrons scattering, optical and electron microscopy and computer simulations have been used to study colloids.

In this work we try to use model systems of star polymers to access their large-scale relaxation mechanisms and how chemistry of the monomers, architecture (linear vs. star) and more specifically functionality (i.e., the number of arms tethered to the same

core) and arm length alter their macroscopic behavior. Their microscopic behavior is related to their short-scale dynamics down to the level of segments and this is why we pay attention also to local dynamics probed mainly by rheology but also using other spectroscopies such as broad band dielectric spectroscopy (in collaboration). The question we try to answer here is *if* and *how* local scale dynamics affect the large-scale relaxation in the case of the simplest branched polymeric systems. Such a study is important to understand the effect of branching in polymers, that may lead to development of materials with designed properties.

In the following, the main experimental tool that we use is rheology, the science of flow of materials under certain deformation. There are different types of rheological measurements such as shear deformation and uniaxial extension. Here we use only shear rheology in the linear viscoelastic regime. Rheology is of particular interest not only for research but also in characterization and quality control. The viscometric parameters of products are important for industries, this is why rheology is one of the most common techniques used in industrial quality control and research and development departments. Some aspects of rheology will be summarized in the next chapter.

We use rheology to link the microscopic properties such as monomeric chemistry and architecture to macroscopic properties such as viscosity and terminal relaxation time. In the following we briefly describe the properties of the materials used in this study, namely star-shaped polymers.

Star polymers are consisted by a core onto which a number of polymer chains are covalently grafted, as described earlier. The main parameters thought when dealing with star polymers are the number of arms (functionality) and the arm length. It has been shown experimentally[15–18] that these parameters largely affect the mechanical response of these materials, but only a quantitative understanding exists. Star polymers have been thought as archetypal for filling the gap between polymers and colloids[19–21]. As Likos et al.[19] showed one can go all the way from polymers to hard colloids when the functionality and arm length are properly selected. Star polymers can swell in the presence of a good solvent to display a soft colloidal suspension, with a conformation in space modeled by Daoud and Cotton[22]. In this model three regimes of concentration have been introduced. The inner near to core melt-like regime, where monomers are stretched, the intermediate unswollen theta-like regime and the outer regime where blobs are swollen and chains from neighboring stars can interpenetrate and interact as in the linear melt case. In the absence of solvent of the melt, stars have to compromise their shape and obey space-filling conditions. They deform and interdigitate when confined giving rise to interesting mechanical properties. The ability to control the functionality and arm length[23–25] of these model systems give to stars the advantage to be best candidates for soft colloids used to link the missing gap between properties of polymeric and colloidal origin[26,27].

Another important class of soft colloids are the microgels[20,28]. These are soft, deformable[29] and penetrable particles with an internal gel-like structure that is swollen by the dispersing solvent. They are interesting soft model materials due to their ability to respond to external stimuli such as temperature[30,31], pH[32], ionic strength[33] etc. The

development of synthetic methods allows to diverge their shape and deformability as well as to control the existence or not of long dangling ends[34].

We will not further refer to the importance of the concentration and phase diagram of colloids since we work only with melts where the concentration is the maximum possible.

Rheology of star polymer melts has been the subject for a large number of studies[15,17,35–41]. It was shown that increasing the functionality, a second relaxation process is necessary for the full relaxation of a star melt. This is attributed to colloidal-like dynamics of the center-of-mass movement, similar to out-of-cage dynamics in hard sphere colloids[42]. Recently the effect of colloidal jamming was investigated[41] for stars of ultra-high functionality where a colloidal plateau that does not relax within the experimentally accessible time was reported. These jammed stars have to overcome an energy potential to diffuse a distance of the order of their own size, but this potential is so high that only local rearrangements are possible. In this study the polymeric nature of the stars was clearly identified, with the presence of the plateau modulus of the linear homopolymer consisting the arms to be successfully reached. For larger times the plateau relax due to disentanglement of the interdigitated arms and the center-of-mass movement is suppressed due to the crowded environment.

Here we further investigate this area of ultra-high functionality stars, but in our case the arms are shorter with their molar mass being lower than the entanglement molecular weight. This feature gives rise to further suppression of the polymeric relaxation dynamics of these materials. Indeed, we found that the clear separation of the polymeric and colloidal plateaus has disappeared and replaced by a unique plateau following the glass rubber transition. Moreover, the plateau modulus in our case is higher than these reported earlier and almost half the plateau modulus of the linear homopolymer, indicating constraints at smaller length scales. The modulus appears unchanged over stars with the same length of unentangled arms but almost three times higher functionality, leading us to the assumption that modulus in this extreme case is dominated by arm length.

Furthermore, the local dynamics of such architectures have never been studied before. In literature no indication of an effect of architecture on local dynamics has been reported, but in this extreme case, architecture is important. The mechanical spectra of these stars revealed differences when shifted at the same temperature distance from glass transition temperature. In the high frequency regime where local dynamics are probed, these model materials exhibit a slowing down of the segmental dynamics. This was first observed with rheology and later confirmed by further experiments with broad band dielectric spectroscopy (BDS). Polybutadiene has only a dipole perpendicular to the polymer backbone, so only local dynamics can be probed. BDS revealed three layers of mobility with the same temperature dependence. The existence of such complicated local dynamics is in agreement this the failure of time-temperature superposition of the isothermal rheological measurements. As the glassy regime is approached from temperatures higher than T_g the existence of more than one relaxation processes with same temperature dependence leads to spectra that do not perfectly overlap in terms of loss tangent factor.

By the other side stars of low and intermediate functionalities have been studied in the past. The majority of studies were made with model systems where the arm length was large enough so entanglements were present. Here we examine the case of stars of unentangled arms and the effect that this feature has in the overall dynamics. The particular chemistry of styrene monomers is highly considered as playing a role. The bulkiness and stiffness of a polystyrene chain alters the configuration of arms near the core where monomers belonging to different arms have to stretch in order to coexist. This phenomenon becomes more and more important as the functionality increases.

We already mentioned the existence of a second colloidal-like plateau in the case of star polymers. In this last case, stars reach the terminal regime but the slopes of the moduli are not those expected for a purely diffusive relaxation. A second relaxation process due to center-of-mass diffusion must be present. An upturn of the storage modulus was found for the lower molar masses and this progressively disappears.

Such measurements are prone to experimental errors due to low signal-to-noise ratio but specific care has been taken to ensure the validity of the data. Two types of deformations have been used here. Small Amplitude Oscillatory Shear was used to access the frequency dependent storage and loss moduli from the glassy regime all the way to the terminal relaxation. Creep experiments is the second type of measurements where a constant stress was applied on the sample near the terminal regime and the induced strain was recorded to yield the creep compliance. The data collected using these two methods were found to be in great agreement, indicating the quality of the measurements.

Finally, we study the local dynamics for these low and intermediate functionality stars. Interestingly we found the existence of a second local relaxation process with the same temperature dependence from analysis of BDS data obtained earlier. This explains the failure of time-temperature superposition observed also for these stars. For some of these stars, Temperature-modulated DSC revealed two T_g's confirming the second local relaxation process.

This thesis is organized as follows:

In Chapter 2 the samples used and the measuring techniques are presented.

In Chapter 3 the data obtained for the large-scale terminal relaxation of all the stars studied here are presented and discussed in detail. Also, the rheology and supportive techniques data obtained on local scale dynamics of low and intermediate functionalities stars are presented and discussed.

In Chapter 4 the rich segmental behavior of the ultra-high functionality stars is presented first as observed in terms of rheology and then the sensitive to local dynamics BDS shed light and the obtained data are briefly presented to understand the physics of relaxation of these macromolecular objects.

1.5 References

(1) M. Doi. *Introduction to Polymer Physics*, Clarendon Press Oxfor.; 1996.
(2) Rubstein, M.; Ralph H. Colby. *Polymer Physics*; 2003.
(3) Edwards, S. F. Statistical Mechanics with Topological Constraints: II. *J. Phys. A: Gen. Phys.* **1968**, *1* (1), 15–28. https://doi.org/10.1088/0305-4470/1/1/303.
(4) Reptation of a Polymer Chain in the Presence of Fixed Obstacles. 9.
(5) Edwards, S. F., D. M. *Theory of Polymer Dynamics*, Oxford Uneversity Press.; Oxford Uneversity Press, 1986.
(6) Graham, R. S.; Likhtman, A. E.; McLeish, T. C. B.; Milner, S. T. Microscopic Theory of Linear, Entangled Polymer Chains under Rapid Deformation Including Chain Stretch and Convective Constraint Release. *Journal of Rheology* **2003**, *47* (5), 1171–1200. https://doi.org/10.1122/1.1595099.
(7) McLeish, T. C. B. Tube Theory of Entangled Polymer Dynamics. *Advances in Physics* **2002**, *51* (6), 1379–1527. https://doi.org/10.1080/00018730210153216.
(8) Read, D. J. Convective Constraint Release with Chain Stretch: Solution of the Rouse-Tube Model in the Limit of Infinite Tubes. *Journal of Rheology* **2004**, *48* (2), 349–377. https://doi.org/10.1122/1.1645515.
(9) Milner, S. T.; McLeish, T. C. B. Reptation and Contour-Length Fluctuations in Melts of Linear Polymers. *Phys. Rev. Lett.* **1998**, *81* (3), 725–728. https://doi.org/10.1103/PhysRevLett.81.725.
(10) van Ruymbeke, E.; Keunings, R.; Bailly, C. Prediction of Linear Viscoelastic Properties for Polydisperse Mixtures of Entangled Star and Linear Polymers: Modified Tube-Based Model and Comparison with Experimental Results. *Journal of Non-Newtonian Fluid Mechanics* **2005**, *128* (1), 7–22. https://doi.org/10.1016/j.jnnfm.2005.01.006.
(11) Colby, R. H.; Fetters, L. J.; Graessley, W. W. The Melt Viscosity-Molecular Weight Relationship for Linear Polymers. *Macromolecules* **1987**, *20* (9), 2226–2237. https://doi.org/10.1021/ma00175a030.
(12) Ball, R. C.; McLeish, T. C. B. Dynamic Dilution and the Viscosity of Star-Polymer Melts. *Macromolecules* **1989**, *22* (4), 1911–1913. https://doi.org/10.1021/ma00194a066.
(13) Marrucci, G. Relaxation by Reptation and Tube Enlargement: A Model for Polydisperse Polymers. *J. Polym. Sci. Polym. Phys. Ed.* **1985**, *23* (1), 159–177. https://doi.org/10.1002/pol.1985.180230115.
(14) Gold, B. J.; Pyckhout-Hintzen, W.; Wischnewski, A.; Radulescu, A.; Monkenbusch, M.; Allgaier, J.; Hoffmann, I.; Parisi, D.; Vlassopoulos, D.; Richter, D. Direct Assessment of Tube Dilation in Entangled Polymers. *Phys. Rev. Lett.* **2019**, *122* (8), 088001. https://doi.org/10.1103/PhysRevLett.122.088001.
(15) Vlassopoulos, D.; Pakula, T.; Fytas, G.; Roovers, J.; Karatasos, K.; Hadjichristidis, N. Ordering and Viscoelastic Relaxation in Multiarm Star Polymer Melts. *Europhys. Lett.* **1997**, *39* (6), 617–622. https://doi.org/10.1209/epl/i1997-00403-3.
(16) Pakula, T. Static and Dynamic Properties of Computer Simulated Melts of Multiarm Polymer Stars. *Computational and Theoretical Polymer Science* **1998**, *8* (1–2), 21–30. https://doi.org/10.1016/S1089-3156(98)00003-8.

(17) Pakula, T.; Vlassopoulos, D.; Fytas, G.; Roovers, J. Structure and Dynamics of Melts of Multiarm Polymer Stars. *Macromolecules* **1998**, *31* (25), 8931–8940. https://doi.org/10.1021/ma981043r.
(18) Kapnistos, M.; Semenov, A. N.; Vlassopoulos, D.; Roovers, J. Viscoelastic Response of Hyperstar Polymers in the Linear Regime. *The Journal of Chemical Physics* **1999**, *111* (4), 1753–1759. https://doi.org/10.1063/1.479436.
(19) Likos, C. N.; Löwen, H.; Watzlawek, M.; Abbas, B.; Jucknischke, O.; Allgaier, J.; Richter, D. Star Polymers Viewed as Ultrasoft Colloidal Particles. *Phys. Rev. Lett.* **1998**, *80* (20), 4450–4453. https://doi.org/10.1103/PhysRevLett.80.4450.
(20) Vlassopoulos, D.; Cloitre, M. Tunable Rheology of Dense Soft Deformable Colloids. *Current Opinion in Colloid & Interface Science* **2014**, *19* (6), 561–574. https://doi.org/10.1016/j.cocis.2014.09.007.
(21) Likos, C. N. Effective Interactions in Soft Condensed Matter Physics. *Physics Reports* **2001**, *348* (4–5), 267–439. https://doi.org/10.1016/S0370-1573(00)00141-1.
(22) Daoud, M.; Cotton, J. P. Star Shaped Polymers : A Model for the Conformation and Its Concentration Dependence. *J. Phys. France* **1982**, *43* (3), 531–538. https://doi.org/10.1051/jphys:01982004303053100.
(23) Roovers, J. E. L.; Bywater, S. Preparation and Characterization of Four-Branched Star Polystyrene. *Macromolecules* **1972**, *5* (4), 384–388. https://doi.org/10.1021/ma60028a010.
(24) Hirao, A.; Hayashi, M.; Tokuda, Y.; Haraguchi, N.; Higashihara, T.; Ryu, S. W. Precise Synthesis of Regular and Asymmetric Star Polymers and Densely Branched Polymers with Starlike Structures by Means of Living Anionic Polymerization. *Polym J* **2002**, *34* (9), 633–658. https://doi.org/10.1295/polymj.34.633.
(25) Hirao, A.; Inoue, K.; Higashihara, T.; Hayashi, M. Successive Synthesis of Well-Defined Star-Branched Polymers by Iterative Methodology Based on Living Anionic Polymerization. *Polym J* **2008**, *40* (10), 923–941. https://doi.org/10.1295/polymj.PJ2008064.
(26) Roovers, J.; Zhou, L. L.; Toporowski, P. M.; van der Zwan, M.; Iatrou, H.; Hadjichristidis, N. Regular Star Polymers with 64 and 128 Arms. Models for Polymeric Micelles. *Macromolecules* **1993**, *26* (16), 4324–4331. https://doi.org/10.1021/ma00068a039.
(27) Vlassopoulos, D.; Cloitre, M. Bridging the Gap between Hard and Soft Colloids. *Soft Matter* **2012**, *8* (15), 4010. https://doi.org/10.1039/c2sm90031a.
(28) Karg, M.; Pich, A.; Hellweg, T.; Hoare, T.; Lyon, L. A.; Crassous, J. J.; Suzuki, D.; Gumerov, R. A.; Schneider, S.; Potemkin, Igor. I.; Richtering, W. Nanogels and Microgels: From Model Colloids to Applications, Recent Developments, and Future Trends. *Langmuir* **2019**, *35* (19), 6231–6255. https://doi.org/10.1021/acs.langmuir.8b04304.
(29) Conley, G. M.; Aebischer, P.; Nöjd, S.; Schurtenberger, P.; Scheffold, F. Jamming and Overpacking Fuzzy Microgels: Deformation, Interpenetration, and Compression. *SCIENCE ADVANCES* **2017**, 8.
(30) Pelton, R. Temperature-Sensitive Aqueous Microgels. *Advances in Colloid and Interface Science* **2000**, *85* (1), 1–33. https://doi.org/10.1016/S0001-8686(99)00023-8.
(31) Berndt, I.; Richtering, W. Doubly Temperature Sensitive Core-Shell Microgels. **2003**, *36* (23), 6.

(32) Ngai, T.; Behrens, S. H.; Auweter, H. Novel Emulsions Stabilized by PH and Temperature Sensitive Microgels. *Chem. Commun.* **2005**, No. 3, 331. https://doi.org/10.1039/b412330a.
(33) Snowden, M. J.; Chowdhry, B. Z.; Vincent, B.; Morris, G. E. Colloidal Copolymer Microgels of N-Isopropylacrylamide and Acrylic Acid: PH, Ionic Strength and Temperature Effects. *Faraday Trans.* **1996**, *92* (24), 5013. https://doi.org/10.1039/ft9969205013.
(34) Witte, J.; Kyrey, T.; Lutzki, J.; Dahl, A. M.; Houston, J.; Radulescu, A.; Pipich, V.; Stingaciu, L.; Kühnhammer, M.; Witt, M. U.; von Klitzing, R.; Holderer, O.; Wellert, S. A Comparison of the Network Structure and Inner Dynamics of Homogeneously and Heterogeneously Crosslinked PNIPAM Microgels with High Crosslinker Content. *Soft Matter* **2019**, *15* (5), 1053–1064. https://doi.org/10.1039/C8SM02141D.
(35) Fytas G., V., D. *From Polymers to Colloids: Engineering the Dynamic Properties of Hairy Particles*; Springer, 2009.
(36) Vlassopoulos, D. Colloidal Star Polymers: Models for Studying Dynamically Arrested States in Soft Matter. *J. Polym. Sci. B Polym. Phys.* **2004**, *42* (16), 2931–2941. https://doi.org/10.1002/polb.20152.
(37) Erwin, B. M.; Cloitre, M.; Gauthier, M.; Vlassopoulos, D. Dynamics and Rheology of Colloidal Star Polymers. *Soft Matter* **2010**, *6* (12), 2825. https://doi.org/10.1039/b926526k.
(38) Helgeson, M. E.; Wagner, N. J.; Vlassopoulos, D. Viscoelasticity and Shear Melting of Colloidal Star Polymer Glasses. *Journal of Rheology* **2007**, *51* (2), 297–316. https://doi.org/10.1122/1.2433935.
(39) Rogers, S. A.; Erwin, B. M.; Vlassopoulos, D.; Cloitre, M. Oscillatory Yielding of a Colloidal Star Glass. *Journal of Rheology* **2011**, *55* (4), 733–752. https://doi.org/10.1122/1.3579161.
(40) Vlassopoulos, D.; Fytas, G.; Pakula, T.; Roovers, J. Multiarm Star Polymers Dynamics. *J. Phys.: Condens. Matter* **2001**, *13* (41), R855–R876. https://doi.org/10.1088/0953-8984/13/41/202.
(41) Gury, L.; Gauthier, M.; Cloitre, M.; Vlassopoulos, D. Colloidal Jamming in Multiarm Star Polymer Melts. *Macromolecules* **2019**, *52* (12), 4617–4623. https://doi.org/10.1021/acs.macromol.9b00674.
(42) van Megen, W.; Schöpe, H. J. The Cage Effect in Systems of Hard Spheres. *The Journal of Chemical Physics* **2017**, *146* (10), 104503. https://doi.org/10.1063/1.4977523.

Chapter 2

Materials and Methods

2.1 Materials

2.1.1 Low and intermediate functionality polystyrene stars

As mentioned in Chapter 1, we have used star polymers in the melt state of varying functionalities and arm lengths. More specifically, we use three different types of stars and we separate them for clarity based on their functionality, i.e., the number of polymer chains bonded onto the same core. The functionality *f* varies from low (order of 10), to intermediate (order of 100) and finally to ultra-high (order of 1000). For the first two groups it holds that $N_{arm}^2 > f$ and for the ultra-high functionalities stars it holds that $N_{arm}^2 \sim f$ in the case of the star with 1110 arms and $N_{arm}^2 < f$ in the case of the star with 2830 arms.

The low and intermediate functionalities stars were synthesized via anionic polymerization under high vacuum[1–4]. The monomer used here is styrene. Synthesis was performed by the group of Professor George Sakellariou in University of Athens. The chemical characteristics are summarized in the following table. The nomenclature used is as follows: the first part of the name refers to the monomer chemistry, the number after that refers to the functionality *f* and the last part refers to the molar mass of the arm M_{arm}. In this way for example the PS8-3.5k sample is a star of polystyrene with 8 arms and molar mass of the arm 3.5 $kgmol^{-1}$.

Sample	Functionality (f)	M_{arm} ($gmol^{-1}$)	M_{arm}/M_e
PS8-3.5k	8	3500	0.2
PS8-6k	8	6000	0.35
PS8-14k	8	14000	0.8
PS8-55k	8	55000	3.2
PS64-8k	64	8000	0.5
PS64-36k	64	36000	2
PS64-52k	64	52000	3
PS64-140k	64	140000	8.2

Table 1. Chemical characteristics of the polystyrene stars of low (*f*=8) and intermediate (*f*=64) functionality stars.

These samples found to contain same traces of solvents from the synthesis, so for all the samples annealing at high temperature was performed under dynamic vacuum. The samples were weighted and placed into a cylindrical mold. The mold has three parts, the cylindrical part drilled at the center with the desired diameter of the yielded disk used for rheological measurements, a bottom base on which the cylindrical part lies and

finally an external cylindrical supporting piece of metal. The mold was fastened mechanically and put in the vacuum oven at the desired temperature overnight. This ensures the annealing of the sample and also the complete evaporation of any traces of remaining solvents. For the entangled samples at least 24 hours annealing was performed. Then the heating of the oven was turned off and the system was left to equilibrate to the ambient temperature. The mold was taken out of the oven and the sample was taken out of the mold in the case of unentangled samples, or further shaping was performed using a heating press under vacuum.

Special treating was needed in the case of the unentangled polystyrene stars samples. These samples are very brittle due to their low molar masses so it was impossible to take them out of the mold without breaking. Initially cold press was tested but when the powder (initial state of samples) was pressed without heating, air was always trapped in the shaped sample, leading to the formation of air bubbles when heated in the convection oven of the rheometer. The method selected for these unentangled samples is the following. We carefully take the sample out of the mold, so two or three pieces were extracted. These pieces were placed on the bottom plate of the rheometer and centered by eye. Then the temperature was increased under nitrogen atmosphere to temperature quite higher than the T_g and the melted sample formed a uniform disc. The upper plate was then carefully brought to the measuring gap. Some tiny arrangement of the sample was done using a spatula and the filling of the gap was ensured optically.

For the entangled samples the standard preparation was used using a heating press under vacuum. The samples were directly shaped at the desired diameter using the corresponding mold.

2.1.2 Ultra-high functionality polybutadiene stars

Details of the synthesis of the ultra-high functionality (*f* of order of 1000) star polymers can be found elsewhere[5]. We think useful to discuss the main points of this advanced in complexity synthesis process for completeness. Carbosilane dendrimers substrates with 64 and 128 peripheral groups were used to provide a chemical core for the stars, similarly as in the case of low and intermediate functionality stars. Short polybutadiene chains of 1,2-polybutadiene addition with small average molar mass of *1200 gmol*$^{-1}$ were grafted onto the cores to form star-like hybrids. Then at a second step, the double bonds of the polybutadiene short chains were used as coupling sites for grafting chlorosilane functional groups. The starlike substrates were finally reacted with 1,4-polybutadienyllithium chains of different molecular weights to generate series of high branching functionality dendrimerarborescent polymer hybrids. The following cartoon depict the synthesis of these ultra-high functionality dendrimerarborescent polymer hybrids, referred to as stars throughout all the thesis for simplicity.

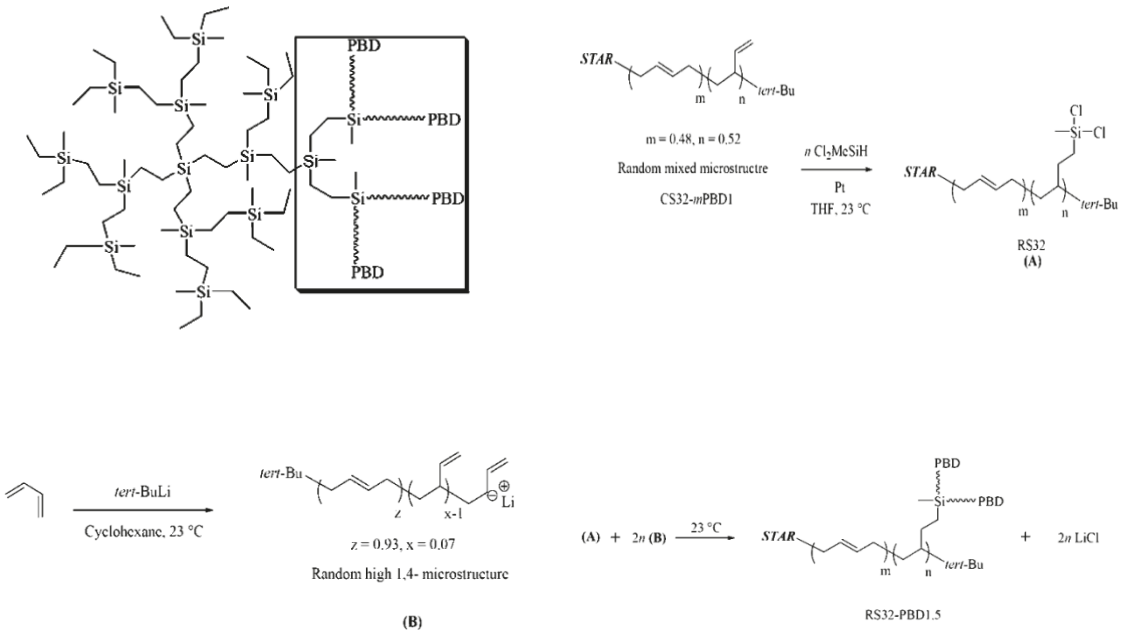

Figure 1. (From top left to bottom right) a. Cartoon of a 16-arms (for clarity) carbosilane dendrimer coupled with short 1,2-polybutadiene, b. addition of random mixed microstructure polybutadiene with hydrosilylation of the vinyl groups of the 1,2-butadiene units, c. addition of the 1,4-polybutadiene chain synthesized independently and d. the final structure of the dendrimerarborescent polymer hybrids.

Here we use two stars with functionalities 1110 and 2830 arms. We will refer to them in the following as PBD1110-1.3k and PBD2830-1.3k, respectively, according to the nomenclature described earlier. The molar mass of the arms is 1.3 $kgmol^{-1}$, lower than the entanglement molecular weight of linear polybutadiene being 1.8 $kgmol^{-1}$. The mechanical spectra of a third star synthesized in the same way were reproduced from Reference[6]. This star has a functionality of 929 arms and the molar mass of the arms is 4 $kgmol^{-1}$.

It is important to clarify that the functionality is not the physical one. The number-average branching functionality f_n was calculated according to:

$$f_n = \frac{(M_n)_{star} - M_c{}'}{(M_n)_{arm}},$$

where $(M_n)_{star}$ represents the absolute number-average molecular weight of the graft polymer (dendrimer-arborescent hybrid), $(M_n)_{arm}$ is the absolute number-average molecular weight of the side chains, and $M_c{}'$ is the molecular weight of the core (substrate). We will refer to this number-average branching functionality f_n as functionality *f* in the following for simplicity.

The polybutadiene stars were stored in glass vials at a lower temperature as close to their glass transition temperature as possible at -67 ℃, to prevent oxidization of the polybutadiene. The samples were taken out of the freezer and left to equilibrate to ambient temperature under vacuum. After this the amount needed for the rheological

measurements was weighted using an analytical scale. A dilute solution of the antioxidant 2,6-di-tert-butyl-p-cresol (>99% purity from Fluka) was prepared and the needed amount of the antioxidant was put in the vial with the sample. Then dichloroethane was used to dissolve fully the stars in order to prepare a low-viscosity solution of the stars. This ensures the complete embodiment of the antioxidant with the stars. Then the solution was left in the protected environment of a hood to evaporate under ambient conditions, and then the complete evaporation of the solvent made sure under vacuum. The evaporation was further confirmed in terms of weighting the melt and compare with the original amount weighted.

In the case of the PBD2830-1.3k sample only few milligrams (less than 30 mg!) were available so all the amount of sample was used. In the case of the PBD1110-1.3k sample only the amount needed for the measurements was prepared as described above, so the rest of the batch is clear of the antioxidant. The sample being melt at room temperature was placed directly on the bottom plate of the rheometer and the upper plate was moved to the measuring gap. Using a spatula, the sample was shaped to fulfil the cylindrical shape needed. Then the gap was decreased by a few microns so the sample was slightly pushed. Then a sharp piece of glass was used to trim the sample and ensure the cylindrical shape.

Sample	Functionality (f)	M_{arm} ($gmol^{-1}$)	M_{arm}/M_e
PBD929-4k	929	4000	2.2
PBD1100-1.3k	1100	1300	0.7
PBD2830-1.3k	2830	1300	0.7

Table 2. Chemical characteristics of the 1,4-polybutadiene stars of ultra-high functionality. The star from Reference[6] is included for completeness.

2.2 Experimental techniques

2.2.1 Rheology

The main technique used in this work in linear rheology. The linear viscoelasticity (LVE) of the samples was measured with two equivalent methods. Small Amplitude Oscillatory Shear (SAOS) was utilized to measure the frequency dependent storage $G'(\omega)$ and loss $G''(\omega)$ moduli. For this reason, two rheometers were employed, a strain-controlled separated motor and transducer ARES rheometer (TA Instruments, USA) equipped with a 2kFRT-N1 torque rebalance transducer. A double headed stress-controlled rheometer MCR702 TwinDrive (AntonPaar, Austria) was also employed especially in the case of the unentangled polystyrene stars due to its better torque resolution. The advantage here is also that creep experiments can be performed without the need of reloading the sample, so experimental errors due to two loadings are minimized. This rheometer is in principle stress-control, but it utilizes an optical encoder to read the position to which the motor has deflected for a certain applied stress,

and then a very fast feedback loop calculates the stress needed to reach the commanded strain and the stress is constantly changing in order to follow the sinusoidal strain profile. This advanced technology allows the rheometer to functionalize both as stress-controlled as well as strain-controlled[7,8] rheometer. Creep experiments were performed using the MCR702 rheometer for the unentangled samples where experiments of few hours were needed. A DSR (TA Instruments, USA) single-headed stress-controlled rheometer was used in the case of the entangled stars where long experiments were needed in order to better manipulate the booking program of the rheometers in the lab. A constant stress within the linear regime was applied to the sample and the strain was recorded in terms of an optical encoder for both rheometers. The creep compliance $J(t)$ was taken from the software of the rheometers and transformed to dynamic moduli using the NLREG software[9–12]. We now briefly discuss the transformation of the creep data into dynamic data.

The software solves nonlinear ill-posed inverse problems using Tikohnov regularization methods. It actually expresses data obtained in the frequency domain into data in the time domain through an integral equation. Since the entire time domain cannot be measured (due to experimental limitations), the conversion is an ill-posed problem, meaning that we cannot get enough experimental information to uniquely calculate the integral. The software uses a nonlinear regularization method to estimate the logarithm of the relaxation time spectrum from the creep data and calculates the equivalent oscillatory elastic and viscous moduli $G'\ and\ G''$. The basic equations used by the algorithm of the software are the following[11]:

The Complex viscoelastic modulus G^* (which is the Fourier transform of the time derivative of $G(t)$), is a simple function of the Fourier-transformed compliance:

$$G^*(\omega) = \frac{1}{i\omega\hat{J}(\omega)}.$$

where $i\omega\hat{J} \equiv J^*$ is sometimes called the dynamic compliance[13]. The problem that arises is due to the fact that the Fourier transform (denoted as $F[...](\omega)$) of the compliance,

$$\hat{J}(\omega) \equiv F[...](\omega) \equiv \int_{-\infty}^{\infty} J(t)e^{-i\omega t}dt.$$

is not a convergent integral, since $J(t)$ grows with increasing time (even for a solid, where $J(t)$ tends to a finite constant at long times, the integral remains undefined).

In oscillatory measurements, the duration of the experiment is many times the inverse of the lowest frequency, because the rheometer needs to perform a few oscillations at this frequency to obtain good signal statistics. Using creep, the lowest measurable frequency is given by the inverse of the duration of the experiment. This is the main advantage of creep measurements. Another important feature of creep measurements is that the torque signal remains constant throughout the experiment, so the dynamic moduli can indirectly be measured even in the viscous terminal relaxation regime, where moduli and so the torque reduce by orders of magnitude. These data were then treated just like the dynamic moduli obtained directly by SAOS to construct the master curves.

Rheology is among the most well-established experimental techniques for studying polymers. Rheological measurements are in general separated into linear and non-linear. Linear are those that the linear viscoelastic regime is probed. This means that the measured rheological quantities are independent of the applied stress or strain. In the other side, non-linear measurements are those that the sample is taken out of its equilibrium by an applied stress or strain that exceeds the linear viscoelastic regime.

In this work we use linear measurements to access the viscoelasticity of the samples under investigation. The time-temperature superposition (tTs) empirical principle introduced by Ferry[13,14] back in the fifties has been proven of excellent importance for experimental study of polymers using rheology. Conventional rheometers cover 4 decades in frequency (in a reasonable experimentally long measurement). The highest frequency accessible in terms of conventional rheometry is of the order of 100 $rads^{-1}$. Older rheometers such as the ARES rheometer used here operates reliably in the frequency regime $10^{-2} \leq \omega \leq 10^{2}\ rads^{-1}$. This is the case also for newer generation rheometers such as the MCR702 proven to be able to reliably measure frequencies as high as 400 $rads^{-1}$, but even this does not change the capabilities significantly. In principle lower frequencies are accessible but the time needed for such low frequencies is more than one day. Non-conventional rheological measurements can be performed by using piezorheometry[15] but even this approach roughly increases the frequency accessible window by two decades. This makes rheology a pure tool compared to other spectroscopic techniques such as broadband dielectric spectroscopy. Despite that the dynamics of polymers are thermally driven by energies of the order of *kT*. This means that we can make the relaxations of polymers faster or slower by changing the measuring temperature, instead of making rheometers to operate at higher of lower frequencies. Increasing the temperature will increase the thermal energy absorbed by polymers making the relaxation processes faster and the vice versa, decreasing the temperature will reduce the thermal energy absorbed by polymers leading to slowing down of the relaxation processes. In this way all the relaxations processes are in principle accessible in terms of rheometry.

The above-mentioned technique of tTs when applicable turn rheology to spectrometric technique. More than 10 decades in frequency are accessible when the sample under investigation is thermorheologically simple. This means that changing the temperature just shift the relaxation times by a single temperature dependent factor. The spectra of dynamic moduli obtained in several isothermal frequency sweeps can be shifted against the spectrum at a reference temperature, to construct a master curve. The frequencies of the spectra obtained at different temperatures need to be shifted in the horizontal frequency axis according to a shift factor. These temperature dependent shift factors can be fitted according to the empirical Williams-Lander-Ferry equation: $loga_T = \frac{-C_1(T-T_{ref})}{C_2+(T-T_{ref})}$. Due to the usually wide temperature window of the measurements the temperature variation of the density of the samples must be taken into consideration according to the $b_T = \frac{\rho(Tref)*Tref}{\rho(T)*T}$, where b_T is a sift factor that multiples the dynamic moduli. In the following Figure 2a, one example of the data obtained at different temperatures are presented without shifting. One can see that these four temperatures nearly capture all the characteristic relaxation processes for this sample (PS64-36k). At

the lowest temperature (data in black) the high frequency glassy regime is captured at the highest frequencies, the transitional regime of Rouse-like dynamics is captured at the lowest frequencies. The data in red represent a higher temperature where the transitional regime is again captured and the dynamic moduli cross each other at the characteristic frequency (or equivalently the time) of relaxation of a Kuhn segment. Then for lower frequencies the plateau is reached which becomes clear at the green data depicting a higher temperature. The plateau modulus of polystyrene of 2.2×10^5 Pa is another typical observation at the minimum of the loss tangent factor ($tan\delta = G'/G''$). Data in blue are obtained for the highest temperature and one can see the third cross-over of the moduli indicating the terminal relaxation modes. Only four temperatures are illustrated here for clarity. In Figure 2b we see the shifted data constructing the master curve. One can see that the moduli do not perfectly overlap. We attribute this to thermorheological complexity originating from the existence of more than one segmental relaxation process as will be discussed further in the next chapter and especially in Chapter 4. Note that in the case of polystyrene only some tiny vertical shifting of the order of 5% is needed to account for the variation of temperature (data shown in the following figure have been not shifted vertically).

More details about the rheological measurements can be found at the part where the data obtained are presented in the following Chapters.

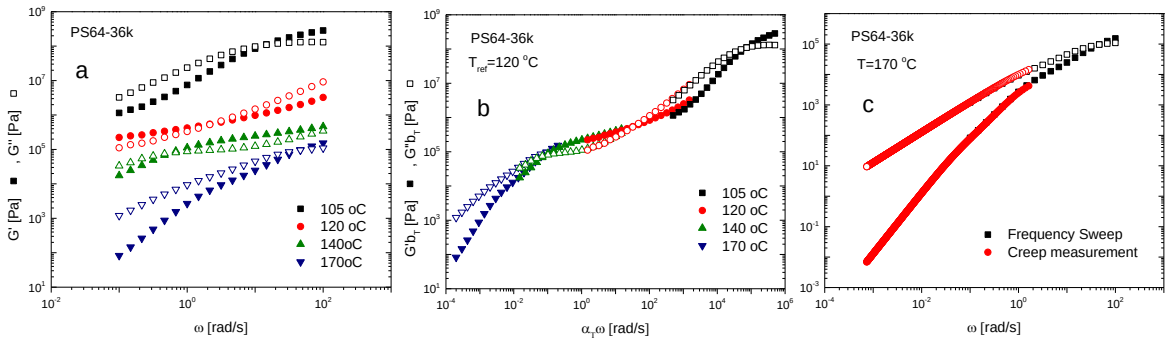

Figure 2a. Frequency sweeps at four selected temperatures, b. Master curve of the data in figure 2a shifted against a reference temperature and c. Dynamic moduli obtained by frequency sweep (black data) and the converted to dynamic moduli data from creep compliance at the same temperature.

In Figure 2b the terminal relaxation of the system could not be accessed in terms of SAOS because the temperature needed to extend the window to lower frequencies would maybe lead to degradation of the sample. To complete the master curve, creep measurements were performed. In the Figure 2c the frequency performed at 170 ℃ is plotted with the data obtained from the transformation of the creep compliance to dynamic moduli.

2.2.2 Temperature-modulated Differential Scanning calorimetry (TM-DSC)

Conventional Differential Scanning Calorimetry (DSC) is the most commonly used technique of thermal analysis. It is based on measuring the flow difference of heat of a sample against a reference sample as a function of temperature when both samples are under the same heating, cooling or isothermal conditions. In the following Figure 3 we can see for instance one of the thermocurves obtained for the PS64-36k sample. Measurements were made using a Q250 calorimeter (TA Instruments, USA). For amorphous samples only the glass transition can be observed in a thermocurve, since no melting or crystallization is possible for non-crystallizing polymers. For all the samples studied here the same protocol was used to determine the glass transition temperature. A small amount of the sample (about 3 mg) was sealed in aluminum pans. The sample was placed in the instrument and heated up to a temperature much higher than the expected T_g and left for 5 minutes. This ensures the erase of thermal history of the sample. Then the sample was cooled down with a constant cooling rate of 10 $℃/minute$ to a temperature lower than the expected T_g and left for 5 minutes to equilibrate. Finally, the sample was heated up with the same constant heating rate as in the cooling. This was done twice to ensure reproducibility. One can see in the inset of Figure 3 the glass transition of the PS64-36k sample as the minimum of the first derivate of the heat flow upon heating.

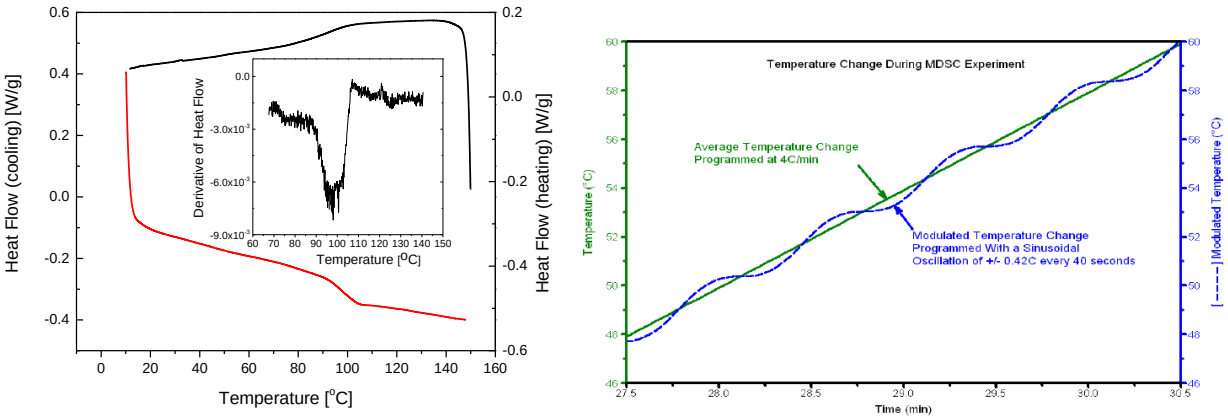

Figure 3 (left) Thermograph of the cooling (black line) and heating (red line) steps during a DSC experiment for the PS64-36k sample. Inset the first derivative of the heat flow upon heating near the glass transition. (Right) The average (green line) and modulated (blue line) temperature change as a function of time in a TM-DSC experiment.

Temperature-modulated DSC (TM-DSC) is a very important technique for studying transitions such as the glass transition[16,17]. It has been also thought as specific heat spectroscopy[18]. The details of handling data obtained with TM-DSC as spectroscopic data can be found elsewhere[19,20]. The difference between conventional and TM-DSC is that on top of the linear temperature profile ($T = T_0 + \beta t$, where β is the heating or

cooling rate) is added a sinusoidally modulated temperature profile according to $T = T_0 + \beta t + B sin\omega t$, where B is the amplitude of the temperature modulation. In other words, the TM-DSC differs from standard DSC in that the TM-DSC uses two simultaneous heating rates, a linear heating rate that provides information similar to standard DSC, and a sinusoidal or modulated heating rate that permits the simultaneous measurement of the sample's heat capacity. Creation of the sinusoidal temperature change requires the operator to select a modulation period (in seconds) and modulation temperature amplitude ($\pm$ ℃) The maximum possible frequency range with this apparatus is between 0.05 and 0.005 Hz (periods between 20-200 seconds) and the maximum amplitude is 1 ℃. The linearity of the amplitude was tested by varying between 0.1, 0.2, 0.5 and 1 ℃, for the higher frequency for each sample. In Figure 3 (right) we can see a temperature profile from a TM-DSC experiment. Figure taken from Reference[21]

In general, the sinusoidal heating rate $\frac{dT}{dt} = \omega B cos\omega t = A_T cos\omega t$, (where A_T is the amplitude of the modulated heating rate) and the sinusoidal heat flow $\frac{dQ}{dt} = A_Q cos\omega t$, (where A_Q is the amplitude of the modulated heat flow) have a phase difference δ based on which the in phase and out of phase components of the heat capacity C_p can be calculated as follows:

$\frac{A_Q}{A_T} cos\delta$=in phase heat capacity

$\frac{A_Q}{A_T} sin\delta$=out of phase heat capacity

In the following we refer to the reversing heat capacity C_p^{rev}, i.e., the real part of the imaginary representation of the complex heat capacity:

$C_p^* = C_p' - iC_p''$, with $C_p' = C_p^{rev} = \frac{A_Q}{A_T} cos\delta$ and $C_p'' = \frac{A_Q}{A_T} sin\delta$.

We use this nomenclature of reversing heat capacity to emphasize to the reversibility of the glass transition, which depends on the heating rate, compared to the non-reversibility of kinetic transitions such as crystallization. Additionally, to the spectrometric advance of the technique, the resolution is sufficiently increased. This is important when more than one processes take place simultaneously such as a glass transition and a melting in a blend, or two glass transitions are very close to each other (as in our case), and this cannot be detected by conventional DSC.

2.2.3 Broadband Dielectric Spectroscopy (BDS)

Dielectric spectroscopy, also known as impedance spectroscopy, measures the dielectric properties of a medium as a function of frequency[22,23]. It is based on the interaction of an external field with the electric dipole moment of the sample, often expressed by permittivity.

It is also an experimental method of characterizing electrochemical systems. This technique measures the impedance of a system over a range of frequencies, and therefore the frequency response of the system, including the energy storage and dissipation properties.

Impedance is the opposition to the flow of alternating current (AC) in a complex system. A passive complex electrical system comprises both energy dissipator (resistor) and energy storage (capacitor) elements. In analogy with rheology one can say that as the storage and loss moduli are measured in rheology as the real and imaginary part of the complex modulus respectively, the real and imaginary parts of the dielectric permittivity $\varepsilon^* = \varepsilon' - i\varepsilon''$ are measured in dielectric spectroscopy. If the system is purely resistive, then the opposition to AC or direct current (DC) is simply resistance.

Polymers display storage and dissipation properties dielectrically, as they display storage and dissipation of energy mechanically, as viscoelasticity. They can be probed either by a step strain where the stress relaxation is recorded as a function of frequency, or they can be equivalently measured by applying an external oscillating electric field that align the dipoles of the polymer and an analyzer probe the relaxation of the aligned dipoles.

The two techniques are sensitive to different physical mechanisms. Unless a component of dipole moment exists to the end-to-end distance in the polymer chain's backbone, BDS can provide information only for local-segmental relaxations. In this study the polymers under investigation, namely polystyrene and polybutadiene have only dipoles perpendicular to their backbones, so only local-segmental relaxation processes can be detected. By the other side, rheology is sensitive to stress relaxation processes, so in principle all the relaxation processes can be detected. This is an advantage of rheology since gives access to relaxation processes from sub T_g relaxations up to terminal viscous relaxations of a polymer. Rheology is not sensitive to processes that overlap or are at the same length scale. This is the case here with the stars under investigation. More than one segmental relaxation processes take place with the same temperature dependence making the rheology pure technique to shed light on them. BDS is not only physically more sensitive to local dynamics, but a wider range of frequencies of the order of 9 decades can be measured at one single temperature, so processes taking place simultaneously, can be nicely mapped. The two techniques together when employed on the same sample, provide complete characterization of the relaxation spectra from length scales of one monomer (beta relaxation) up to terminal relaxation (viscous flow).

Interestingly, rheology is sensitive to the segmental relaxation of a system as it will be clear in the following Chapters, but the complex temperature dependence of more than one local relaxations cannot be detected. This is the reason of the thermorheological complexity shown almost for all the samples studied here, even those of low and intermediate functionality polystyrene stars. Although thermorheological complexity has been reported also for linear polystyrene[24–26], we believe that branching adds an extra complexity to the systems increasing the failure of tTs. This complexity is seen also dielectrically, in the superposition of dielectric loss curves for the ultra-high

functionality stars of polybutadiene. The lack of dielectric spectra for all the polystyrene samples do not allow us to further comment on that.

We will not discuss further technical details of BDS here, but some fundamentals of the fitting process of the dielectric spectra are provided for completeness.

The dielectric relaxation spectra fit to a summation of Havriliak and Negami equations:

$$\varepsilon * (\omega, T) = \varepsilon_{\infty}(T) + \sum_{j=1} \frac{\Delta\varepsilon_j(T)}{[1+(i\omega\tau_{HN,j}(T))^{\alpha_j}]^{\gamma_j}} + \frac{\sigma_0(T)}{i\varepsilon_f\omega}$$

where ε_∞ is the dielectric permittivity at infinite frequency, $\Delta\varepsilon_j$ is the relaxation dielectric strength, $\tau_{HN,j}$ is the H-N characteristic relaxation time, and j is the index of the corresponding relaxation process. At lower frequencies, ε'' rises due to the contribution of the conductivity $\sigma_0/\omega\varepsilon_f$ where σ_0 is the dc conductivity and ε_f is the permittivity of free space. The α_j, γ_j ($0 < \alpha_j$, $\alpha_j\gamma_j \leq 1$) are two shape parameters of the H-N function and describe the symmetrical and antisymmetrical broadening of the distribution of relaxation times.

2.3 References

(1) Hadjichristidis, N.; Iatrou, H.; Pispas, S.; Pitsikalis, M. Anionic Polymerization: High Vacuum Techniques. 24.

(2) Kainthan, R. K.; Muliawan, E. B.; Hatzikiriakos, S. G.; Brooks, D. E. Synthesis, Characterization, and Viscoelastic Properties of High Molecular Weight Hyperbranched Polyglycerols. *Macromolecules* **2006**, *39* (22), 7708–7717. https://doi.org/10.1021/ma0613483.

(3) Roovers, J. E. L.; Bywater, S. Preparation and Characterization of Four-Branched Star Polystyrene. *Macromolecules* **1972**, *5* (4), 384–388. https://doi.org/10.1021/ma60028a010.

(4) Uhrig, D.; Mays, J. W. Experimental Techniques in High-Vacuum Anionic Polymerization. *J. Polym. Sci. A Polym. Chem.* **2005**, *43* (24), 6179–6222. https://doi.org/10.1002/pola.21016.

(5) Gauthier, M.; Munam, A. Synthesis of 1,4-Polybutadiene Dendrimer−Arborescent Polymer Hybrids. *Macromolecules* **2010**, *43* (8), 3672–3681. https://doi.org/10.1021/ma1004056.

(6) Gury, L.; Gauthier, M.; Cloitre, M.; Vlassopoulos, D. Colloidal Jamming in Multiarm Star Polymer Melts. *Macromolecules* **2019**, *52* (12), 4617–4623. https://doi.org/10.1021/acs.macromol.9b00674.

(7) Läuger, J.; Wollny, K.; Huck, S. Direct Strain Oscillation: A New Oscillatory Method Enabling Measurements at Very Small Shear Stresses and Strains. *Rheol Acta* **2002**, *41* (4), 356–361. https://doi.org/10.1007/s00397-002-0231-5.

(8) Läuger, J.; Stettin, H. Differences between Stress and Strain Control in the Non-Linear Behavior of Complex Fluids. *Rheol Acta* **2010**, *49* (9), 909–930. https://doi.org/10.1007/s00397-010-0450-0.

(9) Evans, R. M. L.; Tassieri, M.; Auhl, D.; Waigh, T. A. Direct Conversion of Rheological Compliance Measurements into Storage and Loss Moduli. *Phys. Rev. E* **2009**, *80* (1), 012501. https://doi.org/10.1103/PhysRevE.80.012501.

(10) Kwon, M. K.; Lee, S. H.; Lee, S. G.; Cho, K. S. Direct Conversion of Creep Data to Dynamic Moduli. *Journal of Rheology* **2016**, *60* (6), 1181–1197. https://doi.org/10.1122/1.4961484.

(11) Kim, M.; Bae, J.-E.; Kang, N.; Soo Cho, K. Extraction of Viscoelastic Functions from Creep Data with Ringing. *Journal of Rheology* **2015**, *59* (1), 237–252. https://doi.org/10.1122/1.4904394.

(12) Vyas, B. M.; Orpe, A. V.; Kaushal, M.; Joshi, Y. M. Passive Microrheology in the Effective Time Domain: Analyzing Time Dependent Colloidal Dispersions. *Soft Matter* **2016**, *12* (39), 8167–8176. https://doi.org/10.1039/C6SM00829A.

(13) J. D. Ferry,. *Viscoelastic Properties of Polymers*, 3rd ed.; Wiley, 1980.

(14) Williams, M. L.; Landel, R. F.; Ferry, J. D. The Temperature Dependence of Relaxation Mechanisms in Amorphous Polymers and Other Glass-Forming Liquids. *J. Am. Chem. Soc.* **1955**, *77* (14), 3701–3707. https://doi.org/10.1021/ja01619a008.

(15) Athanasiou, T.; Auernhammer, G. K.; Vlassopoulos, D.; Petekidis, G. A High-Frequency Piezoelectric Rheometer with Validation of the Loss Angle Measuring Loop: Application to Polymer Melts and Colloidal Glasses. *Rheol Acta* **2019**, *58* (9), 619–637. https://doi.org/10.1007/s00397-019-01163-x.

(16) Gracia-Fernández, C. A.; Gómez-Barreiro, S.; López-Beceiro, J.; Tarrío Saavedra, J.; Naya, S.; Artiaga, R. Comparative Study of the Dynamic Glass

Transition Temperature by DMA and TMDSC. *Polymer Testing* **2010**, *29* (8), 1002–1006. https://doi.org/10.1016/j.polymertesting.2010.09.005.
(17) Hensel, A.; Dobbertin, J.; Schawe, J. E. K.; Boller, A.; Schick, C. Temperature Modulated Calorimetry and Dielectric Spectroscopy in the Glass Transition Region of Polymers. *Journal of Thermal Analysis* **1996**, *46* (3–4), 935–954. https://doi.org/10.1007/BF01983612.
(18) Carpentier, L.; Bustin, O.; Descamps, M. Temperature-Modulated Differential Scanning Calorimetry as a Specific Heat Spectroscopy. *J. Phys. D: Appl. Phys.* **2002**, *35* (4), 402–408. https://doi.org/10.1088/0022-3727/35/4/317.
(19) Andreas Boller, B. W.; Yimin Jin. Mathematical Description of Differential Scanning Calorimetry Based on Periodic Temperature Modulation. *Thermochimica Acta* **1994**, *238*, 277–293.
(20) Simon, S. L. Temperature-Modulated Differential Scanning Calorimetry: Theory and Application. *Thermochimica Acta* **2001**, *374* (1), 55–71. https://doi.org/10.1016/S0040-6031(01)00493-2.
(21) Leonard C. Thomas. Modulated DSC® Paper #1 Why Modulated DSC®? ; An Overview and Summary of Advantages and Disadvantages Relative to Traditional DSC. TA Instruments 2005.
(22) Kremer F., Schonhals A., Luck W. *Broadband Dielectric Spectroscopy.*; pringer-Verlag, 2002.
(23) Volkov, A. A.; Prokhorov, A. S. Broadband Dielectric Spectroscopy of Solids. *Radiophysics and Quantum Electronics* **2003**, *46* (8/9), 657–665. https://doi.org/10.1023/B:RAQE.0000024994.15881.c9.
(24) Plazek, D. J.; Schlosser, E.; Schönhals, A.; Ngai, K. L. Breakdown of the Rouse Model for Polymers near the Glass Transition Temperature. *The Journal of Chemical Physics* **1993**, *98* (8), 6488–6491. https://doi.org/10.1063/1.464788.
(25) Santangelo, P. G.; Roland, C. M. Molecular Weight Dependence of Fragility in Polystyrene. *Macromolecules* **1998**, *31* (14), 4581–4585. https://doi.org/10.1021/ma971823k.
(26) Inoue, T.; Onogi, T.; Yao, M.-L.; Osaki, K. Viscoelasticity of Low Molecular Weight Polystyrene. Separation of Rubbery and Glassy Components. *Journal of Polymer Science: Part B: Polymer Physics* **1999**, *37* (389–397), 9.

Chapter 3

Caging and jamming of star polymers of varying functionality and arm length. Consequences on local scale dynamics

3.1 Introduction

The nature of star polymers to display hybrid behavior between polymers and colloids originates from their architecture. Synthetic techniques allow the design and synthesis of star polymers of varying molecular characteristics such as monomer chemistry, functionality and length of the arm. The tunable softness[1] of these macromolecular objects strongly alter their macroscopic properties, such as elasticity and flow behavior. Likos et al.[2] showed that increasing the number of arms that are tethered to a common core, gradually switch from the unbranched polymer chain to hard sphere. Star polymers display a non-uniform monomer density distribution, as described by Daoud and Cotton[3] for solutions. A single star has different regimes of monomer density, due to the fact that for a given number of arms, the monomer concentration in the core region has to be higher because all branches have to join at the center. This means that away the core the density of the monomers decreases, leading eventually to the limit of linear chains for infinitely long arms where excluded volume interactions dominate and arm ends jointed at the same core can be far apart from each other at the outer part of the star. It becomes clear that even for this simplest case of branched polymers, which is the case of one branching point, a variation of local concentration is important. This phenomenon becomes progressively more and more important as the number of arms increases. Synthetic methods allow for extremely high functionalities to be achieved. Ultra-high functionality star polymers (usually referred to as dendrimer-arborescent polymer hybrids) with narrowly distributed molar masses of the arms have been synthesized as described elsewhere[4].The model of blobs[5] originally derived to describe the dynamics of linear polymers can be used to describe the spatial distribution of lengths in a star arm. In this, a part of the arm has locally a single undisturbed chain behavior in a region of size $\xi(r)$. This size increases as the distance from the branching point increases. Overall, three regimes are defined in this model in the case of good solvent conditions. The inner part close to the core, which is melt-like, the intermediate unswollen theta-like regime characterized by ideal blobs that are penetrable from solvent only, and finally the outer, swollen part where blobs are swollen and can interact with other stars via interpenetration. In the absence of solvent in the melt, the mismatch of density and space filling drive the stars to interpenetrate and adjust their shape.

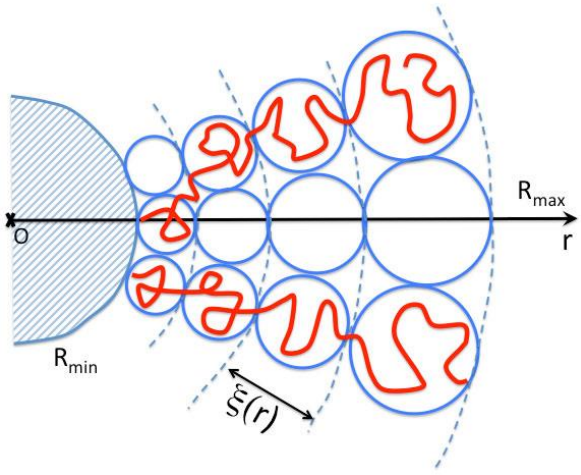

Figure 1. Two-dimensional cartoon of a star within the Daoud and Cotton blob model. The blobs are represented by blue circles with size ξ increasing proportionally to the distance r to the center (Colorized version of the original Daoud and Cotton 1982 drawing.

Star polymers exhibit a rich rheological behavior, with fingerprints of polymers and colloids[6,7]. As the number of arms increases the rheology of these particulate objects changes significantly, in the low frequency regime. A second relaxation process arises in the terminal regime reminiscent of colloidal dynamics[7]. This low frequency, or equivalently long-time response, comes from center of mass rearrangements of the stars, because their cores start to behave cooperatively. This center of mass movement can be thought to obey the dynamics of caging. It is shown that for intermediate functionalities of the order of 10^2 arms, stars order in a liquid-like structure[7], due to the non-uniform monomer density distribution that creates phenomena of macromolecular excluded volume interactions for the cores[8].

In general, stars studied experimentally[9–12] as well as computationally[13,14] obey the condition $N^2 \gg f$, i.e. the number of monomers is much higher than the number of arms. In this case, the mechanical spectra obtained for this type of polymers can be understood considering the following regions of dynamics. At the high frequency regime data reflect local dynamics and are indistinguishable when compared with the high frequency data of the corresponding linear homopolymers, when shifted at same distance from T_g. At intermediate frequencies, a rubbery-like plateau is apparent with a modulus as high as the plateau modulus of the corresponding linear homopolymer. This is a frequency regime where interpenetrated coronas behave as effectively entangled and show dynamics very similar to linear chains. The data at the lowest frequency regime reveal dynamics due the liquid-like ordering of the stars and attributed to a cooperative hoping process akin to cage escape in colloidal glasses[6]. Deviations of this behavior have been observed for the stars with very high functionality and short arms. We will discuss these observations in the last chapter of this thesis in detail. The questions tried to be answered in this study is *if* and *how* extreme functionalities alter the relaxation of star shaped polymers. We will deal here with the case of functionality being comparable to the number of monomers per arm ($N^2 \leq f$).

Data published very recently on star polymer melts with very high functionalities of the order of roughly 10^3 arms[15] ($N^2 \sim f$) reported the absence of terminal relaxation. This dramatic slowing down of the colloidal dynamics indicate a dynamic arrest of this colloidal mode. Interestingly the second plateau found here extends several decades in frequency, indicating that hoping is very slow and in-cage dynamics is the only possible relaxation for these stars. Center-of-mass movements of these particular objects are not favorable due to the energy barrier imposed by the dense packing in the melt. Moreover, the value of the plateau modulus is almost 10 times smaller compared to the entanglement plateau of the linear polymer in this low frequency regime, suggesting large-scale topological constrains. As discussed earlier increasing the functionality leads to the hard sphere limit and one can assume that this is the case for these high functionality stars. For such high functionalities the excluded volume phenomena dramatically slow down their center-of-mass motion resulting in strong caging.

A fundamental question concerns the universality of this behavior and its consequences on the multi-scale dynamics and processing of such materials. So far, the effect is studied only for stars with entangled arms. Also, is the increase of plateau modulus of the center-of-mass relaxation a monotonically increasing function as the functionality increases, and how arm length affects this? Is it possible to reach a colloidal plateau value as high as the entanglement plateau value? In other words, the question to address here is the rheological signature of low functionality stars with short unentangled arms.

Recently the dynamic moduli of low functionality unentangled stars were reported to deviate at the terminal flow regime[16]. The authors mentioned the deviation of the storage modulus from the quadratic frequency dependence, as the frequency becomes smaller. This behavior was also shown in the more sensitive tanδ representation, where a “shoulder” appears before the terminal regime. This behavior was attributed to a new relaxation process that facilitates center-of-mass motion.

To address these questions, we study rheologically two types of stars, namely, stars with very high functionalities of polybutadiene (1,4-addition), PBD, and stars with low or intermediate functionalities, both with short unentangled arms of polystyrene, PS. An interesting distinction between the two chemistries is the bulkiness of the monomer, with PS being bulkier due to the molecular structure of the monomer (see Figure 2). This may have consequences on the local packing near the core. These data complete the picture of universality of jamming in stars. In the second case we study the effect of arm length in the behavior observed, as well.

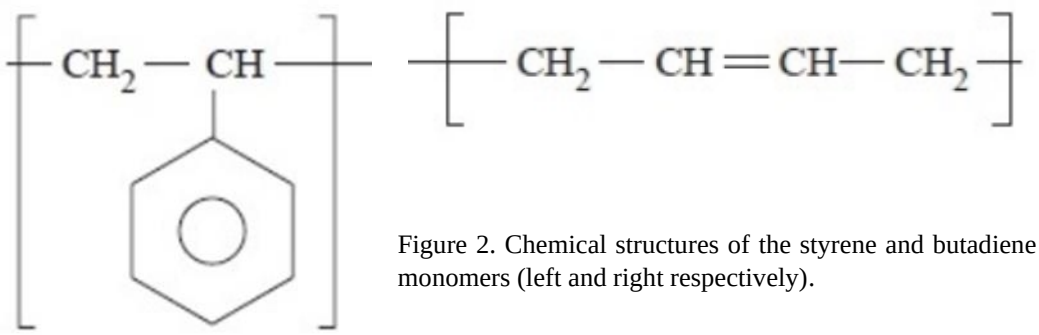

Figure 2. Chemical structures of the styrene and butadiene monomers (left and right respectively).

The systematic rheological study of low functionality stars revealed an upturn of the storage modulus in the terminal flow regime, a rheological behavior never observed before for star polymers. This suggested further investigation for longer arms to elucidate the origin of this peculiarity.

Another question concerns the effect of functionality on this rheological behavior reminiscent of center-of-mass movements. To address this, we used 64-arms stars with molar masses of the arms from unentangled to entangled.

In the following we separate this chapter in two sections. First, we discuss the results on very high functionality stars (($N^2 \leq f$)) with unentangled arms and then we discuss the results on the low (8-arms) to intermediate (64-arms) functionalities stars (($N^2 > f$)) with arms from unentangled to entangled.

More specifically we use a star of 1,4-polybutadiene with functionality comparable to the case studied before[15], namely 1110 arms but here the arm length is reduced by a factor of about 3, with a molar mass of the arm being lower than the entanglement molar mass, M_e of 1.8 kg/mol. We assume that the effect of the core in the large-scale dynamics is roughly the same for theses stars, since according to the Daoud-Cotton model the radius of the core scales as $r_c = bf^{1/2}$, where b is the length of a Kuhn monomer. This means that the radius of the f1110 sample is about 10% larger. The other star studied here has the same chemical composition and molar mass of the arm as the f1110 sample, but a functionality of 2830 arms, i.e. larger by a factor of almost 3. Note that for these stars it holds that ($N^2 \geq f$).

In the second part, we measured the frequency dependent linear viscoelastic moduli for a series of low (8-arms) and intermediate (64-arms) functionalities polystyrene star polymers. These stars have polystyrene arms ($M_e = 17\ kg/mol$) and their molar mass of the arm range from purely unentangled to entangled.

The chemical characteristics for these stars are summarized in the table below:

Sample	Functionality (f)	M_{arm} ($gmol^{-1}$)	M_{arm}/M_e
PBD929-4k	929	4000	2.2
PBD1100-1.3k	1100	1300	0.7
PBD2830-1.3k	2830	1300	0.7

Sample	Functionality (f)	M_{arm} ($gmol^{-1}$)	M_{arm}/M_e
PS8-3.5k	8	3500	0.2
PS8-6k	8	6000	0.35
PS8-14k	8	14000	0.8
PS8-55k	8	55000	3.2
PS64-8k	64	8000	0.5
PS64-36k	64	36000	2
PS64-52k	64	52000	3
PS64-140k	64	140000	8.2

Table 1a. (Top) Chemical characteristics of the high functionality polybutadiene stars. b. (Bottom) Chemical characteristics of the low (f=8) and intermediate (f=64) functionalities polystyrene stars.

In the following we describe the rheological measurements for these two types of stars and present the main findings. We discuss them in three sections for clarity. The first section summarizes the data for the high functionality polybutadiene stars (Table 1a) and the last two sections summarize the data for the low and intermediate functionalities polystyrene stars (Table 1b).

3.2 Results

3.2.1. Stars with very high functionalities and unentangled arms

For the rheological measurements an ARES (TA Instruments, USA) strain-controlled rheometer equipped with a separated motor and a 2kFRTN1 transducer was utilized. Temperature was constant during the experiments with a maximum deviation of 0.1 K. Stainless steel parallel plates (PP) were used to measure the linear viscoelastic properties of the samples. For temperatures near the ambient one, 8 mm parallel plates (PP) were used for the measurements of f1110 sample with a gap of approximately 0.8 mm, whereas 4 mm PP were used for the f2830 sample due to the limited amount of available sample. For the intermediate temperatures, 4 mm PP were used for both samples. The high-frequency regime is not going to be discussed further here, since it is the subject of the last part of this thesis.

Dynamic Frequency Sweep tests were conducted in the range of 0.1 to 100 rad/s. Prior to each test, the linear viscoelastic regime was determined by means of a Dynamic Strain Sweep. Dynamic temperature sweep tests ensured steady conditions for the samples.

Master curves of the storage moduli are shown in figure 3. The Time-Temperature Superposition (tTs) principle[17,18] was applied to obtain the master curves covering nearly 14 decades in frequency and 4 in moduli. A vertical shift was necessary to account for the density variation due to the large temperature window of the measurements. The temperature-dependent density was estimated from ρ(T)=1.04332-5.96426E-4*T [19] and the vertical shift factors were calculated according to $b_T = \frac{\rho(Tref)*Tref}{\rho(T)*T}$. Then, the dynamic moduli were horizontally shifted to obtain the horizontal shift factors (a_T). The later can be fitted with the empirical WLF[18] equation according to $loga_T = \frac{-C_1(T-T_{ref})}{C_2+(T-T_{ref})}$. All curves were shifted at a constant (temperature) distance from the glass transition temperature, such that the reference temperature is given as $T_{ref} = T_g + 13$ K. In the following figure we plot the master curves for the three samples studied here. Note that the measurements for the f929 samples were originally performed by Dr. Leo Gury[15] following the same experimental practices. Some

additional measurements were performed for temperatures near the T_g, with special care in the high frequency glassy regime.

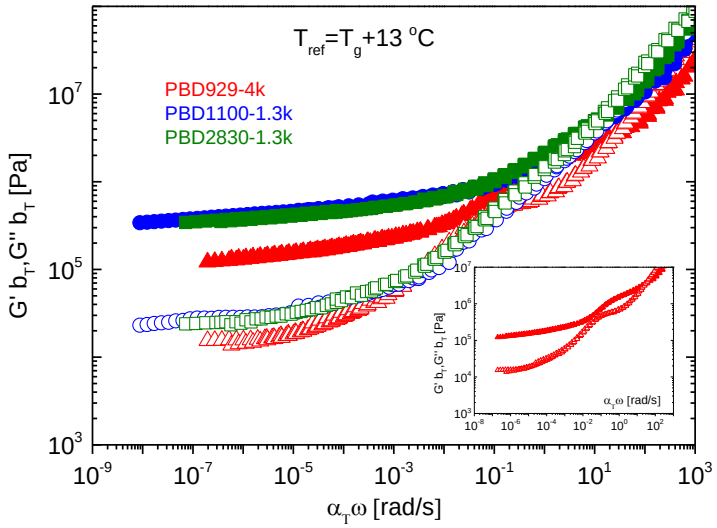

Figure 3. Master curves of storage (filled symbols) and loss (open symbols) moduli for the three stars, shifted at the same temperature distance from T_g. Data for the f929 are reproduced from the publication of Leo et al., for direct comparison. Inset: Master curve of f929 star presented individually plotted for clarity.

First we see the colloidal behavior as expected and found earlier[15]. The colloidal plateau for both stars studied here do not relax in the experimentally accessible frequency window. Additionally, the values of the storage moduli decrease slower compared to the case of f929 star, which appears to decrease in a logarithmic scale. For the stars studied here a more pronounced plateau modulus is detected. This is an interesting finding followed by the magnitude of the plateau modulus, that is roughly half the plateau modulus of the linear homopolymer. One would expect that for a molar mass of the arm close but lower than the entanglement molecular weight of PBD, the modulus at the lowest frequencies should be comparable or even equal to the linear. This is a clear proof that these stars behave as jammed colloidal particles, where the terminal polymeric behavior is suppressed. This is reasonable, in the sense that in the extreme case of tethering a very short polymer chain onto a very dense spherical object, would lead to the hard sphere limit[2].

Another interesting finding is the lack of the well pronounced separation of the polymeric and colloidal modes that ware apparent for the case of the f929 star (see inset of figure 1). For this sample a plateau is present with modulus as high as the one of linear homopolymer. Then the modulus decreases over about two decades in frequency to plateau again to a modulus of about one decade lower. This observation is also apparent in the data representation of tanδ data as function of the frequency, in figure 2. For the f929 sample a local minimum is observed, characteristic of a plateau in the dynamic moduli due to entanglements. The local minimum is replaced by a "shoulder"

at the same frequency regime, indicated by the arrow (about 10^{-1}-10^{1} rad/s) for the unentangled samples studied here. This is another proof of the suppression of the polymeric behavior of the samples, behaving effectively as elastic soft spheres.

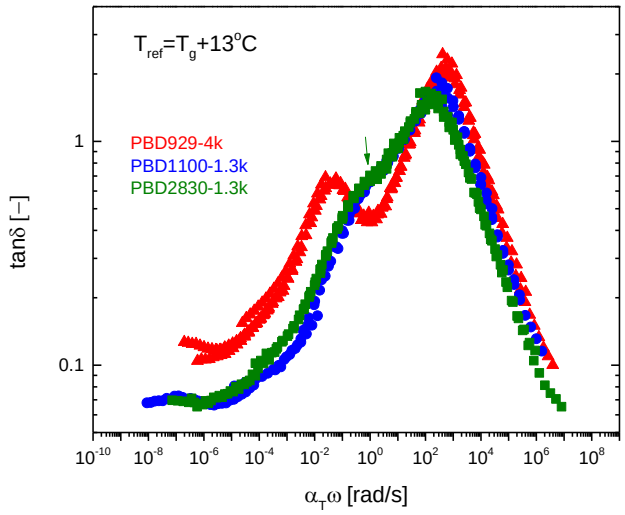

Figure 4. Master curves of tanδ data as function of the frequency for the three stars, shifted at the same temperature distance from T_g.

Storage modulus was found to be more or less the same for both unentangled samples studied here, within the experimental error. Unfortunately, the limited amounts of samples being only few tens of milligrams didn't allow us to use plates of larger diameters to measure with higher accuracy the moduli at the higher temperatures and lower frequencies. Despite that, it is interesting that the stars exhibit the same modulus but with a difference in the number of arms being almost a factor of 3. This is an indication that the plateau modulus is mainly a consequence of the arm length rather than the number of arms. If we directly compare the samples studied here in terms of the colloidal relaxation regime in the lower frequency domain with the other two stars with high functionality and entangled arms presented in Ref 15, we see a clear evolution of the storage modulus increasing upon decreasing the arm length of the arm. The f929 star, with molar mass of arm of 4 kg/mol has a higher colloidal modulus compared to the f875 star, with molar mass of the arm being 5.8 kg/mol, despite the fact that their functionalities are close so the radius of the core being very similar ($r_c \approx \sqrt{f}$), which is attributed to more localized dynamics and stronger caging, because of the reduction of the arm length. Modulus increases as the arm length decreases but remains roughly constant for the same molar mass of the arm even in the case where the functionality becomes 3 times higher. It is likely that a saturated value of the plateau modulus is reached for these dynamically arrested dendrimer-arborescent polymer hybrids.

A dynamic state diagram for star polymers has been proposed in terms of the viscoelastic behavior as a function of the inverse of functionality and number of entanglements[15]. In this data collection literature studies[6,7,20] with stars of varying functionalities and arm lengths the dynamics can be represented to distinguish their viscoelastic behavior into three regimes, namely polymeric, polymeric and colloidal

and last jamming. The key parameters are as already mentioned, the number of entanglements and the inverse of functionality. For the first, the length of the arms has to be small enough so that the core is relatively big and colloidal behavior is observable. In the other side, functionality has to be large enough to increase the effective volume of the core, for the reason described. A significant increase of the functionality leads to increasing the colloidal relaxation time with eventually dynamic arrest of the dense stars. In the following these observations are summarized for the three viscoelastic signatures of star polymers, namely polymeric (arm relaxation), hybrid (polymeric accompanied with colloidal relaxation of center-of-mass motion) and finally jammed (arm relaxation followed by colloidal caging that does not relax with the experimental window).

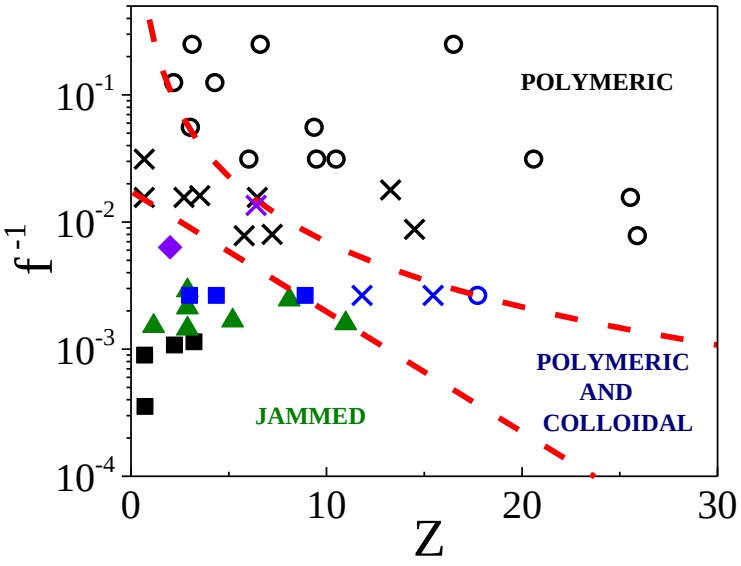

Figure 5. Dynamic state diagram with inverse functionality f-1 (vertical axis) and the number of entanglements Z per grafted chain (horizontal axis). Open circles represent systems whose response is dominated by polymeric arm retraction, cross symbols (X) refer to systems exhibiting hybrid (both polymeric and colloidal) response. Solid squares refer to jammed regime where a clear colloidal mode with extremely long relaxation time, if reached, dominates the mechanical spectra. Blue symbols refer to grafted nanoparticles (data not published yet); black squares refer to the star polymers investigated here and taken from Ref. 15; violet and green symbols are grafted nanoparticles taken from Refs[21–23]. The dashed lines are drawn to guide the eye.

3.2.2 Stars of low functionality and varying molar mass of the arms

We study now stars of low functionality (${N_{arm}}^2 > f$), namely 8 polystyrene arms. In the case of low molar mass arms (below the molar mass of entanglements) these samples are very brittle. Shaping before the rheological measurements is very challenging since molding them in a cylindrical specimen yields to breaking before the extraction from the mold. To overcome this, we use a different preparation protocol to that used for entangled polystyrenes. We put the sample in its initial powder form into a mold consisted of a cylindrical inner part with a concentric hole, a base and a holder. These elements are mechanically fastened together to seal the cylindrical inner part with the base in order to avoid the sample going out of it due to its low viscosity above T_g. Samples are left in a vacuum oven over night at a temperature about 30 degrees above its T_g to anneal and evaporate any traces of remaining solvent from the synthesis. Then heating is turned off and the sample is left to cool down slowly under vacuum. Once the temperature into the vacuum oven is cooled down the sample is removed. The brittleness makes it difficult to remove it without braking. Careful handling allows us to take out the sample in two or three pieces. These pieces are carefully located in the center of the lower moving plate mounted on the motor of the rheometer, which is now much bigger than the upper measuring plate mounted to the transducer. We use this configuration of asymmetric upper and lower plates to better manipulate the pieces of the sample during the loading on the rheometer and also avoid losing the sample during unloading. Once the temperature inside the convection oven goes higher than the T_g, the sample melts and the upper tool is moved gradually to the measuring gap. The surface tension makes the sample to fill the gap, and appropriate pre shear in terms of a large amplitude oscillating shear guarantees the complete fill of the gap.

For the rheological measurements a MCR 702 TwinDrive (Anton Paar, Austria) rheometer was used. Dynamic frequency sweep measurements were performed in a wide temperature range and master curves were obtained by shifting the isothermal data along the frequency axis. A tiny vertical shifting was performed in the case of polystyrene, according to the temperature dependence of the density given by $\rho(T) = 1{,}25 - 6{,}05 * 10^{-4} * (T)$ [19] giving a vertical shift factor of roughly 5% at most. The weak temperature dependence of the density in the case of polystyrene has been reported for a wide range of molar mass samples[24], but here we use this vertical shifting for consistency and completeness.

We see a deviation from the quadratic frequency dependence of the dynamic modulus in the terminal flow regime. While the loss modulus scales as $G'' \propto \omega^1$, the storage modulus scales as $G' \propto \omega^{\sim 1.8}$. Additionally, we observe an upturn of the storage modulus for lower frequencies. For the PS8-3.5k sample, the storage modulus decreases again but data do not expand a decade in the frequency axis, thus we cannot extract the frequency dependence at this regime safely.

These data are sensitive to experimental artifacts. When measuring low magnitudes of moduli of the order of 1 Pa or even smaller, the torque resolution of the measuring apparatus has to be carefully checked. A rheometer working in dynamic (oscillating) mode measures stress, i.e., the magnitude of the complex modulus (G*) as well as the

phase angle between strain and stress signals. Experimentally it is challenging to accurately measure the phase angle between the storage and loss moduli of these samples at the terminal regime where the loss modulus is more than one order of magnitude higher than the storage modulus. The phase angle in this case is close to 90 degrees, so rheometers equipped with transducers built to measure highly elastic samples will not be able to accurately measure small differences in the phase angle far from the purely elastic behavior that is the case here. This is true for the rheometers equipped with torque rebalance transducers. The stiffness of this type of transducers is different for apparatuses suitable for highly elastic or highly viscous samples. To explore the low frequency regime where samples are purely viscous, a rheometer built for viscous samples should be used, but in this case measuring a glass forming liquid is experimentally tricky, since the normal force as well as the torque rebalance transducers are not able to withstand loads produced during loading or unloading the samples. By the other side, transducers built to measure elastic samples are by default calibrated using a nearly purely elastic sample, usually a specimen made by stainless steel. This allows for calibrating efficiently the instrument in the phase angle regime of purely elastic samples, so measurements are mostly favorable in the phase angle regime close to zero degrees, assuming that this is enough for all the values away of the purely viscous behavior limit of 90 degrees. In addition, torque rebalance transducers have a torque resolution of about 4-5 decades, in contrast with the newest technology transducers that have by far larger torque resolution. Finally, another very important aspect of these measurements is the method used by the firmware embedded in the rheometer to define the phase angle between the imposed strain and the acquired stress. Older rheometers use the zero-cross method, the phase angle is defined by the time lag that the stress and strain signals cross the zero within the oscillations performed for each frequency. Noisy signals (see figure below) can lead to considerably large errors in the phase angle measured by a rheometer utilizing this method[25]. Nowadays, rheometers utilize electronics much better, allowing to acquire and analyze larger amounts of data and digitization of the signals accompanied with numerical analyses, allow for reliable measurements[26] of the phase angle even in the case of approaching the 90 degrees limit.

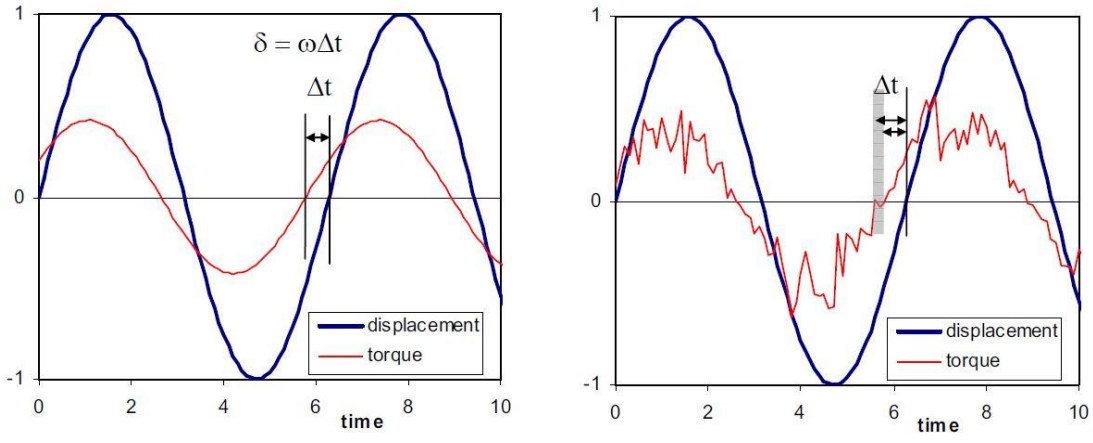

Figure 6. Left) The zero crossing of the sinusoidal displacement and torque signals give the phase lag, from which the phase angle δ can be calculated. Right) If the one or both of the signals are noisy, it will cause some uncertainty in the zero crossing (illustrated by the shaded line), and hence in measuring δ). Figure was reproduced from reference 10.

Indeed, in the case of using a rheometer equipped with a torque rebalance transducer, the data in the regime of the upturn of the storage modulus were noisy (data not shown here). Additionally, the limited resolution does not allow us to explore frequencies low enough. In the case of the MCR 702 rheometer data are more reliable. To further investigate the validity of the data we systematically performed strain sweeps at fixed frequencies. The frequencies selected were same as those measured in the isothermal frequency sweep. We systematically performed this study to validate the existence of the upturn in the storage modulus, for the PS8-3.5k sample. As illustrated in figure 4 at low strains the moduli are scattered, despite the fact that the torque is higher than the theoretical resolution of the instrument. Note also that for some points the phase angle is 90 degrees. These data are below the resolution of the instrument, so the firmware report arbitrarily values for the phase angle as well as the storage modulus. As the strain increases the torque increases as well so the phase angle data become constant and the moduli appear consistent for all the strains within the linear viscoelastic regime. For the largest strains the onset of non-linearity yields to an increase of the phase angle but our data are not affected from this. It is crucial here to discuss the torque resolution of the instrument. In oscillating mode there are two contributions to the torque signal, namely the elastic contribution (storage modulus) and the viscous contribution (loss modulus). Here we care about the elastic contribution since we are interested in the validity of the storage modulus data. One has to be careful since a difference between storage and loss moduli of approximately two orders of magnitude, means that equivalently the elastic contribution of the torque is going to be two orders of magnitude lower than the viscous, respectively. The total torque resolved by the rheometer may be much higher than the lower limit, but the elastic contribution can be lower. In figure 7b the elastic torque is plotted for the data of the strain sweeps plotted in figure 8. One can see that the lower limit of elastic torque resolution is about 10^{-2} μNm. This is the value that we account as the lower limit of torque resolution for our measurements.

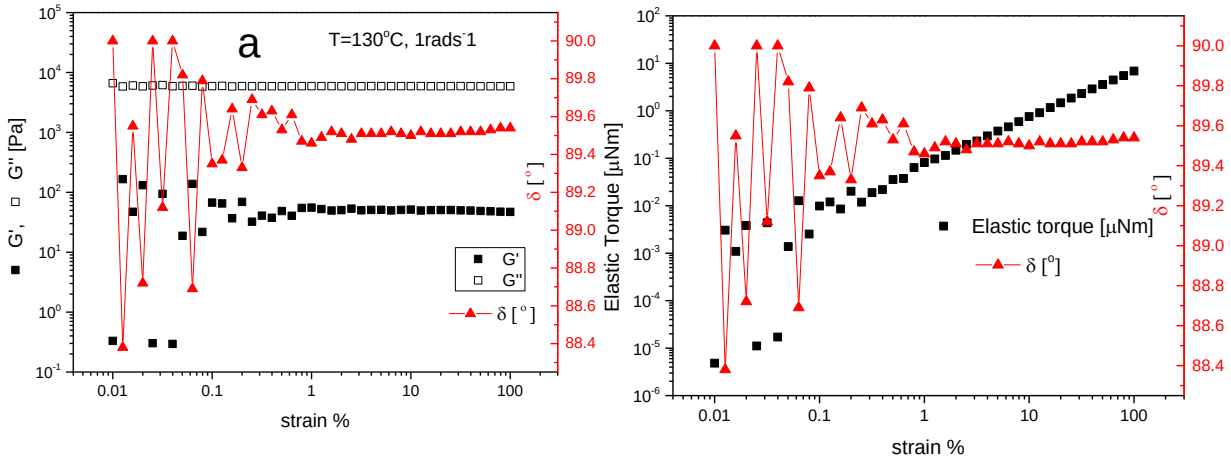

Figure 7. a) Strain sweep performed for a constant frequency for the PS8-3.5k. For low strains phase angle is noisy, yielding to scattered storage modulus values. As the strain increase, the phase angle becomes roughly constant and the storage modulus data become consistent. b) The elastic contribution of total torque measured by the instrument for the phase angles plotted previously in figure 4.

In figure 8 we compare data obtained by conventional frequency sweep and the single frequency strain sweeps. We see excellent agreement between the data obtained with the two experimental procedures. In the insets of figures 8a and 8b we can see that this lower limit of elastic torque is respected, for the data of the conventional frequency sweeps used to construct the master curves. This supports the validity of the data at this low frequency regime, despite the fact that the 90 degrees limit has been reached. Measurements were performed for two temperatures, covering nearly 5 decades in the vertical axis.

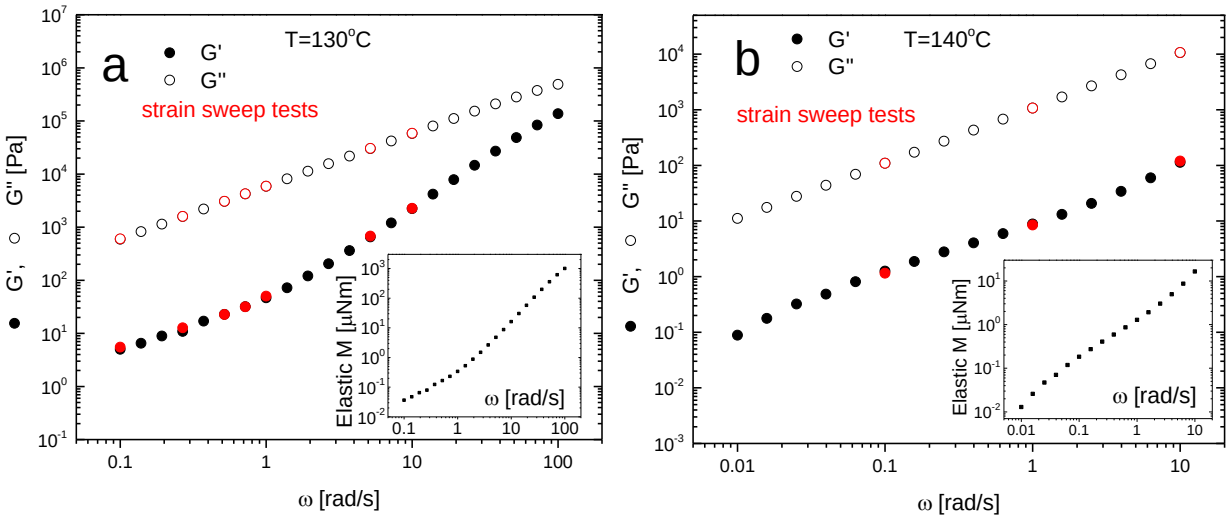

Figure 8. Comparison of the storage and loss moduli of the PS8-3.5k sample obtained by conventional frequency sweep (black data) and strain sweep (red data) tests, for some selected frequencies and temperatures (left 130ºC and right 140 ºC). Insets illustrate the elastic component of the torque for the frequency sweep data used for the construction of the master curves.

In figure 9a the master curve of PS8-3.5k is plotted at a reference temperature of 120 ºC. First, we see that storage modulus remains below loss modulus until the glassy transition, as expected for unentangled polymers. Just before the glassy regime is reached, G' remains below G'' and they both rise in a nearly parallel fashion for more than a decade. In this frequency regime both moduli scale roughly as $G' = G'' \sim \omega^{3/4}$. Such behavior has been observed for hyperbranched polymers of unentangled polystyrene melts[27]. Another study of hyperbranched polymer melts of poly(ε-caprolactone)s, reported the upturn in the storage modulus at the lowest frequencies[28]. Authors in this work attributed this upturn to the slow secondary relaxation mode due to the different molecular mechanisms. Interestingly this behavior was found in the case

of the linear polymer, as well. Solutions of very high molecular weight hyperbranched polyglycerols were studied[29] rheologically and same behavior was found, with the upturn of storage modulus being slightly or highly apparent, depending on the molar mass of the branches. For low molar mass the upturn roughly covers a decade in frequency. For intermediate molar mass the upturn expands almost two decades in frequency. For the highest molar mass, where storage and loss moduli coincide at high frequencies and increase in parallel over more than 3 decades of frequency, a behavior characteristic of gel-like and highly branched structures, the upturn of storage modulus in the lowest frequency regime seems to disappear.

In figure 9a the frequency regime between about 10^0 and 10^2 seems to be the terminal regime for this sample, but G' does not follow the quadratic frequency dependence. A non-purely diffusive relaxation occurs in this frequency regime, followed by the upturn of the G'. For even lower frequencies, G' decreases again, but the limitations in the measurements due to torque resolution has been reached. It is likely that G' eventually reaches the $G' \propto \omega^2$ dependence, but data do not exceed a decade in frequency thus we cannot conclude.

It is important at this point to comment on the time-temperature superposition of the data. When tTs is validated, shifting the data along the frequency axis, allow to construct a master curve where data of isotherms superimpose by a frequency-scaling factor (a_T). The superposition fails as can be seen in the inset of figure 9a, where a discontinuity of the loss tangent factor exists between about 10^1 to 10^3 in the frequency axis. This failure of the superposition has been observed for all the unentangled samples studied here. We believe that this discontinuity originates from the existence of more than one local relaxation process. We will discuss this in more detail in the following.

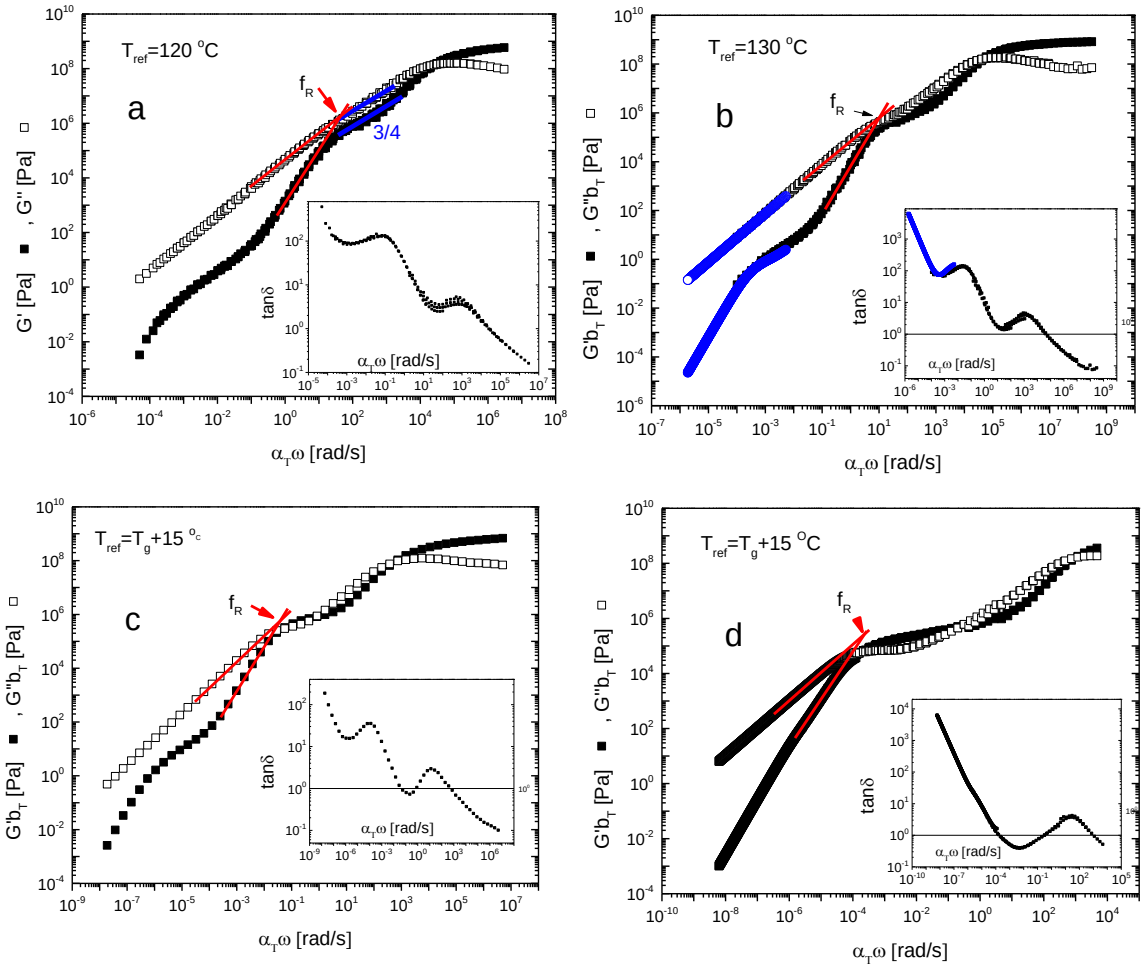

Figure 9. Master curves of storage and loss moduli for the a) PS8-3.5k, b) PS8-6k, c) PS8-14k and d) PS8-55k samples. Insert shifted data of loss tangent (tanδ=G''/G') with the same reference temperature. Red lines are the extrapolations consider to estimate the arm relaxation time as the inverse of the frequency where moduli cross (f_R).

The master curve for the PS8-6k sample is depicted in figure 9b. The glassy regime is carefully measured utilizing 3 mm in diameter stainless steel parallel plates. One can see that G' plateaus reaching a modulus as high as 10^9 Pa. Following the transitional regime, the moduli come close to each other but they do not cross and both decrease indicating the arm relaxation. At sufficiently low frequencies the storage modulus decreases in a slower mode and eventually decrease to reach a quadratic frequency dependence as shown in the blue filled circles (converted data from creep compliance). Here we take advantage to measure the creep compliance of the sample in this terminal regime, since the available amount of sample is a few hundreds of milligrams. The creep compliance data obtained using a single headed stress-controlled rheometer (DSR, TA Instruments, USA), were converted into dynamic moduli using the NLREG program[30,31]. The good agreement between data measured in oscillating and steady deformation modes are representative of the quality of the measurements and the validity of this peculiar behavior. The experimental limitations mentioned above are

not the case for creep experiments. First the torque signal is not decreasing as the measuring frequency decreases (or in this case as time increases), rather maintain constant. This means that once the torque is higher than the minimum able to be measured, the creep compliance can be measured with the same uncertainty for several orders of magnitude. This is very helpful in this case, since in a frequency sweep where the moduli decrease by orders of magnitude the measured torque decreases in the same way. For creep this is not the case. Using a parallel plate of 8 mm in diameter and a gap of approximately 1 mm we obtained the creep compliance data (not shown here) for several stresses, checking for linearity and the average of the creep compliances for at least 3 different stresses over time were converted as described above. An additional advantage of creep measurements is that the phase angle is not directly measured by the rheometer, but rather calculated, so experimental errors described earlier are of minor importance.

Of particular interest is the obtained master curve of the PS8-14k sample depicted in figure 9c. Following the glassy regime, the transitional regime is followed by a frequency regime where moduli cross two times, behavior reminiscent of entanglement plateau. This is also seen in the master curve of loss tangent in the inset of figure 9c, where the tanδ equals to one two times before the moduli cross in the glassy regime, giving the third point. The minimum in tanδ is also a characteristic of rubber elasticity. The modulus in this case is almost three times higher than the plateau modulus of polystyrene (G_N'~$2.2 \times 10^5\ Pa$). This plateau is not due to rubber elasticity since the molar mass of the arm is lower than the critical molecular weight for the creation of entanglements being M_c~$2 \times (M_e = 17\,\frac{kg}{mol})$. This behavior has been attributed to the maximum amount of molecular orientation per unit of stress[32] and has been seen for other branched polymers such as bottle brushes[33,34]. In ref. 33 the rheological behavior of unentangled polystyrene brushes was studied reveling similarities with our data.

To further investigate this plateau formation, we calculated the retardation spectra for all the samples studied here. For this reason, we used the Orchestrator software. First the dynamic compliances (J' and J'') where calculated by the dynamic moduli and then the relaxation spectrum (H(λ)) was the intermediate step for the final transformation to the retardation spectrum (L(τ)). The data shown in Figure 11b.

We discuss now the rheology for a well entangled star with molar mass of the arm of 55kg/mol, named PS8-55k. The master curve is illustrated in Figure 9d. Entangled molar mass of polystyrene is about 17kg/mol, so the arm is about 3 entanglements long. In figure 10 we see the master curve of the dynamic moduli for this sample. In the inset the loss tangent factor data are plotted. As one can see typical behavior of entangled polystyrene is observed. A plateau modulus with value of about $G' = 2.2 \times 10^5$ Pa is reached at the frequency where G'' is minimum. For higher frequencies crossover of the moduli corresponds to the characteristic relaxation of a Kuhn segment and then moduli rapidly increase to reach another crossover in the glassy regime. Of particular interest is the low frequency regime, where loss modulus scales as $G' \propto \omega^1$ but storage modulus scales again as $G' \propto \omega^{1.7}$. The arm relaxation process takes place before the storage modulus reach the quadratic frequency dependence indicating the center-of-mass relaxation for these entangled polystyrene stars. This is also apparent in the tanδ

data representation where tanδ equals to one indicating a crossover of the moduli and the increases with a slope different than -1 for fully diffusive process and reaches the slope of -1 at the lowest frequency regime. Note also that the superposition is much more reasonable (as indicated in the data representation of tanδ versus frequency), compared to the cases of the unentangled samples, presented earlier.

Data presented here strongly support a secondary relaxation mechanism at low frequencies. Earlier studies of branched polymers have not revealed such rheological observations, namely the deviation of the terminal flow regime from the quadratic frequency dependence of storage modulus as well as the upturn of storage modulus, while being lower than the loss modulus. A reasonable question is whether this behavior originates from the architecture, namely the polymer chains tethered to a common core, or this is something coming from the polymeric chain itself. In a study where low molar mass polystyrene samples were investigated rheologically, the failure of the tTs process

was reported for low molar mass polystyrene, below the entanglement threshold[35]. Thermorheological complexity for low molar mass polystyrene has been reported in the literature[36]. To further investigate this, we measured a linear polystyrene sample of a molar mass of 2.5 kg/mol, that we will refer to as PS2.5k, with particular interest in the low frequency regime. For consistency we use here the same experimental protocol used for the stars. Master curve of the moduli in figure 10a are plotted against the data reproduced from ref. 35 for roughly same molar mass sample. Our data are in good agreement with the data published before, and surprisingly an upturn in the storage modulus occurs at the lowest frequencies measured. Harmandaris et al.[37] reported the viscoelastic data of a linear polystyrene sample of molar mass of about 1.9 kg/mol. The lack of superposition can be seen in the spectrum of dynamic moduli where storage modulus appears as scattered data, but authors did not comment on that. Interestingly data of the storage modulus were reported for shorter frequency regime than the one of the loss modulus. This upturn of the storage modulus should be reached but authors did not report it. This is also the case for the data of Ref. 35 plotted in figure 10a.

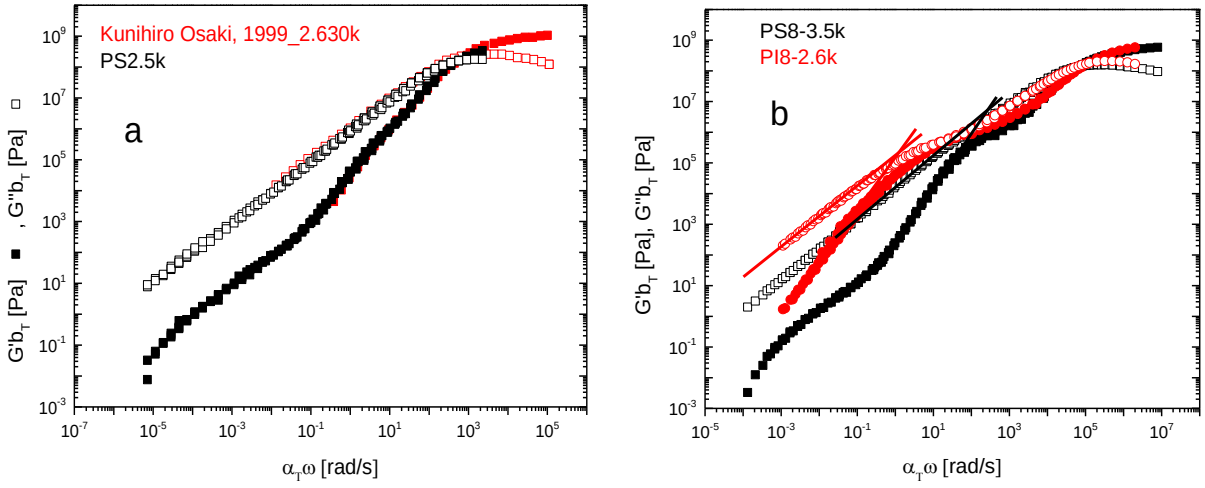

Figure 10a. Master curves of nearly same molar mass polystyrene. Data are arbitrarily shifted because shift factors were not reported for the data reproduced, so a shifting to the same temperature distance from T_g is not possible. b. Master curves of the storage (filled symbols) and loss (empty) moduli for the PI8-2.6k at a reference temperature of -40 °C. Inset: master curve of the tanδ at the same reference temperature.

The existence of this upturn even in the case of the linear polystyrene of low molar mass, has been observed for several samples in our laboratory (not shown here). It is interesting to note that this upturn does not affect the viscosity dependence that scales with the first power of molar mass, as shown in figure 13b.

We now compare the rheological behavior of the star PS8-3.5k and the linear PS2.5k. These samples have different architecture but the arm of the star has molar mass close enough to that of the linear. Starting from the low frequency regime, we see an upturn of the G' for both samples, being always below G'', until the glassy regime. Interestingly we see differences in the regime before the glass transition, where for the case of the star both moduli increase in a parallel fashion with a scaling of $G' = G'' \sim \omega^{3/4}$. One can say that branching of low molar mass polymers on a common core, significantly alters their dynamics, at local scales for short unentangled arms.

Further investigations are needed to shed lights on these interesting findings. Two are the main questions that arise here. What is the critical value of molar mass for the linear polystyrene above which only a purely dissipative relaxation process is taking place? Also, if the upturn observed in the case of the star originates from the chemistry of the repeating unit, is the critical molar mass the same for different architectures, namely linear chains and stars? Finally does chemistry of the monomer play a role? In other words what is the effect of a bulky high T_g monomer of styrene, to the dynamics of a star?

To further investigate the possible effect of the styrene monomer to the dynamics of the star we measured also an 8-arm star of polyisoprene, named PI8-2.6k. The molecular weight of the arm is 2.6 kg/mol. The molar mass of styrene is ~104 g/mol, so the PS8-3.5k star has about ~34 repeating units per arm. For the isoprene the molar mass is ~68 g/mol, yielding to ~38 repeating units per arm. We can then compare the two stars, having reasonably close number of monomers. In this case measurements were much easier since polyisoprene is melted at room temperature. We combine measurements performed with two rheometers. A strain-controlled rheometer with a 2kFRTN1 torque rebalance transducer was utilized to measure the temperatures lower than the ambient (temperature control using liquid nitrogen). The MCR 702 was used to measure the temperatures where torque is weak. The tTs principle allowed us to construct the master curve as described earlier. A vertical shifting was necessary to account for the temperature dependent density given by $\rho(T) = 0{,}9283 - 0{,}61 * 10^{-3} * (T)$ [19]. Note that the superposition breaks for the lower frequencies, at the terminal flow regime. Interestingly the upturn of the storage modulus is not present here, at least at the frequencies where moduli could be reliably measured. For frequencies lower than the glassy regime both moduli increase parallel and their slope is roughly 3/4 for two decades in frequency. For lower frequencies a regime where

moduli almost cross is apparent, despite the fact that the molar mass of the arms is quite lower than the entanglement threshold for polyisoprene, being about 6.8 kg/mol[38]. Then the moduli start decreasing and two regimes can be seen. The first is at frequencies of 0.1 to 1 rad/s (indicated also as a shoulder in the tanδ master curve) and the other where storage modulus decrease with a slope of about 2. The fact that for the case of polyisoprene the upturn of storage modulus does not occur can be explained in terms of the simple chemical structure of the isoprene. In contrast, styrene is a bulky and relatively stiff monomer, so tethering a short polymeric chain of a few monomers onto a common core can alter the center of mass relaxation of the stars in the melt state.

Now we compare the master curves of the two stars having roughly the same number of monomers, namely PS8-3.5k and PI8-2.6k. To do so, we arbitrary shift the master curves to collapse at the glassy regime. We observe in figure 10b the differences for the two stars.

As one can see in figure 10b, when master curves are shifted arbitrarily to collapse to the same high frequency regime, the dynamics appear similar at the regime before the glass and both samples exhibit a frequency regime where both moduli increase parallel with slope of 3/4. Interestingly the terminal flow regime is reached for quite different times. If we extrapolate the moduli in the terminal regime to estimate the terminal relaxation time, this is more than two orders of magnitude slower in the case of the PI8-2.6k sample.

We compared two stars with same functionality and same number of different repeating units, namely polyisoprene and polystyrene. We see that in this case of tethering short arms onto the same core, dynamics are different in the low frequency regime. We attribute this to the difference in the repeating unit. Polyisoprene has a smaller more compact and more symmetric monomeric chemical structure compared to polystyrene[39]. This leads to increased interactions of the flexible isoprene segments in the corona that slows down the terminal relaxation.

Below we present the data in a comprehensive way. Figure 11a compares the data as phase angle (δ) versus complex modulus (G^*), known as Van-Gurp Palmen plot. Note that in this representation data of the isothermal experiments need no shifting. The data for the linear PS2.5k sample are added as well. We also use recently published data[40] of an entangled linear polystyrene sample with molar mass of 185 kg/mol (cyan symbols). We see that despite the architecture varying between linear and low functionality stars, as well as low (unentangled) to high (entangled) molar masses, data in the high modulus regime collapse onto a master curve as expected. This is the corresponding high frequency regime, where local dynamics of the same chemistry monomer are probed. This is another proof of the quality of data.

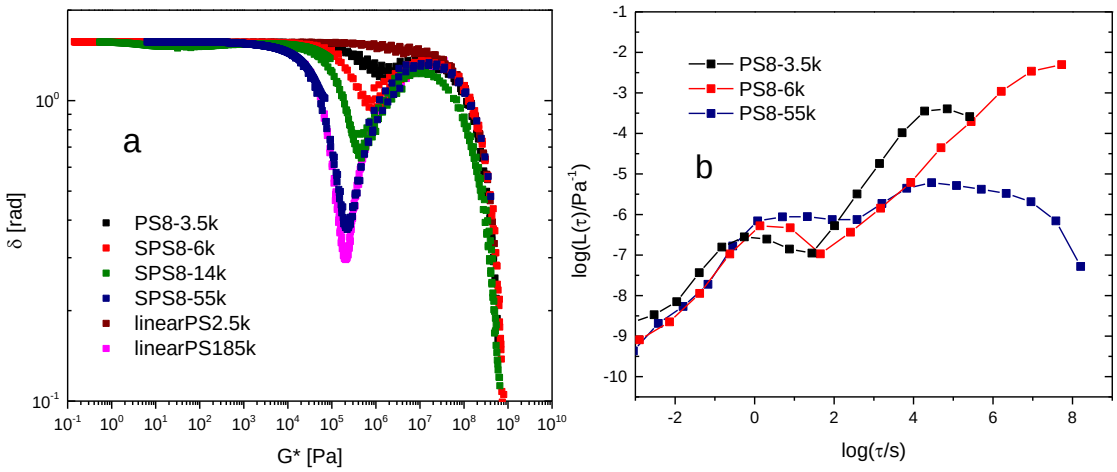

Figure 11a. Van-Gurp Palmen plot of the four stars compared with two linear samples. b. Retardation spectra for the samples where the transformation of dynamic moduli was possible.

Careful comparison of the data at the high modulus regime, reveal same non-negligible differences for the PS8-14k sample. This is because this specific sample was synthesized with a slightly different way. A few (3-4) monomers of butadiene where first grafted to the core, and then the polystyrene chains were grafted to the formers. This of course leads to same detectable differences when so local dynamics are probed. These few monomers plasticize the polystyrene chain, so the experimentally (calorimetrically) measured T_g was quite lower for this sample[41]. To overcome this, the data were shifted horizontally to meet the high frequency data of all the rest samples, included the linear ones. Then the horizontal (a_T) WLF coefficients were used to estimate the corresponding the T_g and found to be reasonable (See Figure 16).

For moduli lower than the glassy an interesting feature appears for the unentangled polystyrene samples. One can see that the low molar mass PS of 2.5 kg/mol goes to a plateau of the phase angle without displaying any minimum. By the other side, we observe a progressively deeper and deeper (lower values of phase angle) minimum for all the stars studied here. This minimum shifts to lower values of the complex modulus (G^*) for increasing the molar mass of the arm. For the well entangled sample (PS8-55k) this minimum is located at the same complex modulus as the well entangled linear one (PS185k). Following the fact that this minimum is due to entanglements elasticity in the case of entangled samples, we attribute the minima observed for the unentangled samples to more local (and as a consequence higher complex modulus) constraints. Branching of the short linear chains consisted of stiff monomers leads to higher degree of correlation for these stars giving rise to elasticity due to local orientational conformations. This becomes less important as the molar mass of arms approach the entanglement limit.

This interpretation is supported also in the retardation spectra of these samples shown in Figure 11b. In this two peaks with similar heights should exist for entangled samples[32]. This is the case for the PS8-55k star. The other two samples, display peaks with heights separated by orders of magnitude. We assume here that this would be also

the case for the PS8-14k sample where a plateau of the storage modulus was found, but the data could not be transformed.

3.2.3 Stars of intermediate functionality and varying molar mass of the arms

Polystyrene stars with intermediate functionality of 64 arms (${N_{arm}}^2 > f$) were studied for varying molar masses of the arms (See Table 1b). The arms are consisted of polystyrene and synthesized as the 8-arm stars studied here, with the difference that a few monomers of polybutadiene were first grafted to the core, to ensure the complete grafting to process of the chains onto the crowded core. The core diameter is $r_c \sim \sqrt{f}$, so the core of these intermediate functionalities stars is approximately 3 times bigger.

The experimental protocols were kept the same as before to ensure consistency. Four samples were measured and the mechanical spectra are depicted in Figure 12. Creep measurements were performed to extend the experimental window accessible in terms of the isothermal Frequency Sweeps. Great agreement between dynamic and steady deformation data was observed as in the case of the 8-arm stars. The limited amount of the PS64-53k sample did not allow us to perform creep measurements, since the high temperature and long-time experiment would possibly lead to degradation of the sample.

The rheological signatures for these stars are discussed below. First the upturn of storage modulus is present also here for the lowest molar mass star (PS64-8k). Another interesting finding is the regime between the transitional and the terminal one. One can see (inset of Figure 12a) that moduli cross marginally two times, as forming a plateau of the storage modulus for less than a decade in the frequency axis. The storage modulus is as high as about $G' \sim 2 \times 10^5\ Pa$, close to the entanglement plateau modulus of polystyrene. This is not expected for molar mass of the arm of 8 kg/mol. Note that here the molar mass of the arm is about 3 times higher compared to the case of PS8-3.5k, but the functionality is quite higher. By the other side, the size of the core is roughly 3 times bigger as explained earlier,

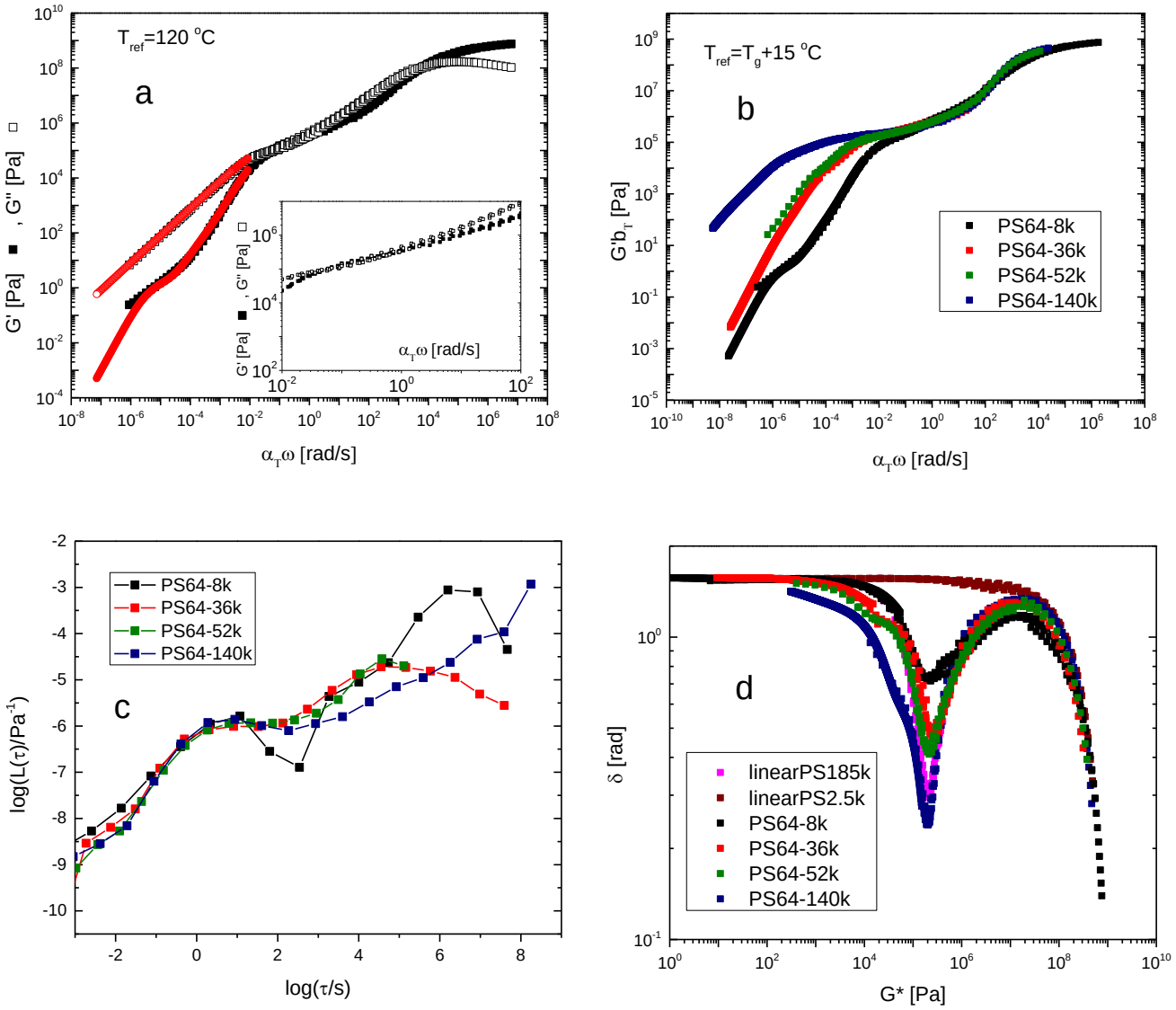

Figure 12a. Master curve of the PS64-8k sample. b. Master curves of storage moduli for the four 64-arms stars. The loss modulus data are not shown here for clarity. c. Retardation spectra for all 64-arms stars and d. Van-Gurp Palmen plot for all 64-arms stars.

so, one can say that these two samples have a comparable ration of arm length and core size. Despite the behavior at the terminal zone, the intermediate frequency regime appears quite different. In the case of the PS64-8k sample, the intermediate frequency regime is reminiscent of entangled polymers, where the existence of such a frequency regime where G' and G'' cross each other is apparent only for samples with $M > \sim 4M_e$[24].

It is impressive that the transition from the glassy to terminal zone is almost identical for the PS64-8k sample compared to the rest well-entangled samples!! The sample behaves as entangled with the formation of a clear plateau modulus for polystyrene. Branching of such a low molar mass chains onto a common core of intermediate functionality leads to significant orientation of the chains that leads to very strong

interpenetration of the monomers far from the star core. This gives rise to unusual rheological behavior reminiscent of entangled polymers. The data representation of phase angle versus complex modulus reveals another peculiarity. This sample not only display a minimum, but this minimum is almost for at the same position as the minima for the well entangled samples!! Finally, one can see similarities in the retardation spectra of the samples in Figure 12c. The creation of two peaks can be assumed for this sample very similar with those of the entangled samples.

The other three entangled samples display similar behavior. A plateau modulus of polystyrene is reached before the terminal processes. For the PS64-36k, where creep measurements extended the spectrum until center-of-mass relaxation with storage modulus scaling as $G' \propto \omega^2$. For higher frequencies, two distinct regimes are observed and the frequency dependences are $G' \propto \sim\omega^{1.6}$ and $G' \propto \sim\omega^{0.85}$, respectively.

The rheological behavior of the PS64-52k sample appears to be similar with the cross-over of the moduli to be shifted to lower frequencies as expected. Also, the two regimes described earlier are apparent here and the point of transition between the two regimes is shifted also to lower frequency here. We assume this is the case for the second regime and eventually the center-of-mass relaxation occurs.

Finally, we measured a star with quite high molar mass of the arm (about 10.5 entanglements), namely 140 kg/mol, named as PS64-140k. In this case the terminal flow regime was not accessible in terms of tTs, since temperature required to access these frequencies were high and sample would degrade. To measure the frequencies lower than those accessible long time creep experiments were conducted. Initially, a constant stress was applied to be about 1/1000 the stress at the plateau modulus. The stress was applied for 1000 seconds and then other stresses were applied to check the linearity (different stresses yield to the same creep compliance J (t)). The stress within the linear viscoelastic regime with the best torque signal was selected and applied for roughly 10^5 seconds. Then the obtained creep compliance J(t) was converted into storage and loss moduli, as described earlier. The data obtained by isothermal frequency sweeps and the converted compliances into dynamic moduli are in good agreement. Note that the terminal flow regime with $G'' \propto \omega^1$ and $G' \propto \omega^2$ was not accessible even with these long creep measurements. For a large molar mass of the arms the arm retraction is entropically unfavorable and stress relaxation slows down exponentially with increasing arm lengths[42,43], so the final center-of-mass relaxation was not accessible experimentally.

Finally, we combine data from the literature and our work to understand the relaxation of arms for different functionalities and molar masses of the arms. Data of the literature[20] display a quadratic dependence of the arm relaxation time normalized with the segmental relaxation time, over the number of monomers (N_a). We follow here the same analysis to be able to combine the data sets in order to see the effect of branching quite short chains onto a common core. Then the zero-shear viscosity of all the samples studied in this chapter are summarized and plotted against the zero-shear viscosity of a wide range of molecular weights of linear polymers. We see that the zero-shear viscosity remain higher than the linear with the same span molecular weight ($2 \times M_a$). Notice the departure of the PS64-8k sample from the quadratic dependence of zero-

shear viscosity over molar mass. We attribute this to strong caging and slowing down of the center-of-mass movement of the stars in the melt.

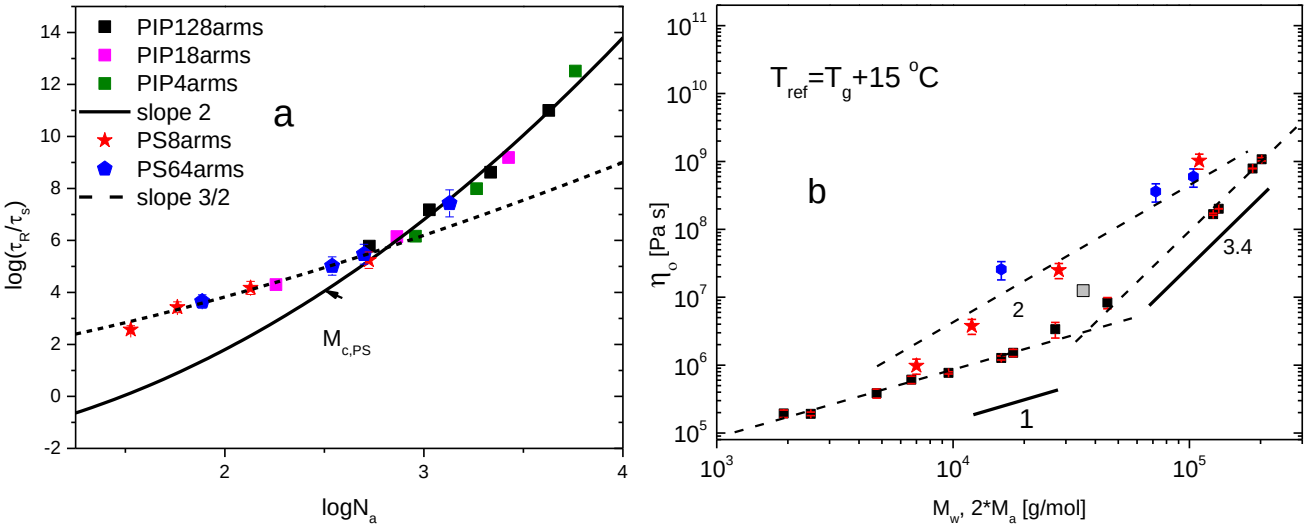

Figure 13a. Arm relaxation time normalized by the segmental relaxation times versus the number of monomers for all the stars studied here (both 8-arms and 64-arms stars) plotted with data from the literature. b. Zero-shear viscosity versus molecular weight for linear polymers and span molecular weights ($2 \times M_a$) for stars.

3.2.4 Effect of branching at local scale dynamics

We described in the previous the rheological behavior of three regimes of functionalities of star polymers. We have shown the important impact of branching at large scales and we focused on the terminal relaxation regime. Here we investigate the local segmental dynamics for the polystyrene stars studied previously. The case of extremely highly branched hybrids is so rich in terms of local dynamics that we discuss them separately in the next chapter of this work.

For this investigation two techniques are utilized. Rheology with particular interest in the high frequency glassy regime, where local dynamics are probed. In advance we systematically used Temperature-Modulated Differential Scanning Calorimetry (TM-DSC) to access the segmental relaxation of our systems, using an independent technique.

Experimentally it is tricky to measure the dynamic moduli of a glass forming liquid, for reasons that are analytically described in the next chapter. Briefly, such measurements are dramatically affected from compliance of the measuring apparatus. When the stiffness of the sample becomes progressively important if not comparable

with the stiffness of the parts of the rheometer, measurements are prone to experimental errors. To overcome this challenge, we used small diameter ($\leq 3\ mm$) parallel plates for moduli higher than say 1MPa, to eliminate the torque produced from the sample.

The WLF coefficients[18] C_1 and C_2 obtained from the tTs process at the arbitrarily chosen reference temperature, were used to calculate the corresponding coefficients at the T_g, a_{T,T_g}, according to $C_1^{T_g} = (C_1 C_2)/C_2 + T_g - T_{ref}$ and $C_2^{T_g} = C_2 + T_g - T_{ref}$. Then using the calculated shift factors a_{T,T_g} we can shift the master curves to the T_g and estimate the segmental relaxation time, as the inverse frequency where the loss tangent factor is maximum in the high frequency glassy regime. Assuming that the segmental relaxation time is shifted in time (or frequency) having the same temperature dependence as the shift factors a_{T,T_g}, we multiply the segmental relaxation time with the shift factors a_{T,T_g} found with reference temperature the T_g to estimate the segmental relaxation time at different temperatures.

A differential scanning calorimeter (TA Q250, USA) was utilized to perform the TM-DSC measurements to access the segmental relaxation. The glass transition temperature was first measured upon heating at a constant rate with conventional calorimetry. Then the width of T_g was investigated by applying a time-modulated oscillating heating profile (see inset of Figure 14). This gives information about the activated process of glass-to-melt transition, responsible for the de-froze of the segmental dynamics. More specifically we applied the time-modulated oscillating heating profile for a broad temperature window in the vicinity of previously measured T_g. During such an experiment the period of the oscillating heating profile was changed to explore the maximum time window allowed by the instrument. The heating profile is as follows. We calculate the heating rate according to $\beta = \frac{\Delta T_g}{n*P} * 60\ s/min$. Here ΔT_g is the temperature width of the glass transition, *n* is the number of oscillations per period and *P* is the period in seconds. We tried several numbers of oscillations and found that the best data were recorded for *n=6*. On top of this heating rate was added the oscillating profile with a temperature amplitude found to be best for 1 ℃ (maximum for this instrument). We systematically performed this for the broader period window possible with the instrument, namely 20-200 s. Then the glass-to-melt transition temperature

that is slightly different for each heating rate, was used to yield the segmental relaxation time as $\tau_s = period\ /\ (2 \times \pi)$.

TM-DSC has another important advantage compared to conventional calorimetry. The oscillating heating profile allows for separation of glass-to-melt transitions that cannot be separated with conventional calorimetry when the two processes have close temperature difference or the strength of one process is relatively small. We found two glass transition temperatures for some of the stars studied here as one can see for instance in the Figure 14 for the PS64-8k star. One can see the main glass transition temperature due to alpha relaxation indicated in the following Figure as the first peak in the first derivative of the heat capacity and another T_g indicated as a muck smaller step on heat capacity and a weaker peak at the derivative. This behavior is reminiscent for a second local relaxation process. Interestingly, a careful analysis in the BDS spectra of the PS8-55k star revealed two segmental relaxation processes with the same VFT temperature dependence as shown in Figure 15c. Unfortunately, possible lack of strength for a second process in the calorimetric measurements as well as lack of BDS spectra for all the samples studied here do not allow us to conclude.

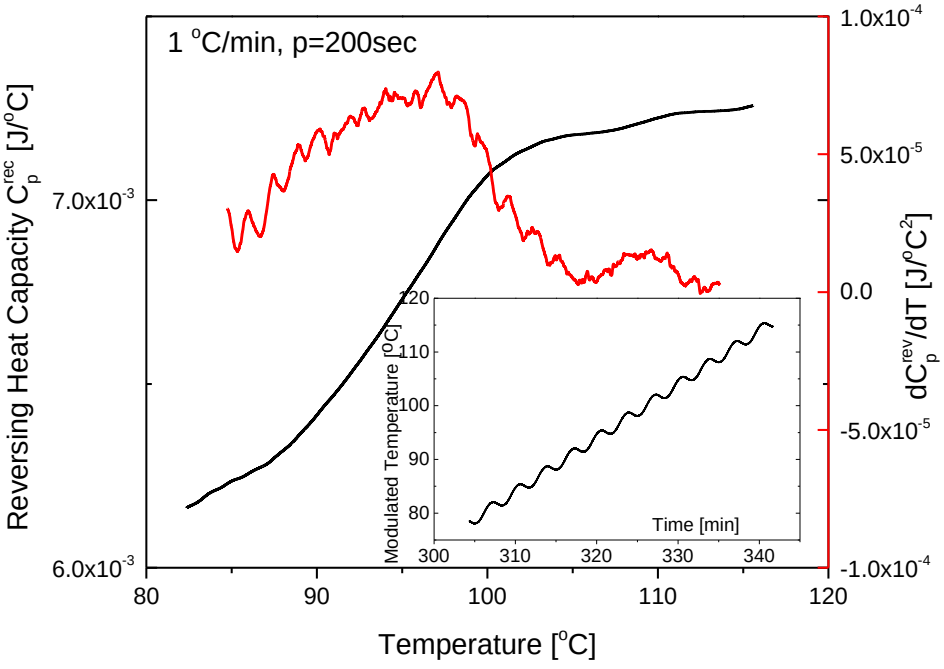

Figure 14. Indicative Reversing Heat capacity C_p^{rev} versus Temperature for the PS64-8k sample at a heating rate of 1 $°C/min$ corresponding to a period of 200 seconds, indicating to steps corresponding to two T_gs. Right part of the plot derivate over temperature showing two peaks the T_gs. Inset the modulated temperature versus time applied on the sample.

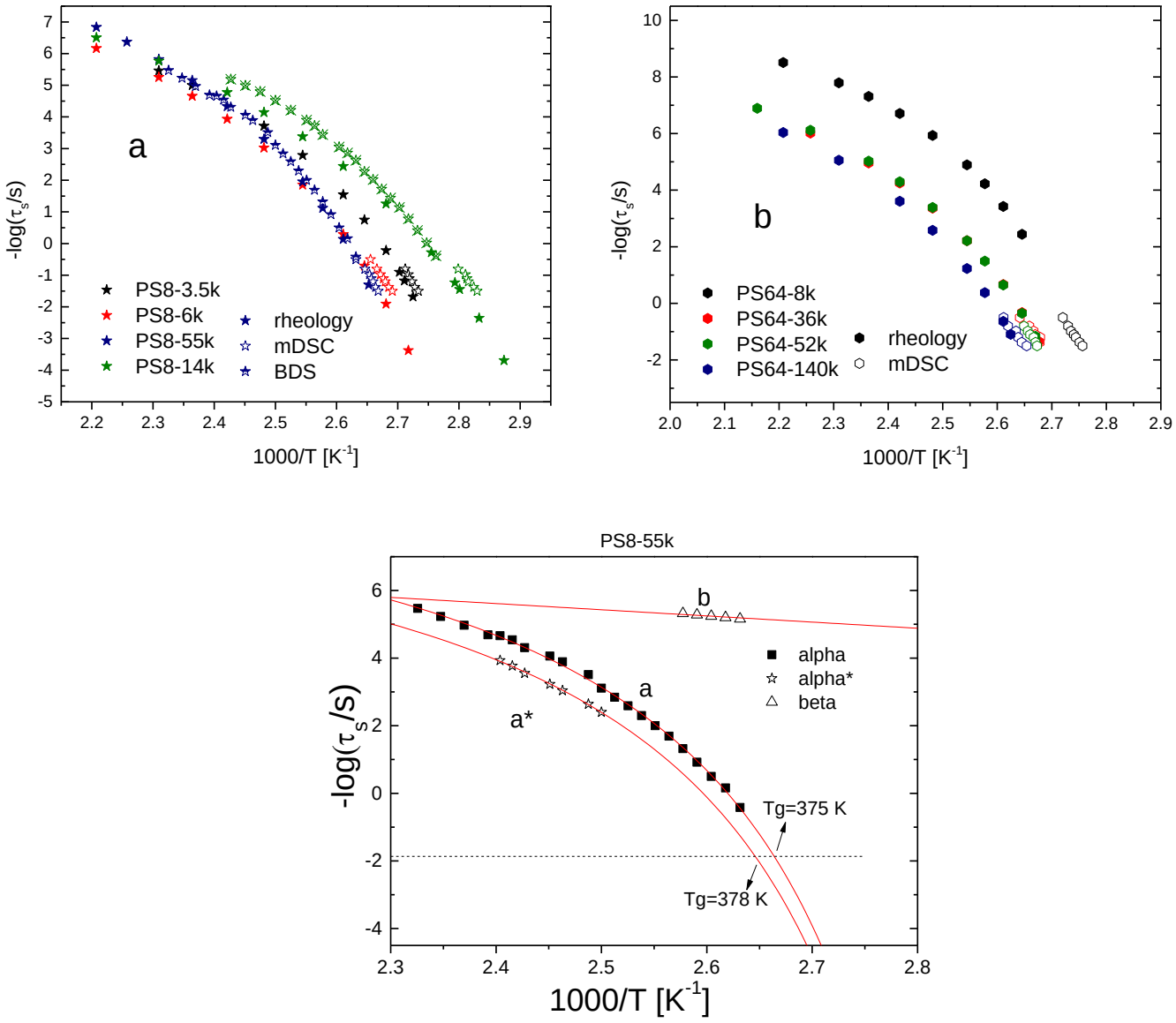

Figure 15.a Relaxation maps for the 8-arms polystyrene stars (Left) and b. 64-arms polystyrene stars (Right). Filled symbols correspond to data from rheology, empty data correspond to TM-DSC and in the case of PS8-14k and PS8-55k stars, semi-filled correspond to BDS. c. Relaxation map of the PS8-55k sample obtained by BDS, indicating two local relaxation processes with the same VFT temperature dependence.

We now plot the data obtained with TM-DSC and rheology as described earlier in the Figure below to create a relaxation map. Available measurements of Broad Band Dielectric spectroscopy (BDS) performed earlier in the University of Michigan are also plotted for the PS8-14k and PS8-55k samples. We see a good agreement among the three techniques. BDS is sensitive only to local segmental relaxations since polystyrene have only a dipole perpendicular to the chain. Also, MT-DSC is also sensitive to

segmental dynamics, since measures the energy needed to de-froze them. In this context the agreement of data obtained rheologically are of impressive accuracy and indicate the quality of the measurements.

First, in the case of the PS64-8k sample its segmental dynamics appear faster compared to the other stars. We attribute this to the addition of a few polybutadiene monomers on

the core to ensure the complete grafting on the crowded core. These few monomers plasticize the polystyrene as mentioned earlier, but also increase the mobility locally, so when the local dynamics of such a short chain are probed, they are significantly faster. This is why the PS8-14k sample has so weird behavior. It is the only one star prepared with the addition of PBD. The rest 8-arms stars are pure polystyrene. Then for the PS64-36k and PS64-52k samples this effect is more or less the same, so the local dynamics look indistinguishable. For the larger arm of 140 $kgmol^{-1}$ the dynamics look slower due to the fact that the plasticization is minimized.

The effect of the addition of these few butadiene monomers is also seen in the T_g for these stars. In the following plot we plot the glass transition temperatures as they were obtained by conventional calorimetry. For comparison we also plot data for linear polystyrene homopolymers to comment on the effect of branching short polymeric arms on a common core. The increase of the T_g for the branched polymers is quite high as seen in the case of PS8-3.5k and PS8-6k samples. One can see an increasement of about 10 ^oC between linear and these two star polymers. Then the addition of polybutadiene plasticizes the polystyrene but even in this case the PS64-8k sample has higher T_g. The PS64-36k and PS64-52k samples have lower T_gs values again due to plasticization and in the case of the PS8-55k (without addition of butadiene) as well as the PS64-140k sample where the effect of plasticization is minimum the T_gs are the expected within the experimental error.

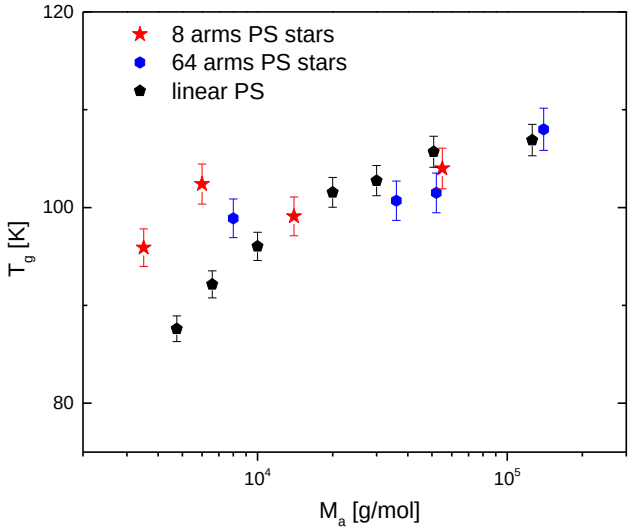

Figure 16. Glass transition temperatures for the star polymers studied here as well ass linear polystyrenes with relative molar masses.

3.3 Discussion

The dynamics of a wide range of star polymers were studied that capture three regimes, $({N_{arm}}^2 > f)$, $({N_{arm}}^2 \sim f)$ and the unexplored regime where $({N_{arm}}^2 < f)$ using mainly rheology, supported by other techniques, namely TM-DSC and broad-band dielectric spectroscopy. First the global dynamics of a three ultra-high functionality stars were studied and found to display strong slowing down of the center-of-mass relaxation yielding to colloidal dynamic arrest of these soft colloids. We observed a plateau modulus that decreases slowly over several decades and does not relax within the experimentally accessible frequency window. The modulus was found to depend on the arm length in a previous work[15], increasing as the molar mass of the arm decreases. Here we studied two samples with unentangled arms. The functionality is comparable to the one previously studied (~1100 arms) $({N_{arm}}^2 \sim f)$ and in the second case almost 3 times higher (~2830 arms) $({N_{arm}}^2 < f)$. Interestingly we found that for both samples the plateau modulus was higher than the samples previously studied as expected, but is unchanged for the two samples with same arm length, indicating that modulus is mainly a function of arm length rather than the functionality. The local dynamics of these stars were studied as well and presented in the last part of this work.

Then we studied the dynamics of low (8-arms) and intermediate (64-arms) stars $({N_{arm}}^2 > f)$ with varying molar mass of the arm. In the case of unentangled samples, for both functionalities an upturn of the storage modulus was found in the terminal flow regime of the mechanical spectra, indicating that the center-of-mass relaxation of these stars deviates from the frequency dependence of the dynamic moduli expected. Systematic study of the instrumental limitations of the rheometer, proved the good torque resolution of the storage moduli measured. Additionally, creep experiments facilitated the measurements in this terminal regime. The fact that the phase angle is not directly measured and thus prone to experimental errors additionally with the fact that the torque signal remains constant throughout the experiment, in contrast with the isothermal frequency sweep where the torque signal is reduced by orders of magnitude as the moduli decrease with almost quadratic frequency dependence, ensure the validity of the mechanical spectra.

These stars have a relatively high core to size ration, so the size of the core cannot be neglected. Once the arms relax and reach the terminal flow regime, the cores become correlated to some extent, so the existence of a second relaxation process can explain this anomalous rheological behavior.

For the stars with entangled arms, the upturn in the storage modulus disappears and a second relaxation process is apparent in the mechanical spectra. This second process is more clearly observed in the tanδ representation where a shoulder is followed by the terminal relaxation. This shoulder becomes less and less prominent as the molar mass of the arm increases.

Another interesting finding is the minimum of phase angle as function of complex modulus (van-Gurp Palmen) plot. Direct comparison of the minimum for linear and star polymers, reveal the importance of architecture on the dynamics. More specifically, a

clear minimum is observed in the case of PS64-8k sample. This was not expected for unentangled arms. Not only that but the depth of this minimum is similar with those for well entangled homopolymers. This is indicative of the strong impact of branching in the local dynamics. As the molar mass of the arm increases, the minimum becomes deeper and deeper, as expected, and interestingly the PS64-140k sample has deeper minimum than the linear homopolymer of higher molar mass (PS185k).

The possible effect of monomer chemistry of the high T_g bulky polystyrene was examined. A star with arms of polyisoprene having the same functionality and nearly the same number of monomers, was measured rheologically and the absence of the upturn in storage modulus was confirmed to the extent of the current experimental abilities. This strongly suggests that in the case of low molar mass of the arms where core to arm ratio is small the bulkiness of polystyrene make the cores of the stars more correlated in the melt. We can assume that stretching of the monomers near the core, suggested by the Daoud-Cotton model is stronger for styrene, compared to the smaller more compact and more symmetric monomeric chemical structure of isoprene.

The high frequency segmental dynamics of these stars have been also studied. Rheological data in the high frequency regime collapse onto a master curve, when shifted at the same temperature-distance from T_g. This was expected for samples with same chemistry and different architecture. The estimated relaxation map for these samples agrees well with data obtained with TM-DSC and the alpha relaxation process obtained with BDS when spectra were available. The definition of the segmental relaxation time from rheological data, reveal another peculiarity.

Failure of the superposition of isothermal frequency spectra in the transition to the glassy regime, is observed for all the samples studied here. Data from BDS available for the PS8-55k sample, show that the alpha relaxation process is not the only one. Another slower local relaxation process with the same temperature dependence occurs as one can see in figure 15c.

It is likely that the common temperature dependence of the two relaxation processes is the reason for the discontinuity in the transition to the glassy regime in the mechanical spectra. We account this discontinuity as a limitation of rheology to measure stress relaxation processes governed by more than one temperature dependences, rather than a failure of tTs.

3.4 Conclusions

The global dynamics for stars of varying functionality and length of the arms were studied rheologically. Stars of ultra-high functionality (of the order of ~10^3) and sufficiently short arms display a dramatic slowdown of the dynamics for large time scales, where center-of-mass movements take place. This dynamic arrest is due to jamming of these soft colloids that have to overcome a large energy barrier to move a distance of their own size. Plateau modulus for these stars was found to be roughly constant for stars with same molar mass of the arms even in the case where the functionality becomes almost three times higher. This strongly suggest that modulus is primarily a function of the length of the arm and independent of the functionality.

Another class of star polymers is that of stars with quite lower functionalities typically found in the literature, namely 8 and 64-arms stars. The rarely studied case of stars with such functionalities but short unentangled arms, revealed the existence of an extra relaxation attempt indicated as an upturn of the storage modulus in the terminal regime of these stars due to their non-negligible core to arm ratio, making their cores roughly correlated at large times. For entangled arms the existence of a second relaxation process in the terminal regime observed as a shoulder in the tanδ master curves is another fingerprint of the rheological behavior of such samples. The phase angle versus complex modulus data reveal sights of entangled polymers for arm molar mass as low as 8 kg/mol for a star of intermediate functionality, presenting a minimum in the above-mentioned data representation, not expected for unentangled polymers.

The existence of two local relaxation processes with the same temperature dependence for the stars observed in BDS spectra, make the discontinuity of the rheological data at the glass transition reasonable. Rheology is able to detect the segmental relaxation process for these stars, but stress relaxation is not sensitive to more than one processes with same temperature dependence.

Finally, the high frequency glassy regime for the low and intermediate functionality stars appears indistinguishable when master curves of mechanical spectra are shifted at the same temperature-distance from T_g. A good agreement of the segmental relaxation times obtained with rheology, BDS and TM-DSC is observed supporting the good quality of the measurements performed and presented here.

3.5 References

(1) Vlassopoulos, D.; Cloitre, M. Tunable Rheology of Dense Soft Deformable Colloids. *Curr. Opin. Colloid Interface Sci.* **2014**, *19* (6), 561–574. https://doi.org/10.1016/j.cocis.2014.09.007.

(2) Likos, C. N.; Löwen, H.; Watzlawek, M.; Abbas, B.; Jucknischke, O.; Allgaier, J.; Richter, D. Star Polymers Viewed as Ultrasoft Colloidal Particles. *Phys. Rev. Lett.* **1998**, *80* (20), 4450–4453. https://doi.org/10.1103/PhysRevLett.80.4450.

(3) Daoud, M.; Cotton, J. P. Star Shaped Polymers : A Model for the Conformation and Its Concentration Dependence. *J. Phys.* **1982**, *43* (3), 531–538. https://doi.org/10.1051/jphys:01982004303053100.

(4) Gauthier, M.; Munam, A. Synthesis of 1,4-Polybutadiene Dendrimer−Arborescent Polymer Hybrids. *Macromolecules* **2010**, *43* (8), 3672–3681. https://doi.org/10.1021/ma1004056.

(5) M. Rubinstein, H. Colby. *Polymer Physics*.

(6) Kapnistos, M.; Semenov, A. N.; Vlassopoulos, D.; Roovers, J. Viscoelastic Response of Hyperstar Polymers in the Linear Regime. *J. Chem. Phys.* **1999**, *111* (4), 1753–1759. https://doi.org/10.1063/1.479436.

(7) Vlassopoulos, D.; Fytas, G.; Pakula, T.; Roovers, J. Multiarm Star Polymers Dynamics. *J. Phys. Condens. Matter* **2001**, *13* (41), R855–R876. https://doi.org/10.1088/0953-8984/13/41/202.

(8) Pakula, T. Static and Dynamic Properties of Computer Simulated Melts of Multiarm Polymer Stars. *Comput. Theor. Polym. Sci.* **1998**, *8* (1–2), 21–30. https://doi.org/10.1016/S1089-3156(98)00003-8.

(9) Vlassopoulos, D.; Pakula, T.; Fytas, G.; Roovers, J.; Karatasos, K.; Hadjichristidis, N. Ordering and Viscoelastic Relaxation in Multiarm Star Polymer Melts. *Europhys. Lett. EPL* **1997**, *39* (6), 617–622. https://doi.org/10.1209/epl/i1997-00403-3.

(10) Matsumiya, Y.; Masubuchi, Y.; Inoue, T.; Urakawa, O.; Liu, C.-Y.; van Ruymbeke, E.; Watanabe, H. Dielectric and Viscoelastic Behavior of Star-Branched Polyisoprene: Two Coarse-Grained Length Scales in Dynamic Tube Dilation. *Macromolecules* **2014**, *47* (21), 7637–7652. https://doi.org/10.1021/ma501561y.

(11) Adams, C. H.; Hutchings, L. R.; Klein, P. G.; McLeish, T. C. B.; Richards, R. W. Synthesis and Dynamic Rheological Behavior of Polybutadiene Star Polymers. *Macromolecules* **1996**, *29* (17), 5717–5722. https://doi.org/10.1021/ma951893w.

(12) Roovers, J. Properties of the Plateau Zone of Starbranched Polybutadienes and Polystyrenes. *Polymer* **1985**, *26* (7), 1091–1095. https://doi.org/10.1016/0032-3861(85)90234-4.

(13) Fan, J.; Emamy, H.; Chremos, A.; Douglas, J. F.; Starr, F. W. Dynamic Heterogeneity and Collective Motion in Star Polymer Melts. *J. Chem. Phys.* **2020**, *152* (5), 054904. https://doi.org/10.1063/1.5135731.

(14) Chremos, A.; Glynos, E.; Green, P. F. Structure and Dynamical Intra-Molecular Heterogeneity of Star Polymer Melts above Glass Transition Temperature. *J. Chem. Phys.* **2015**, *142* (4), 044901. https://doi.org/10.1063/1.4906085.

(15) Gury, L.; Gauthier, M.; Cloitre, M.; Vlassopoulos, D. Colloidal Jamming in Multiarm Star Polymer Melts. *Macromolecules* **2019**, *52* (12), 4617–4623. https://doi.org/10.1021/acs.macromol.9b00674.
(16) Johnson, K. J.; Glynos, E.; Sakellariou, G.; Green, P. Dynamics of Star-Shaped Polystyrene Molecules: From Arm Retraction to Cooperativity. *Macromolecules* **2016**, *49* (15), 5669–5676. https://doi.org/10.1021/acs.macromol.6b00456.
(17) Williams, M. L.; Landel, R. F.; Ferry, J. D. The Temperature Dependence of Relaxation Mechanisms in Amorphous Polymers and Other Glass-Forming Liquids. *J. Am. Chem. Soc.* **1955**, *77* (14), 3701–3707. https://doi.org/10.1021/ja01619a008.
(18) J. D. Ferry,. *Viscoelastic Properties of Polymers*, 3rd ed.; Wiley, 1980.
(19) Zoller, P.; David J. Walsh. *Standard Pressure-Volume-Temperature Data for Polymers*; Technomic, 1995.
(20) Pakula, T.; Vlassopoulos, D.; Fytas, G.; Roovers, J. Structure and Dynamics of Melts of Multiarm Polymer Stars. *Macromolecules* **1998**, *31* (25), 8931–8940. https://doi.org/10.1021/ma981043r.
(21) Liu, X.; Abel, B. A.; Zhao, Q.; Li, S.; Choudhury, S.; Zheng, J.; Archer, L. A. Microscopic Origins of Caging and Equilibration of Self-Suspended Hairy Nanoparticles. *Macromolecules* **2019**, *52* (21), 8187–8196. https://doi.org/10.1021/acs.macromol.9b01473.
(22) Agarwal, P.; Qi, H.; Archer, L. A. The Ages in a Self-Suspended Nanoparticle Liquid. *Nano Lett.* **2010**, *10* (1), 111–115. https://doi.org/10.1021/nl9029847.
(23) Sakib, N.; Koh, Y. P.; Huang, Y.; Mongcopa, K. I. S.; Le, A. N.; Benicewicz, B. C.; Krishnamoorti, R.; Simon, S. L. Thermal and Rheological Analysis of Polystyrene-Grafted Silica Nanocomposites. *Macromolecules* **2020**, *53* (6), 2123–2135. https://doi.org/10.1021/acs.macromol.9b02127.
(24) Majeste, J.-C.; Montfort, J.-P.; Allal, A.; Marin, G. Viscoelasticity of Low Molecular Weight Polymers and the Transition to the Entangled Regime. *Rheol. Acta* **1998**, *37* (5), 486–499. https://doi.org/10.1007/s003970050135.
(25) Sachin S. Velankar; David Giles. How Do I Know If My Phase Angles Are Correct? *Rheol. Bull.* **2007**, *76, Number 2*.
(26) Läuger, J.; Wollny, K.; Huck, S. Direct Strain Oscillation: A New Oscillatory Method Enabling Measurements at Very Small Shear Stresses and Strains. *Rheol. Acta* **2002**, *41* (4), 356–361. https://doi.org/10.1007/s00397-002-0231-5.
(27) Dorgan, J. R.; Knauss, D. M.; Al-Muallem, H. A.; Huang, T.; Vlassopoulos, D. Melt Rheology of Dendritically Branched Polystyrenes. *Macromolecules* **2003**, *36* (2), 380–388. https://doi.org/10.1021/ma020612z.
(28) Seung-Yeop Kwak; Jeongsoo Choi; Hee Jae Song. Viscoelastic Relaxation and Molecular Mobility of Hyperbranched Poly(ε-Caprolactone)s in Their Melt State. *Chem. Mater. 17*, 1148–1156.
(29) Kainthan, R. K.; Muliawan, E. B.; Hatzikiriakos, S. G.; Brooks, D. E. Synthesis, Characterization, and Viscoelastic Properties of High Molecular Weight Hyperbranched Polyglycerols. *Macromolecules* **2006**, *39* (22), 7708–7717. https://doi.org/10.1021/ma0613483.
(30) Weese, J. A Regularization Method for Nonlinear Ill-Posed Problem~. 12.
(31) Honerkamp, J.; Weese, J. A Nonlinear Regularization Method for the Calculation of Relaxation Spectra. *Rheol. Acta* **1993**, *32* (1), 65–73. https://doi.org/10.1007/BF00396678.

(32) Plazek, D. J.; Echeverría, I. Don't Cry for Me Charlie Brown, or with Compliance Comes Comprehension. *J. Rheol.* **2000**, *44* (4), 831–841. https://doi.org/10.1122/1.551117.
(33) Alexandris, S.; Peponaki, K.; Petropoulou, P.; Sakellariou, G.; Vlassopoulos, D. Linear Viscoelastic Response of Unentangled Polystyrene Bottlebrushes. *Macromolecules* **2020**, *53* (10), 3923–3932. https://doi.org/10.1021/acs.macromol.0c00266.
(34) Hu, M.; Xia, Y.; McKenna, G. B.; Kornfield, J. A.; Grubbs, R. H. Linear Rheological Response of a Series of Densely Branched Brush Polymers. *Macromolecules* **2011**, *44* (17), 6935–6943. https://doi.org/10.1021/ma2009673.
(35) Inoue, T.; Onogi, T.; Yao, M.-L.; Osaki, K. Viscoelasticity of Low Molecular Weight Polystyrene. Separation of Rubbery and Glassy Components. *J. Polym. Sci. Part B Polym. Phys.* **1999**, *37* (389–397), 9.
(36) R.W.Gray. Dynamic Viscoelastic Behavior of Low-Molecular-Mass Polystyrene Melts.
(37) Harmandaris, V. A.; Floudas, G.; Kremer, K. Temperature and Pressure Dependence of Polystyrene Dynamics through Molecular Dynamics Simulations and Experiments. *Macromolecules* **2011**, *44* (2), 393–402. https://doi.org/10.1021/ma102179b.
(38) Abdel-Goad, M.; Pyckhout-Hintzen, W.; Kahle, S.; Richter, D.; Fetters, L. J. Rheological Properties of 1,4-Polyisoprene over a Large Molecular Weight Range. **2004**, *37* (21), 10.
(39) Plazek, D. J.; Schlosser, E.; Schönhals, A.; Ngai, K. L. Breakdown of the Rouse Model for Polymers near the Glass Transition Temperature. *J. Chem. Phys.* **1993**, *98* (8), 6488–6491. https://doi.org/10.1063/1.464788.
(40) Parisi, D.; Ahn, J.; Chang, T.; Vlassopoulos, D.; Rubinstein, M. Stress Relaxation in Symmetric Ring-Linear Polymer Blends at Low Ring Fractions. *Macromolecules* **2020**, *53* (5), 1685–1693. https://doi.org/10.1021/acs.macromol.9b02536.
(41) Roovers, J. E. L.; Toporowski, P. M. The Glass Transition Temperature of Star-Shaped Polystyrenes. *J. Appl. Polym. Sci.* **1974**, *18* (6), 1685–1691. https://doi.org/10.1002/app.1974.070180609.
(42) Milner, S. T.; McLeish, T. C. B. Parameter-Free Theory for Stress Relaxation in Star Polymer Melts. *Macromolecules* **1997**, *30* (7), 2159–2166. https://doi.org/10.1021/ma961559f.
(43) van Ruymbeke, E.; Keunings, R.; Bailly, C. Prediction of Linear Viscoelastic Properties for Polydisperse Mixtures of Entangled Star and Linear Polymers: Modified Tube-Based Model and Comparison with Experimental Results. *J. Non-Newton. Fluid Mech.* **2005**, *128* (1), 7–22. https://doi.org/10.1016/j.jnnfm.2005.01.006.

Chapter 4

Local dynamics of densely packed macromolecular objects

4.1. Introduction

As we discussed in the previous chapters, star polymer melts display a hybrid rheological behavior that interpolates between polymers and colloids. Their rheological signature was discussed for both low and ultra-high functionalities. Their colloidal-like behavior was discussed in the context of viscous flow. So far, when comparing the viscoelastic spectra of different stars no clear indication for deviations in local (high-frequency) dynamics has been reported, however the extreme case of very high functionality and short arms deserves attention, as the literature is limited to intermediate functionality stars with entangled arms[1,2]. In general, it has been shown that branched polymers, such as combs or stars, display segmental dynamics that are indistinguishable when compared to linear polymers of the same chemistry[3–5]. Indeed, the high frequency regime data were shown to collapse onto a master curve, indicating the same segmental behavior.

From the above, a fundamental question arises: Is these indistinguishable local dynamics behavior unique for polymers with same chemistry, irrespectively of the architecture? This question was triggered by the rheological investigation of star polymers in the limit of ultra-high functionalities (of the order of 10^3) with relatively short, unentangled or marginally entangled arms. These are the same PBD stars studied in the previous chapter. We observed differences in the high-frequency linear viscoelastic moduli for these samples that inspired us to further study their local response. In this chapter, we investigate the dynamics of such star melts rheologically, as well as employing calorimetric techniques and broad band dielectric spectroscopy in collaboration.

The conformation of a single star in good solvent was described by Daoud and Cotton more than 30 years ago[6]. The authors showed that a single star comprises different regimes of monomer concentration, due to the fact that for a given number of arms, the monomer concentration in the core region is higher because all branches have to join at the center. This means that away from the core the density of the monomers decreases, reaching eventually the limit of linear chains in the case of infinitely long arms. The idea of blobs[7] originally derived for linear chains can be used to describe the spatial distribution of lengths in a star arm. In this, a part of the arm exhibits locally single chain behavior in a region of size $\xi(r)$. This size increases with distance from the branching point. Overall, three regimes are defined in this model: The inner part close to the core, which is melt-like, the intermediate unswollen theta-like regime, characterized by ideal blobs that are penetrable to solvent only, and finally the outer swollen part where blobs are swollen and can interact with arms from other stars via interpenetration. In the absence of solvent in the melt, the mismatch of monomer density drives the stars to interpenetrate and adjust their shape. We will see that these characteristics are of great importance in the following.

The challenge emerging from this picture is to understand if and how the local segmental dynamics are affected by the branching of short polymeric chains onto a crowded core and how different are they compared to corresponding linear homopolymers (same molar mass with arms).

Stars with arms having molar mass below the entanglement molar mass, M_e, are rare in the literature but still exist for functionalities below 100.[8] The influence of molar mass in the neighborhood of M_e was studied for polybutadiene stars of low functionality[9], where changes in fast dynamics and T_g were found to depend on total molar mass but not on the architecture.

Simulations of star melts above T_g revealed no difference in density between linear and star polymers for very long arms.[10] However, when rationalizing the molecular characteristics of a star, as the functionality increases and the length of the arm decreases, the inherent density heterogeneity of the region close to the core cannot be ignored.

In order to address the above questions, we combine different spectroscopic techniques, namely rheology and broadband dielectric spectroscopy.

Rheometry in the glassy regime is challenging for several reasons, briefly discussed in the following.

The measurements can be strongly influenced by instrumental (transducer) compliance, when the temperature is close or even below the T_g. In this temperature regime where polymers undergo a liquid-to-solid transition, mechanical moduli rapidly increase reaching values of the order of GPa. This means that the stiffness of the sample is becoming comparable with the stiffness of the mechanical parts of the rheometer. In other words, the mechanical components of the rheometer configuration, namely the moving motor and the measuring transducer are not perfectly stiff.

One has to be very careful in order to obtain reliable data in this temperature regime. The key for measuring reliably the dynamic moduli of such stiff samples is a combination of small diameter tools and large gaps (sample thicknesses)[11]. Note that the sample stiffness is proportional to the forth power of the plate diameter[12] and transducer torque to third power. A corroborating technical issue is that compliance is frequency, tool and sample dependent. This means that a torque rebalance transducer is not able to compensate for the compliance in the same way for varying stiffness and measuring frequency for a given measuring set of tools and this becomes stronger at higher frequencies because its time response is not ideal (instantaneous). Recently, a protocol was proposed to correct the errors originated by instrumental compliance[13]. According to this, the specific compliance of a measuring system (rheometer) is measured before the experiments are performed. The measuring tools are fastened together with a glue at a small gap between the two measuring plates. The idea is that the compliance measured under these conditions is the highest possible, so the effect will be reasonably smaller for the case of polymers undergoing glass transition. This is why a gap of a few tens of micrometers is usually selected in such a test, since it will give a rather higher compliance compared to measurements at gaps being usually more than 1 mm. Once the tools are fastened, an oscillating torque sweep is performed and

the deflection angle is monitored for each applied torque signal. The slope of the diagram of deflection angle versus torque is the compliance of this specific measuring system. Such compliances are known (since they have been determined) and used to some extend here. In this work, we account for the effects of instrumental compliance and consider them minimized.

Another challenge with measuring mechanical properties of samples approaching their glass transition is their extreme temperature dependence[14,15]. It is known that the rheological properties such as relaxation time and viscosity, increase by more than 15 orders of magnitude in the temperature window of the experiments. This phenomenon becomes more and more important when approaching the glass transition temperature. This is clear from the form of the William-Launder-Ferry (WLF) equation where the horizontal (frequency) shift factors increase rapidly close to T_g[14]. Practically, despite the high accuracy of the environmental control system (nitrogen convection oven with nominally ±0.1K accuracy) even the slightest deviations in temperature (including possible temperature gradient within the sample or between sample and plates) can yield bad data in the temperature regime of the glass transition. Another origin of possible experimental errors is the fact that the measurements performed here are well below room temperature. This means that one has to load the sample at room temperature and then cool down to the desired temperature, with the correction of the thermal expansion of the tools described below being crucial. To this end, the zero-gap position of the tools was determined after equilibration at the test temperature by using an independent calibration of the thermal expansion of the tools. Finally, another challenge of these measurements is that limited time is provided for them for two reasons. To achieve such low temperatures liquid nitrogen must be used, with condensation of humidity forming ice all over the rheometer to be only partially avoidable and secondly due to the high resistance induced on the motor of the rheometer which is believed to suffer from creation of ice inside itself that can affect its function or even damage it, if it is exposed to so low temperatures for very long times. Nevertheless, it was ensured that samples did not exhibit time dependence when their properties were probed.

4.2 Results

4.2.1 Rheology

For the rheological measurements an ARES (TA Instruments, USA) strain-controlled rheometer equipped with a separated motor and a 2kFRT-N1 transducer was utilized. Temperature control was achieved in terms of a convection oven and a liquid nitrogen dewar. Temperature was constant during the experiments with a maximum deviation of 0.1 K. Stainless steel parallel plates (PP) were used to measure the linear properties of the samples, with varying diameters to achieve the best combination of torque resolution and minimization of transducer compliance effects. For temperatures near the ambient one, 8 mm parallel plates (PP) were used for the measurements of

PBD1110-1.3k sample with a gap of approximately 0.8 mm, whereas 4 mm PP were used for the PBD2830-1.3k sample due to the limited amount of available sample. For the intermediate temperatures, 4 mm PP were used for both samples and finally for the lowest temperatures, 2 mm PP were used, again in order to minimize the effects of transducer compliance in the vicinity of T_g. Additional measurements to those originally made by Dr. Leo Gury[5] were performed only near T_g for the PBD929-4k sample to obtain the high-frequency data.

Dynamic Frequency Sweep tests were conducted in the range of 100 to 0.1 rad/s. Prior to each test, the linear viscoelastic regime was determined by means of a Dynamic Strain Sweep. Strains in the regime where the dynamic moduli are strain independent were used for the frequency sweeps performed for at least two different strains to ensure linear behavior and good torque resolution. In the cases that the normal force was not zero after a change in temperature, a small correction of the order of few microns was necessary to achieve the correct gap. Dynamic temperature sweep tests ensured steady conditions for the sample.

Master curves of the storage moduli are shown in Figure 1. The Time-Temperature Superposition (tTs) principle was applied to obtain the master curves covering nearly 14 decades in frequency and 4 in moduli. A vertical shift was necessary to account for the density variation due to the large temperature window of the measurements. The temperature-dependent density was estimated from ρ(T)=1.04332-5.96426E-4*T [16] and the vertical shift factors were calculated according to $b_T = \frac{\rho(Tref)*Tref}{\rho(T)*T}$. Then, the dynamic moduli were horizontally shifted to obtain the horizontal shift factors (a_T). The later can be fitted with the empirical WLF equation according to $loga_T = \frac{-C_1(T-T_{ref})}{C_2+(T-T_{ref})}$. All curves were shifted at a constant (temperature) distance from the glass transition temperature, such that the reference temperature is given as $T_{ref} = T_g + 13$ K.

Before moving to the discussion of the data, a discussion of the superposition of the isothermal dynamic rheological data is in order. Superposition of the dynamic data obtained at different temperatures yields a master curve when the sample is thermorheologically simple. This means that when tTs is validated, one unique frequency-scaling allows to superimpose the data, hence scale the fundamental rheological quantities like relaxation time and viscosity. It becomes clear in the data, that the imperfections in the carefully constructed master curve render the present samples thermorheologically complex. Deviations from the thermorheological simplicity have been reported in the past for polybutadiene, with particular emphasis in the microstructure, namely the amounts of 1,2-polybutadiene and the amounts of 1,4-polybutadiene[17]. Our observations likely do not originate from the microstructure of the arms, since their microstructure is nearly uniform (more than 95% pure 1,4-polybutadiene). A sensitive way to appreciate thermorheological complexity is the data representation in the form of tanδ versus frequency master curves (Figure 2a), or even better the so-called van-Gurp Palmen plot of phase angle versus complex modulus (Figure 2b). The superposition breaks-down to some extent, as one can see clearly in the latter plot where data are scattered in the range of the complex modulus from about 10^7 to 10^8 Pa. This is also the case for the data in the frequency range between 10^2 to

10^4 in Figure 2a. It is tempting to attribute this behavior to measurement artifacts. Indeed, equilibration problems or technical difficulties, such as those described above, could be the reason for the scattered data in the superposed plots. However, the overall analysis suggests that this cannot be the only explanation for the local (or partial) failure of the superposition. We believe that this discontinuity of the rheological moduli in the regime of glassy transition is an intrinsic property of the measured samples and originates from the complex temperature dependence of the local relaxation processes, likely reflecting heterogeneities, as will be further discussed in the context of comparison with other techniques. Measurements of the glass transition temperatures were performed on a Discovery DSC Q250 (TA Instruments, USA) for the samples used in this study. Samples were sealed in aluminum pans provided by the instrument manufacturer and the measurements were conducted under nitrogen atmosphere to avoid oxidation. The samples were first heated to 50 ˚C and equilibrated for 10 minutes, to erase any thermal history and then cooled to -115 ˚C under constant cooling rate of 10 ˚C/min and equilibrated for 5 minutes before the final heating to 50 ˚C. The glass transition temperature was defined from the latter heating step for a constant rate of 10 ˚C/min, as the minimum of the first derivate of the heat flow versus temperature. This process was repeated for the equilibration time before cooling several times. Curves were identically same even for 24 hours equilibration at 50 ˚C.

The glass transition temperatures were higher compared to entangled linear polybutadienes measured with the same protocol, for the two samples with same molar mass of the arms (PBD1110-1.3K and PBD2830-1.3K). The PBD929-4k sample has a Tg close to the linear entangled homopolymer. This is a first indication of different segmental dynamics, since glass transition temperature reflects the freezing of the segments.[18]

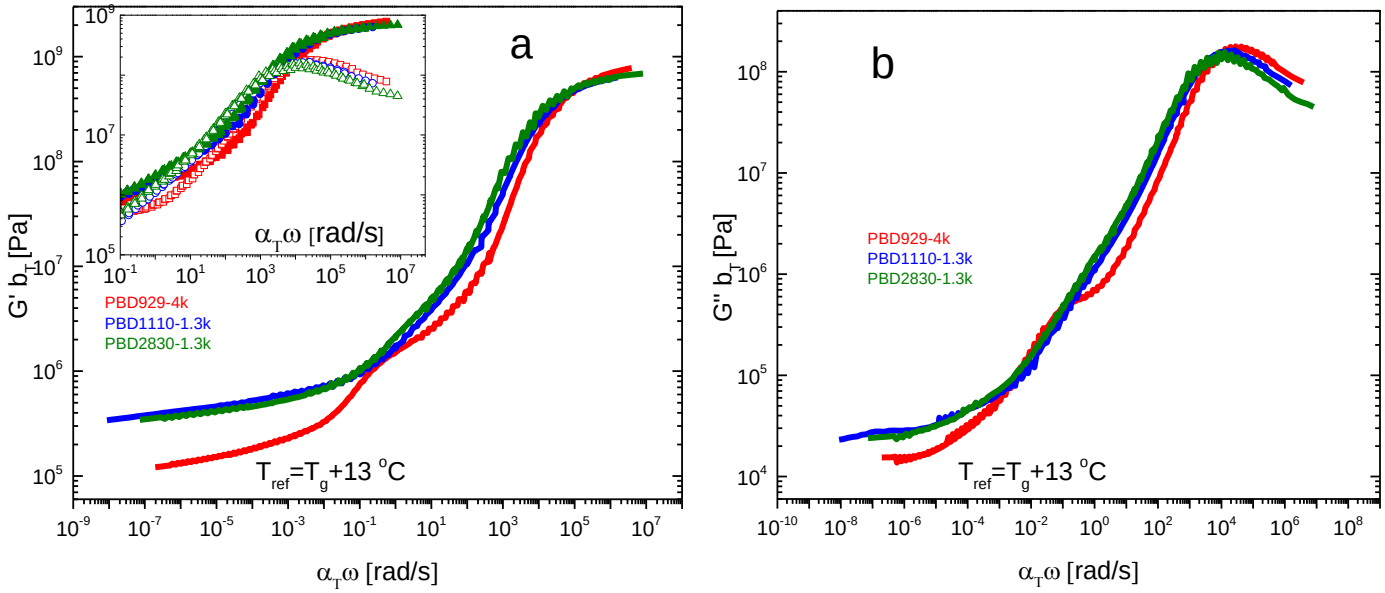

Figure 1: Master curves of (a) storage and (b) loss moduli for the three PBD stars investigated. Data were obtained by tTs and are presented at the same temperature distance from T_g. Inset of 1a. Zoom at the glassy regime for both dynamic moduli and for all three samples.

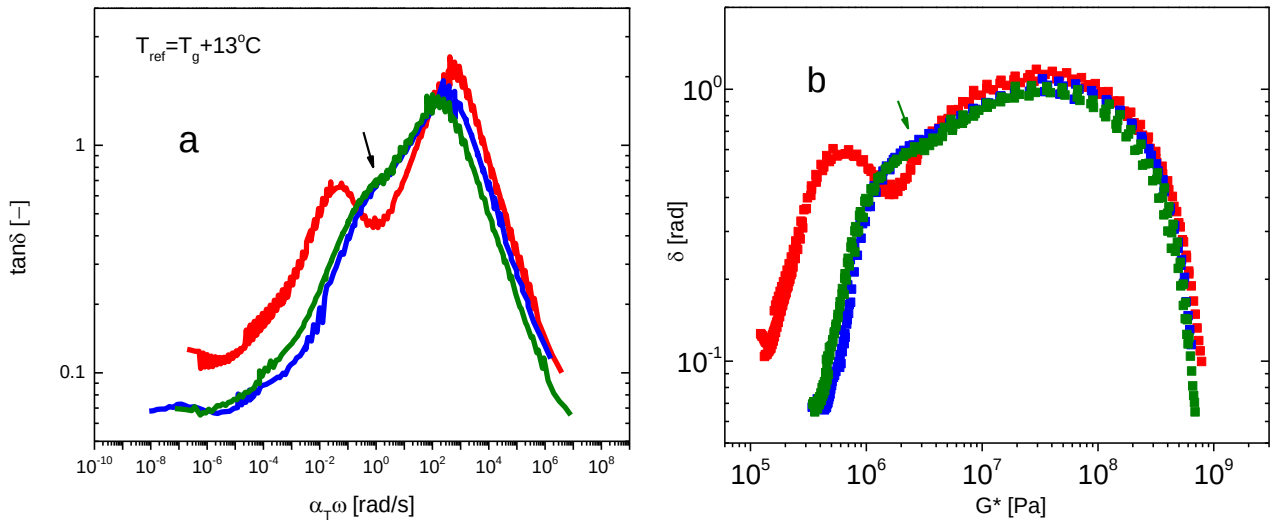

Figure 2a. Master curve of loss factor tanδ=G''/G' shifted at the same temperature distance from T_g. b. Van-Gurp Palmen plot (phase angle versus complex modulus). Note that no shifting has been performed as it is not necessary in this representation.

We focus now on the high frequency regime, where local segmental dynamics are probed. While the high-frequency regime was not the focus of earlier investigations of multiarm star polymer rheology, we note that no difference among stars or stars and linear chains was reported in this regime[2,5]. However, data reveals differences at this regime. These differences are clear when one carefully measures the mechanical moduli of these samples using the techniques described in the Introduction. Data shifted at iso-frictional conditions, i.e., at the same temperature distance from glass transition temperature allow for direct comparisons. It is evident that these high-frequency data do not collapse for all samples. After this initial observation, long-time annealing of the PBD1110-1.3k sample was performed before measuring again all the master curves with this new protocol. The sample was kept for three weeks in a vacuum oven at 40 ^oC, almost 150 ^oC above its glass transition temperature. This was to make sure that the observations reported here are not artifacts due to lack of annealing.

These observations are apparent in Figure 1. The dynamic moduli do not superimpose in the high-frequency regime when shifted at the same temperature distance from T_g. These deviations are also apparent in the data representation of tanδ(=G''/G') master curves. First, the deviation of the moduli at the highest frequencies is apparent at the right part of the plot. The shifting of this part to lower and lower frequencies is clear and describes slower segmental dynamics. In this representation a relaxation time is indicated as local extrema or equality to 1. Usually, the alpha relaxation corresponds to

the maximum of the loss modulus. If we account this frequency as the inverse of the segmental relaxation time this is a frequency where tanδ is not local extreme or equal to 1. The alpha relaxation process corresponds to the crossover of moduli at the highest frequency, or equivalently to the frequency where tanδ=1 at the highest frequency in tanδ master curves. The regime between the alpha relaxation and the second frequency where tanδ equals 1 at lower frequencies is the regime between the segmental relaxation and the relaxation of a Kuhn length. The values of the tanδ data are reduced in this regime, indicating different dynamics at these length scales. Also, a shifting of the peak to lower frequencies is observed. At even lower frequencies in the case of the PBD929-1.3k sample, a minimum in tanδ indicates the rubbery-like plateau that is not present in the samples studied here. The minimum has been replaced by a "shoulder" for both samples at the same frequency regime (see the arrows in the Figure 2a and 2b).

4.2.2 Temperature-Modulated Differential Scanning Calorimetry

To shed light on the unusual high-frequency response reported above, we systematically performed temperature-modulated differential scanning calorimetry (TM-DSC) measurements to obtain independent information on segmental relaxation. TM-DSC has been proven a valuable calorimetric technique to probe dynamics in the vicinity of the glass transition temperature[19]. It has been established as a useful technique[20] and it is often used to support or extend the data obtained on segmental relaxation times by broadband dielectric spectroscopy[21–24], as will be further elaborated here as well. The principles of the technique are described briefly in Chapter 2.

Measurements were conducted with a Discovery DSC Q250 (TA Instruments, USA) at different heating rates and oscillation periods ranging between 20 and 200 seconds. The imposed heating rate β was calculated from the equation[22]: $\beta = \frac{\Delta T_g}{n*P} * 60\ s/min$

where ΔT_g is the full width at the half height of the T_g, n is the number of oscillations within the T_g width and P is the oscillation period. The temperature oscillation amplitude was set at 1 ˚C for all measurements. Samples were initially left to equilibrate at 50 ˚C for 10 minutes to erase the thermal history, and then cooled down to the lowest possible temperature with this setup (-115 ˚C, below the full T_g width) by means of nitrogen flow which was supplied by a chiller. This temperature was kept for 5 minutes and then the heating rate was applied up to a temperature above the highest temperature of the T_g width (-80 ˚C). Temperature modulation was achieved as an oscillating heating wave which enabled the precise measurement of the reversing c_p^{rev} and non-reversing $c_p^{n,rev}$ heat capacity. Data were provided by the instrument software (Trios), and the glass transition temperature for each heating rate was calculated as the minimum of the first derivate of the heating capacity as function of temperature. We can define the segmental relaxation time as the modulation period divided by $2 \times \pi$. The T_g is slightly different for each heating rate.

In order to compare directly the segmental relaxation times from rheology and TM-DSC, we used the WLF coefficients C_1 and C_2 from rheometry and calculated their

values at reference temperature T_g (determined from conventional DSC) according to[25] $c_1^g = C_1C_2/(C_2 + T_g - T_{ref})$ and $c_2^g = C_2 + T_g - T_{ref}$. Subsequently, we shifted the entire master curve at T_g and defined the segmental relaxation time as the inverse frequency where tanδ=1 at the high-frequency glassy regime. The extracted times were multiplied by the horizontal shift factors calculated at T_g to yield estimated segmental relaxation times at different temperatures, assuming that they follow the WLF temperature dependence. This process allows us to construct a relaxation map rheologically. Despite the ambiguity in the definition of the segmental relaxation time at T_g and the slight uncertainty of shift factors and the shifting to another temperature, the rheological relaxation map provides reliable information about the temperature dependence of the segmental relaxation time. Indeed, the segmental relaxation times obtained by TM-DSC and directly by the rheometric data at different temperatures are in very good agreement, as seen in figure 3.

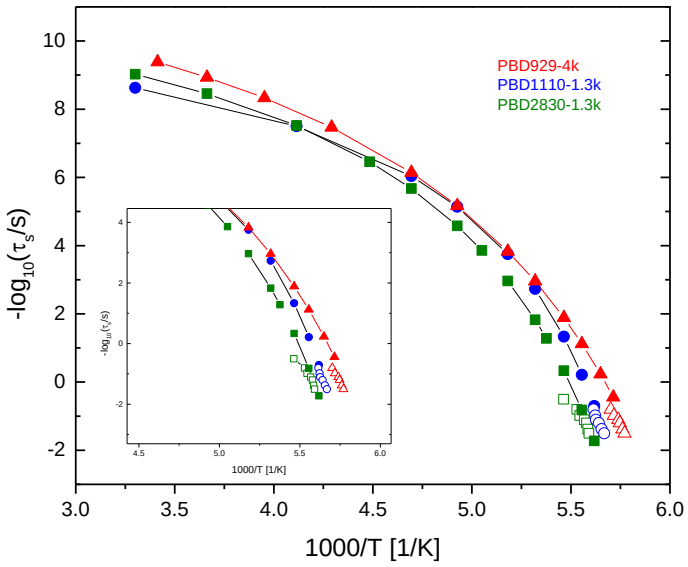

Figure 3: Relaxation map of segmental relaxation times obtained rheologically and with the aid of TM-DSC.

4.2.3 Broadband Dielectric Spectroscopy

These findings render the need to obtain further insights on the local dynamics of the present star polymers imperative, hence the samples were also investigated by means of broadband dielectric spectroscopy (BDS) in collaboration with the lab of Professor George Floudas.

The segmental dynamics obtained by BDS confirm the differences in local dynamics probed rheologically and described earlier. This provides further support to the rheological data and to the emerging picture of local dynamics in the present multiarm star polymers. Indeed, the qualitative agreement between the two techniques reflects their sensitivity to study local dynamics. It should be noted that these two techniques probe different physical processes. Rheology measures the frequency dependence of stress relaxation upon the application of an oscillatory linear strain. It is able to probe dynamics at different time and length scales, from the segmental motion all the way to the terminal relaxation. This means that ideally all relaxation modes can be measured. On the other hand, BDS measures the relaxation of permanent electric dipoles that align with the imposed external oscillatory electric field. In the case of polybutadiene (1,4-addition), the only one dielectric dipole is perpendicular to the macromolecular backbone, so only local relaxation mechanisms can be detected, i.e., the technique is selective. An advantage of this technique is that a very broad frequency spectrum is accessible for an isothermal experiment, so if mechanisms with different temperature dependencies coexist, they can be easily identified.

Interestingly, more than one local relaxation processes were probed by BDS. For all samples studied here, a third relaxation process was found, unlike the linear homopolymer with the same molecular weight as the arm, where only two, the segmental alpha (α) and a faster beta (β) processes are present[26]. Another important finding is that the faster local relaxation process, the beta process, appears to be faster in the case of the stars studied here, when compared to linear. The slower relaxation process (α*) is detected only in the present stars and has the same temperature dependence as the intermediate alpha (α) process. For the PBD1110-1.3k sample an even slower segmental relaxation time is found, as seen in Fig. 6.

It is also interesting that the lack of superposition of different isotherms that was observed rheologically, is also observed in the BDS spectra, as seen in Figure 4. These data support the argument discussed before about the discontinuities of the superposition of mechanical spectra. The complex temperature dependence of the relaxation processes leads to discontinuities even in the case where a wide range of frequencies is accessible in one isotherm.

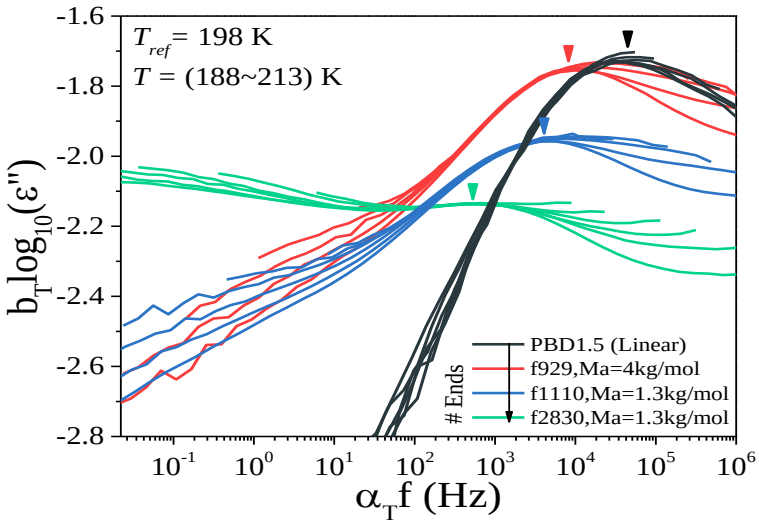

Figure 4. Comparison of superposition of dielectric loss curves of PBD2830-1.3k (green line), PBD1110-1.3k (blue line) and PBD929-1.3k (red line) and PBD1.5 (black line) at a reference temperature of 198 K. The vertical arrows indicate the α-process of each sample. When the star functionality increases, the α-process shift to lower frequencies and the dielectric strength is reduced.

Figure 5 depicts representative BDS data for the PBD1110-1.3k sample. We can clearly see the two local relaxation mechanisms (beyond the beta relaxation) and in addition the slowest process is also evident. The data corresponding to the latter are close to the resolution of the instrument but it is clear that this mechanism is not an artifact. Whereas it is more clearly observed for this sample, it is likely that exists also in the spectra of the other two samples but cannot be well discerned, presumably due to its low signal.

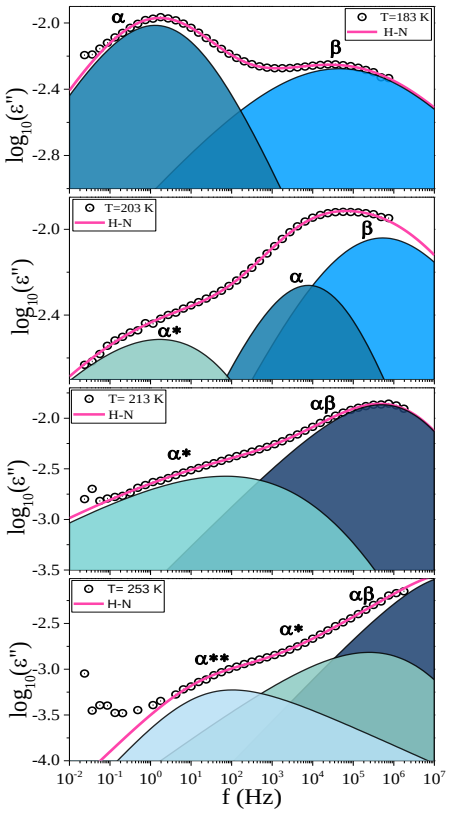

Figure 5. Dielectric loss spectra as a function of frequency of PBD1110-1.3k sample at some selected temperatures. The curves are given at four temperatures: *T*=183 K, *T*=203 K, *T*=213 K and *T*=253 K. The pink lines are result of fits with a summation of Havriliak-Negami functions. Each process is represented with different hue of blue color.

The data obtained from BDS are summarized in two relaxation maps. One is for the two stars (PBD1110-1.3k and PBD2830-1.3k, Figure 6) with the same molar mass per arm, of about 1.3 kg/mol < *Me*. The other is for the PBD929-4k star with arm molar mass of about 4 kg/mol > *Me* (Figure 7). All the experimental data are described through a VFT fitting (the respective data are not shown here for clarity).

In figure 6 a relaxation process labeled as alphabeta (αβ) is nothing more than the merge of alpha and beta processes at some temperatures[27]. At these high temperatures these mechanisms appear indistinguishably and has a VFT with different temperature dependence from the alpha and beta when measured independently.

Lastly, the α**-relaxation is assigned to the dynamics of those PBD segments in the vicinity of the core. At the star core crowding of the chains excludes shaking motions, leading to a much slower segmental relaxation. Within the time scale of the α**-relaxation, some contribution from 1,2-PBD segments is expected.

The disparate dynamics of the *outer*, *intermediate* and near-*core* PBD segments can be discussed with the help of Figures 6b,c as a function of functionality. In Figure 6b the magnitude of the difference of the outer and intermediate dynamic layers, $\tau_\alpha/\tau_{\alpha*}$, has a power law dependence on functionality as $f^{-1.3}$. Additional data from rheology,

corresponding to the arm relaxation mechanism, are included in the figure (Ref. [5]). The apparent agreement of the time scale for the segmental α*-relaxation with the arm relaxation found in rheology can be explained as follows: as the PBD arm undergoes a slow and hindered retraction mechanism, segments are displaced from the star periphery to the intermediate layer – as the approach to the core is prohibited – thus contributing to the dielectrically active α*-relaxation. For the α**-relaxation the difference in the outer and core dynamic layers, $\tau_\alpha/\tau_{\alpha^{**}}$, exhibits another power law dependence as $f^{-2.0}$. In the same plot, simulation data from star polymer melts with a lower functionality are included corresponding to the near-core segments Ref. [10]. Interestingly, the simulation data (for N=20 and N=40) show a dependence on functionality as $f^{-1.63}$, *i.e.*, intermediate to the power laws obtained in the experiment. Nevertheless, both simulated and experimental results clearly demonstrate that functionality enhances the intra-molecular dynamic heterogeneity in the highly branched arborescent hybrids.

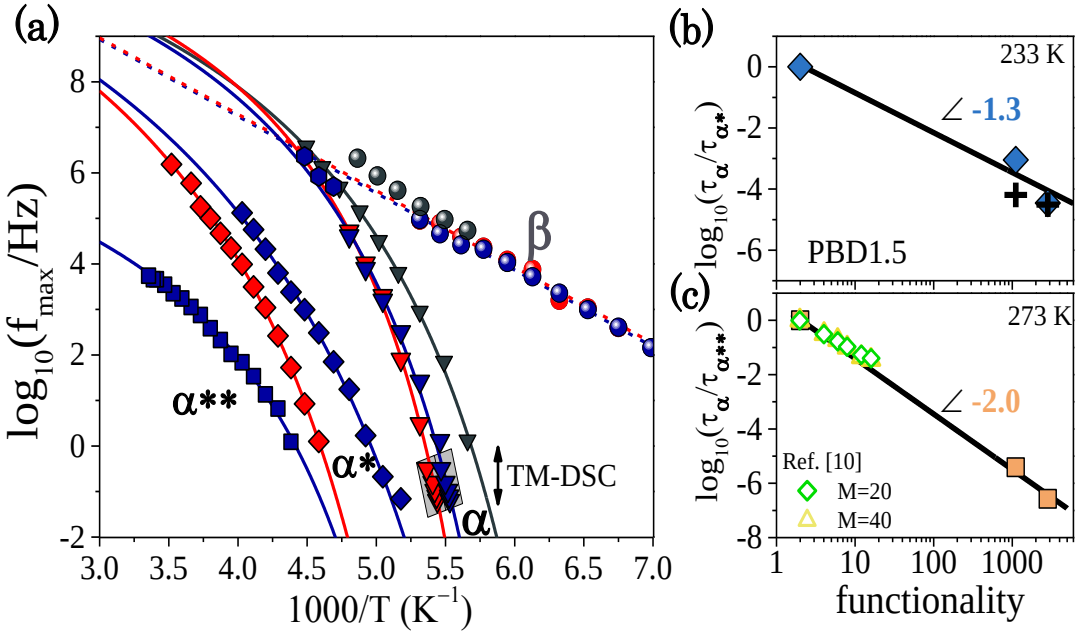

Figure 6. (a) Arrhenius relaxation map for a series of 1,4-PBD arborescent hybrids with a similar arm molecular weight but increasing number of arms: segmental α-relaxation (down triangles), local β-relaxation (circles), α*-relaxation (rhombi) for different functionalities: PBD2830-1.3k (red), PBD1110-1.3k (blue) and PBD1.5 (black). A slower α**-relaxation (squares) is evident in PBD1110-1.3k. Data inside the gray box were obtained from TM–DSC. The curved and the straight lines represent fits to the VFT and the Arrhenius equations, respectively. (b), (c) Structural relaxation time ratios, ($\tau_\alpha/\tau_{\alpha^*}$) and ($\tau_\alpha/\tau_{\alpha^{**}}$), as a function of functionality. Simulation data for different numbers of repeating units, M, are included from Ref. [10]. Crosses in (b) are from rheology Ref. [5].

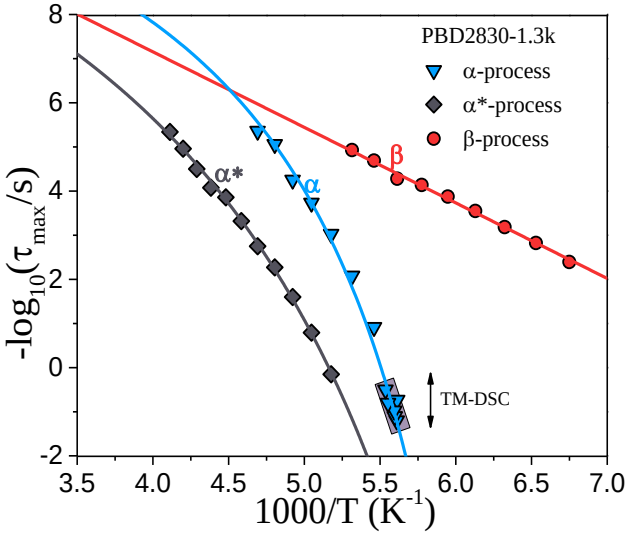

Figure 7. Arrhenius relaxation map of the multiple processes of f929 sample. The red circles, the blue down triangles and the gray rhombus correspond to the β-process, the α-process and the α*-process respectively. The data inside the gray box were obtained from TM-DSC. The curved lines represent VFT fits.

4.3 Discussion

The combination of rheology, broadband dielectric spectroscopy and temperature-modulated differential scanning calorimetry allow us to explore the local dynamics of multiarm star polymers in great detail. In the case of extremely high functionalities and length of the arm ranging from unentangled to marginally entangled, these densely crowded macromolecular objects exhibit unprecedented and unique local dynamics. Rheologically, we observe a slower segmental relaxation time as the functionality increases and the length of the arm decreases. Using BDS we confirm these findings and further explore these interesting dynamics that are not visible with rheology. The experimental fact of slowing-down of the local dynamics in polymers with same chemistry and complex densely packed architecture is an important finding.

The existence of more than one local processes with the same VFT temperature dependence, suggests that distinct layers with different mobilities coexist within one single multiarm star. The dynamics of polymers has been reported to be different in case of confinement compared to the bulk, both experimentally[26,28–31] and in simulations[32,33]. It is tempting to think that changes in the local dynamics of stars in the bulk signify local confinement because of the stretching of the segments near the core. One can assume that distinct corona (i.e., arms) layers with different dynamics coexist in one single star, as a function of the distance from the core. For the segments adjuscent to the core, where monomers of neighboring chains touch each other, the dynamics are

strongly altered due to the densely crowded environment. On the other hand, toward the free chain end stretching and crowding decays (Daoud-Cotton effect), affecting the local relaxation processes. Recall that for the PBD1110-1.3k sample four local segmental processes were identified, with the alpha (α) and alpha* (α*) exhibiting the same temperature dependence and the slowest alpha** (α**) to have a different temperature dependence. We attribute the slowest (α**) mode to the response of the near-core segments, due to stronger stretching and geometric confinement by monomers of neighboring arms. Its distinct temperature dependence is attributed to the interference with the chemical core, where polymer dynamics may coexist with dynamics of the carbosilane dendrimers comprising the core. Importantly the ratios of local relaxations times $\tau_{\alpha}/\tau_{\alpha^*}$, has a power law dependence on functionality as $f^{-1.3}$ and $\tau_{\alpha}/\tau_{\alpha^{**}}$, exhibits another power law dependence as $f^{-2.0}$ meaning that functionality enhances the intra-molecular dynamic heterogeneity in the highly branched arborescent hybrids.

It is therefore important to discuss the effect of the core on the overall dynamics. Synthetically, to achieve a larger number of the arms, a larger core is needed. At the same time, decreasing the length of the arm (i.e., its molar mass) increases the core-to-shell (arm) ratio. This means that for the stars studied here, and in particular for the PBD1110-1.3k and PBD2830-1.3k, both having Ma=1.3kg/mol, the core occupies a non-negligible part of the star and is proportionally larger in the latter case. This is of course apparent in the local dynamics, as well as in global dynamics discussed in the previous chapter. Once the segments are far away from the core, their dynamics become polymeric, so processes with common temperature dependence arise. It becomes clear that we are far from the limit of infinitively long chains tethered to one common core, the situation primarily addressed in the context of star dynamics in the past, i.e., for star polymers where the size of the core is effectively negligible. For these stars, the tube model can describe the dynamics of the arms. We are probing here the extreme case, where the core size becomes non-negligible and the dynamics studied experimentally reflect the importance of architecture. In other words, by progressively reducing the arm length we are able to identify the effect of tethering a large number of polymeric chains onto a common core. If we consider naively that the contribution of different segments (with different local dynamics) to the overall dielectric (or other) signal is weighted in proportion to their population, it is then evident that in the case of long well-entangled arms the effect of the dynamics near the core cannot be discerned experimentally, since the ratio of signal coming from the segments near to the core is negligible. Hence, here we clearly have the case that the information comes from the part that cannot be accessible experimentally for the long arm stars.

4.4 Conclusions

We studied rheologically the effect of tethering a very large number of very short polymeric chains on a common core. The functionality was close enough for two of the samples studied here but with different arm length, namely, totally unentangled and marginally entangled. A third sample with a functionality almost three times higher and unentangled arms completes the picture of the effect of branching on the segmental dynamics of these crowded macromolecular objects.

We performed careful rheological measurements with particular interest in the high-frequency regime in order to elucidate the rich local dynamics. Rheology was proven to be a sensitive to changes in segmental dynamics, despite the limited frequency spectrum accessible with a rheometer during an isothermal measurement. Our main finding is the slowing-down of the segmental relaxation as the number of arms increases and the length of the arm decreases. We found the same qualitative results using TM-DSC. These stars were found to be thermorheologically complex, an important finding that can be explained in terms of the existence of more than one local relaxation processes with the same or different temperature dependence.

The complementary BDS data proved to be crucially important, not only for confirming the above findings, but further to shed light into the origin of local dynamics. BDS is clearly the appropriate technique to study segmental processes due to the fact that they are directly for the particular polymer in question, and their complex temperature dependencies are unambiguously resolved; this is because a BDS spectrum of several orders of magnitude can be accessed at a constant temperature. The discontinuity of superposition of isotherms is present here as well. An additional ultraslow segmental process was clearly identified for one of the samples (PBD1110-1.3k), without excluding its presence in the other two samples. This process was found to have a different temperature dependence compared to the other two alpha-type local relaxation processes, suggesting that different layers with distinct mobilities do coexist in a single multiarm star. We attribute this to the effect of tethering a very large number of short arms onto a common core. Strong stretching and crowding effects must be present here as well as density heterogeneity that is maximum near the core that affect the local dynamics of this densely crowded melt.

4.5 References

(1) Kapnistos, M.; Semenov, A. N.; Vlassopoulos, D.; Roovers, J. Viscoelastic Response of Hyperstar Polymers in the Linear Regime. *J. Chem. Phys.* **1999**, *111* (4), 1753–1759. https://doi.org/10.1063/1.479436.

(2) Vlassopoulos, D.; Fytas, G.; Pakula, T.; Roovers, J. Multiarm Star Polymers Dynamics. *J. Phys. Condens. Matter* **2001**, *13* (41), R855–R876. https://doi.org/10.1088/0953-8984/13/41/202.

(3) Kapnistos, M.; Vlassopoulos, D.; Roovers, J.; Leal, L. G. Linear Rheology of Architecturally Complex Macromolecules: Comb Polymers with Linear Backbones. *Macromolecules* **2005**, *38* (18), 7852–7862. https://doi.org/10.1021/ma050644x.

(4) Pakula, T.; Vlassopoulos, D.; Fytas, G.; Roovers, J. Structure and Dynamics of Melts of Multiarm Polymer Stars. *Macromolecules* **1998**, *31* (25), 8931–8940. https://doi.org/10.1021/ma981043r.

(5) Gury, L.; Gauthier, M.; Cloitre, M.; Vlassopoulos, D. Colloidal Jamming in Multiarm Star Polymer Melts. *Macromolecules* **2019**, *52* (12), 4617–4623. https://doi.org/10.1021/acs.macromol.9b00674.

(6) Daoud, M.; Cotton, J. P. Star Shaped Polymers : A Model for the Conformation and Its Concentration Dependence. *J. Phys.* **1982**, *43* (3), 531–538. https://doi.org/10.1051/jphys:01982004303053100.

(7) M. Rubinstein, H. Colby. *Polymer Physics*.

(8) Ruymbeke, E. van; Muliawan, E. B.; Vlassopoulos, D.; Gao, H.; Matyjaszewski, K. Melt Rheology of Star Polymers with Large Number of Small Arms, Prepared by Crosslinking Poly(n-Butyl Acrylate) Macromonomers via ATRP. *Eur. Polym. J.* **2011**, *47* (4), 746–751. https://doi.org/10.1016/j.eurpolymj.2010.09.037.

(9) Kisliuk, A.; Ding, Y.; Hwang, J.; Lee, J. S.; Annis, B. K.; Foster, M. D.; Sokolov, A. P. Influence of Molecular Architecture on Fast and Segmental Dynamics and the Glass Transition in Polybutadiene. *J. Polym. Sci. Part B Polym. Phys.* **2002**, *40* (21), 2431–2439. https://doi.org/10.1002/polb.10295.

(10) Chremos, A.; Glynos, E.; Green, P. F. Structure and Dynamical Intra-Molecular Heterogeneity of Star Polymer Melts above Glass Transition Temperature. *J. Chem. Phys.* **2015**, *142* (4), 044901. https://doi.org/10.1063/1.4906085.

(11) Mackay, M. E.; Halley, P. J. Technical Note: Angular Compliance Error in Force Rebalance Torque Transducers. *J. Rheol.* **1991**, *35* (8), 1609–1614. https://doi.org/10.1122/1.550247.

(12) Liu, C.-Y.; Yao, M.; Garritano, R. G.; Franck, A. J.; Bailly, C. Instrument Compliance Effects Revisited: Linear Viscoelastic Measurements. *Rheol. Acta* **2011**, *50* (5–6), 537–546. https://doi.org/10.1007/s00397-011-0560-3.

(13) Laukkanen, O.-V. Small-Diameter Parallel Plate Rheometry: A Simple Technique for Measuring Rheological Properties of Glass-Forming Liquids in Shear. *Rheol. Acta* **2017**, *56* (7–8), 661–671. https://doi.org/10.1007/s00397-017-1020-5.

(14) Williams, M. L.; Landel, R. F.; Ferry, J. D. The Temperature Dependence of Relaxation Mechanisms in Amorphous Polymers and Other Glass-Forming Liquids. *J. Am. Chem. Soc.* **1955**, *77* (14), 3701–3707. https://doi.org/10.1021/ja01619a008.

(15) Erwin, B. M.; Colby, R. H. Temperature Dependence of Relaxation Times and the Length Scale of Cooperative Motion for Glass-Forming Liquids. *J. Non-Cryst. Solids* **2002**, *307–310*, 225–231. https://doi.org/10.1016/S0022-3093(02)01464-3.
(16) Zoller, P.; David J. Walsh. *Standard Pressure-Volume-Temperature Data for Polymers*; Technomic, 1995.
(17) Zorn, R.; McKenna, G. B.; Willner, L.; Richter, D. Rheological Investigation of Polybutadienes Having Different Microstructures over a Large Temperature Range. *Macromolecules* **1995**, *28* (25), 8552–8562. https://doi.org/10.1021/ma00129a014.
(18) Bueche, F. Segmental Mobility of Polymers Near Their Glass Temperature. 7.
(19) Simon, S. L. Temperature-Modulated Differential Scanning Calorimetry: Theory and Application. *Thermochim. Acta* **2001**, *374* (1), 55–71. https://doi.org/10.1016/S0040-6031(01)00493-2.
(20) Carpentier, L.; Bustin, O.; Descamps, M. Temperature-Modulated Differential Scanning Calorimetry as a Specific Heat Spectroscopy. *J. Phys. Appl. Phys.* **2002**, *35* (4), 402–408. https://doi.org/10.1088/0022-3727/35/4/317.
(21) Hensel, A.; Dobbertin, J.; Schawe, J. E. K.; Boller, A.; Schick, C. Temperature Modulated Calorimetry and Dielectric Spectroscopy in the Glass Transition Region of Polymers. *J. Therm. Anal.* **1996**, *46* (3–4), 935–954. https://doi.org/10.1007/BF01983612.
(22) Politidis, C.; Alexandris, S.; Sakellariou, G.; Steinhart, M.; Floudas, G. Dynamics of Entangled *Cis* -1,4-Polyisoprene Confined to Nanoporous Alumina. *Macromolecules* **2019**, *52* (11), 4185–4195. https://doi.org/10.1021/acs.macromol.9b00523.
(23) Nikovia, C.; Theodoridis, L.; Alexandris, S.; Bilalis, P.; Hadjichristidis, N.; Floudas, G.; Pitsikalis, M. Macromolecular Brushes by Combination of Ring-Opening and Ring-Opening Metathesis Polymerization. Synthesis, Self-Assembly, Thermodynamics, and Dynamics. *Macromolecules* **2018**, *51* (21), 8940–8955. https://doi.org/10.1021/acs.macromol.8b01905.
(24) Alexandris, S.; Franczyk, A.; Papamokos, G.; Marciniec, B.; Graf, R.; Matyjaszewski, K.; Koynov, K.; Floudas, G. Dynamic Heterogeneity in Random Copolymers of Polymethacrylates Bearing Different Polyhedral Oligomeric Silsesquioxane Moieties (POSS). *Macromolecules* **2017**, *50* (10), 4043–4053. https://doi.org/10.1021/acs.macromol.7b00660.
(25) J. D. Ferry,. *Viscoelastic Properties of Polymers*, 3rd ed.; Wiley, 1980.
(26) Alexandris, S.; Papadopoulos, P.; Sakellariou, G.; Steinhart, M.; Butt, H.-J.; Floudas, G. Interfacial Energy and Glass Temperature of Polymers Confined to Nanoporous Alumina. *Macromolecules* **2016**, *49* (19), 7400–7414. https://doi.org/10.1021/acs.macromol.6b01484.
(27) Arbe, A.; Richter, D.; Colmenero, J.; Farago, B. Merging of the ⌴ and ᴺʟ Relaxations in Polybutadiene: A Neutron Spin Echo and Dielectric Study. 17.
(28) Hu, H.-W.; Granick, S. Viscoelastic Dynamics of Confined Polymer Melts. *Science* **1992**, *258* (5086), 1339–1342. https://doi.org/10.1126/science.258.5086.1339.
(29) Glomann, T.; Schneider, G. J.; Allgaier, J.; Radulescu, A.; Lohstroh, W.; Farago, B.; Richter, D. Microscopic Dynamics of Polyethylene Glycol Chains Interacting with Silica Nanoparticles. *Phys. Rev. Lett.* **2013**, *110* (17), 178001. https://doi.org/10.1103/PhysRevLett.110.178001.

(30) Agarwal, P.; Kim, S. A.; Archer, L. A. Crowded, Confined, and Frustrated: Dynamics of Molecules Tethered to Nanoparticles. *Phys. Rev. Lett.* **2012**, *109* (25), 258301. https://doi.org/10.1103/PhysRevLett.109.258301.
(31) Holt, A. P.; Roland, C. M. Segmental and Secondary Dynamics of Nanoparticle-Grafted Oligomers. *Soft Matter* **2018**, *14* (42), 8604–8611. https://doi.org/10.1039/C8SM01443D.
(32) Denissov, A.; Kroutieva, M.; Fatkullin, N.; Kimmich, R. Segment Diffusion and Nuclear Magnetic Resonance Spin-Lattice Relaxation of Polymer Chains Confined in Tubes: Analytical Treatment and Monte Carlo Simulation of the Crossover from Rouse to Reptation Dynamics. *J. Chem. Phys.* **2002**, *116* (12), 5217. https://doi.org/10.1063/1.1451242.
(33) Thompson, P. A.; Grest, G. S.; Robbins, M. O. Phase Transitions and Universal Dynamics in Confined Films. *Phys. Rev. Lett.* **1992**, *68* (23), 3448–3451. https://doi.org/10.1103/PhysRevLett.68.3448.